Universitat Politècnica de València
Departamento de Máquinas y Motores Térmicos

Optimization and analysis by CFD of mixing-controlled combustion concepts in compression ignition engines

Doctoral Thesis
Presented by:
Alberto Hernández López
Directed by:
Prof. Jesús Vicente Benajes Calvo
and
Dr. Ricardo Novella Rosa

Valencia, March 27, 2018

Doctoral Thesis

Optimization and analysis by CFD of mixing-controlled combustion concepts in compression ignition engines

Presented by: Alberto Hernández López
Directed by: Prof. Jesús Vicente Benajes Calvo
Dr. Ricardo Novella Rosa

Examining Board:

President: Prof. José M Desantes
Secretary: Prof. Tommaso Lucchini
Examiner: Prof. Rosario Ballesteros

Reviewing Board:

Prof. Magin Lapuerta
Prof. Federico Millo
Prof. Tommaso Lucchini

Valencia, March 27, 2018

Resumen. El trabajo presentado en esta Tesis está motivado por la necesidad de los motores de combustión interna alternativos de reducir el consumo de combustible y las emisiones de CO_2 mientras se satisfacen las cada vez más restrictivas regulaciones de emisiones contaminantes. Por lo tanto, el objetivo principal de este estudio es optimizar un sistema de combustión de encendido por compresión controlado por mezcla para probar su potencial como motores de futura generación. Con esta meta se ha desarrollado un sistema automático que combina CFD con métodos de optimización avanzados para analizar y entender las configuraciones óptimas.

Los resultados presentados en este trabajo se dividen en dos bloques principales. El primero corresponde a la optimización de un sistema de encendido por compresión convencional alimentado con diésel. El segundo se centra en un concepto de combustión avanzado donde se ha sustituido el fuel por Dimetil-eter. En ambos casos, el estudio no sólo halla una configuración óptima sino que también se describen las relaciones causa/efecto entre los parámetros más relevantes del sistema de combustión.

El primer bloque aplica métodos de optimización no-evolutivos a un motor medium-duty alimentado por diésel tratando de minimizar consumo a la vez que se mantienen las emisiones contaminantes por debajo de los estándares de emisiones contaminantes impuestos. Una primera parte se centra en la optimización de la geometría de la cámara de combustión y el inyector. Seguidamente se extiende el estudio añadiendo los settings de renovación de la carga de y de inyección al estudio, ampliando el potencial de la optimización. El estudio demuestra el limitado potencial de mejora de consumo que tiene el motor de referencia al mantener los niveles de emisiones contaminantes. Esto demuestra la importancia de incluir parámetros de renovación de la carga e inyección al proceso de optimización.

El segundo bloque aplica una metodología basada en algoritmos genéticos al diseño del sistema de combustión de un motor heavy-duty alimentado con Dimetil-eter. El estudio tiene dos objetivos, primero la optimización de un sistema de combustión convencional controlado por mezcla con el objetivo de lograr mejorar el consumo y reducir las emisiones contaminantes hasta niveles inferiores a los estándares US2010. Segundo la optimización de un sistema de combustión trabajando en condiciones estequiométricas acoplado con un catalizador de tres vías buscando reducir consumo y controlar las emisiones contaminantes por debajo de los estándares 2030. Ambas optimizaciones incluyen tanto la geometría como los parámetros más relevantes de renovación de la carga y de inyección. Los resultados presentan un sistema de combustión convencional óptimo con una notable mejora en rendimiento y un sistema de combustión estequiométrica que es capaz de ofrecer niveles de NOx menores al 1% de los niveles de referencia manteniendo niveles competitivos de rendimiento.

Los resultados presentados en esta Tesis ofrecen una visión extendida de las ventajas y limitaciones de los motores MCCI y el camino a seguir para reducir las emisiones de futuros sistemas de combustión por debajo de los estándares establecidos. A su vez, este trabajo también demuestra el gran potencial que tiene el Dimetil-eter como combustible para futuras generaciones de motores.

Resum. El treball presentat en esta Tesi està motivat per la necessitat dels motors de combustió interna alternatius de reduir el consum de combustible i les emissions de CO_2 mentres se satisfan les cada vegada més restrictives regulacions d'emissions contaminants. Per tant, l'objectiu principal d'este estudi és optimitzar un sistema de combustió d'encesa per compressió controlat per mescla per a provar el seu potencial com a motors de futura generació. Amb esta meta s'ha desenrotllat un sistema automàtic que combina CFD amb mètodes d'optimització avançats per a analitzar i entendre les configuracions òptimes. Els resultats presentats en este treball es dividixen en dos blocs principals. El primer correspon a l'optimització d'un sistema d'encesa per compressió convencional alimentat amb dièsel. El segon se centra en un concepte de combustió avançat on s'ha substituït el fuel per Dimetil-eter. En ambdós casos, l'estudi no sols troba una configuració òptima sinó que també es descriuen les relacions causa/efecte entre els paràmetres més rellevants del sistema de combustió.

El primer bloc aplica mètodes d'optimització no-evolutius a un motor medium-duty alimentat per dièsel tractant de minimitzar consum al mateix temps que es mantenen les emissions contaminants per davall dels estàndards d'emissions contaminants impostos. Una primera part se centra en l'optimització de la geometria de la cambra de combustió i l'injector. A continuació s'estén l'estudi afegint els settings de renovació de la càrrega de i d'injecció a l'estudi, ampliant el potencial de l'optimització. L'estudi demostra el limitat potencial de millora de consum que té el motor de referència al mantindre els nivells d'emissions contaminants. Açò demostra la importància d'incloure paràmetres de renovació de la càrrega i injecció al procés d'optimització.

El segon bloc aplica una metodologia basada en algoritmes genètics al disseny del sistema de combustió d'un motor heavy-duty alimentat amb Dimetil-eter. L'estudi té dos objectius, primer l'optimització d'un sistema de combustió convencional controlat per mescla amb l'objectiu d'aconseguir millorar el consum i reduir les emissions contaminants fins nivells inferiors als estàndards US2010. Segon l'optimització d'un sistema de combustió treballant en condicions estequiomètriques acoblat amb un catalitzador de tres vies buscant reduir consum i controlar les emissions contaminants per davall dels estàndards 2030. Ambdós optimitzacions inclouen tant la geometria com els paràmetres més rellevants de renovació de la càrrega i d'injecció. Els resultats presenten un sistema de combustió convencional òptim amb una notable millora en rendiment i un sistema de combustió estequiomètrica que és capaç d'oferir nivells de NOx menors al 1% dels nivells de referència mantenint nivells competitius de rendiment.

Els resultats presentats en esta Tesi oferixen una visió estesa dels avantatges i limitacions dels motors MCCI i el camí que s'ha de seguir per a reduir les emissions de futurs sistemes de combustió per davall dels estàndards establits. Al seu torn, este treball també demostra el gran potencial que té el Dimetil-eter com a combustible per a futures generacions de motors.

Abstract. The work presented in this Thesis was motivated by the needs of internal combustion engines (ICE) to decrease fuel consumption and CO_2 emissions, while fulfilling the increasingly stringent pollutant emission regulations. Then, the main objective of this study is to optimize a mixing-controlled compression ignition (MCCI) combustion system to show its potential for future generation engines. For this purpose an automatic system based on CFD coupled with different optimization methods capable of optimizing a complete combustion system with a reasonable time cost was designed together with the methodology to analyze and understand the new optimum systems.

The results presented in this work can be divided in two main blocks, firstly an optimization of a conventional diesel combustion system and then an optimization of a MCCI system using an alternative fuel with improved characteristics compared to diesel. Due to the methodologies used in this Thesis, not only the optimum combustion system configurations are described, but also the cause/effect relations between the most relevant inputs and outputs are identified and analyzed.

The first optimization block applies non-evolutionary optimization methods in two sequential studies to optimize a medium-duty engine, minimizing the fuel consumption while fulfilling the emission limits in terms of NOx and soot. The first study targeted four optimization parameters related to the engine hardware including piston bowl geometry, injector nozzle configuration and mean swirl number. After the analysis of the results, the second study extended to six parameters, limiting the optimization of the engine hardware to the bowl geometry, but including the key air management and injection settings. The results confirmed the limited benefits, in terms of fuel consumption, with constant NOx emission achieved when optimizing the engine hardware, while keeping air management and injection settings. Thus, including air management and injection settings in the optimization is mandatory to significantly decrease the fuel consumption while keeping the emission limits.

The second optimization block applies a genetic algorithm optimization methodology to the design of the combustion system of a heavy-duty Diesel engine fueled with dimethyl ether (DME). The study has two objectives, the optimization of a conventional mixing-controlled combustion system aiming to achieve US2010 targets and the optimization of a stoichiometric mixing-controlled combustion system coupled with a three way catalyst to further control NOx emissions and achieve US2030 emission standards. These optimizations include the key combustion system related hardware, bowl geometry and injection nozzle design as input factors, together with the most relevant air management and injection settings. The target of the optimizations is to improve net indicated efficiency while keeping NOx emissions, peak pressure and pressure rise rate under their corresponding target levels. Compared to the baseline engine fueled with DME, the results of the study provide an optimum conventional combustion system with a noticeable NIE improvement and an optimum stoichiometric combustion system that offers a limited NIE improvement keeping tailpipe NOx values below 1% of the original levels.

The results presented in this Thesis provide an extended view of the advantages and limitations of MCCI engines and the optimization path required to achieve future

emission standards with these engines. Additionally, this work showed how DME is a promising fuel for future generation engines since it is able to achieve future emission standards while maintaining diesel-like efficiency.

Agradecimientos

Lo primero quiero agradecer al CMT todo el apoyo que me han dado durante estos anos. Especialmente a mi director de Tesis Jesús Benajes y mi codirector Ricardo Novella ya que ellos han sido un apoyo incondicional y una fuente infinita de conocimientos. También me gustaría agradecer a José Manuel Pastor, quien ha completado el equipo, junto con Ricardo Novella, y con el cual hemos sacado adelante innumerables proyectos. Y finalmente agradecer a todo el equipo de secretaría que sin él no sería posible sacar adelante ningún documento.

También me gustaría agradecer a mi familia y amigos todo su apoyo incondicional, en especial a la última parte en unirse, Amparo, ya que ha estado conmigo para sufrir las partes malas y celebrar las buenas.

Querría también agradecer a la beca de Formación del Proferosado Universitario (FPU 13/02817) su constante y puntual apoyo mensual ya que de aire no se vive y de amor por los motores tampoco.

Finally, I would lke to switch to english to express my sincere gratitude to Sage Kokjohn and the University of Wisconsin Madison to help me with all their knowledge and resources because half of this Thesis would not had been possible without them.

Table of Contents

Index of Figures

Index of Tables

Nomenclature

Latin

b	Bias
$^{\circ}C$	Celsius degrees
$CA90abs$	Angle when 90% of the injected energy is released
d/B	Geometric parameter that refers to the piston bowl width
dP/da	Pressure gradient
dS	Cell size
Exp	Experimental
$G1-G15$	Geometric parameters
K	Reentrant parameter for the non-evolutionary optimization
Kd	Reentrant parameter for the evolutionary optimization
$maxD$	Maximum depth
$MaxGen$	Maximum number of generations
$maxPRR$	Maximum pressure rate
$maxW$	Maximum width
$p1h-p5h$	Horizontal dimension of the bezier points 1 to 5
$p1v-p5v$	Vertival dimension of the bezier points 1 to 5

Greek

$\tau_{GA,0}$	Initial time constant
σ	Convergence constant

Initials and acronyms

ACT	Apparent combustion time
ANN	Artificial neural network
BDC	Bottom dead center

$BSFC$	Brake specific fuel consumption
cad	Crank angle degree or deg aTDC
$CARB$	California air resources board
CCD	Central composite design
CD	Combustion duration
CDC	Conventional diesel engine
CFD	Computational fluid dynamics
CI	Compression ignition
CP	Current position
CR	Compression ratio
DEF	Diesel exhaust fluid
DME	Dimethyl ether
DPF	Diesel particle filter
$Dnoz$	nozzle hole diameter
EGR	Exhaust gas recirculation
ERC	Engine research center
EVO	Exhaust valve opening
FSN	Filter Smoke number
$FTIR$	Fourier transform infrared
GA	Genetic algorithm
GBP	Global best position
GHG	Green house gas
GIE	Gross indicated efficiency
GIW	Gross indicated work
HC	Hydrocarbon
HD	Heavy-duty
HRR	Heat release rate
$HSDI$	High-speed direct injection
HT	Heat transfer
ICE	Internal combustion engine
IP	Injection pressure
$IMEP$	Indicated mean effective pressure
$IRDI$	Discharge rate curve indicator
$ISFC$	Indicated specific fuel consumption

IVC	Intake valve closing
IW	Inertia weight
$LDEF$	Lagrangian-Drop and Eulerian-Fluid
LIV	Last iteration velocity
LNT	Lean NOx trap
LPG	Liquefied petroleum gas
LTC	Low temperature combustion
$MCCI$	Mixing-controlled compression ignition
MD	Medium-duty
NIE	Net indicated efficiency
NSD	New search direction
PBP	Personal best position
$Pcyl$	In-cylinder pressure
$PIVC$	In-cylinder pressure at IVC
PM	Particulate matter
$Pmax$	Maximum pressure
PP	Peak pressure
PSA	Particle swarm algorithm
RMS	Root mean square
RSM	Response surface method
SCR	Selective catalytic reduction
SI	Spark ignition
SOI	Start of injection
TDC	Top dead center
TWC	Three way catalyst
WSR	Well stirred reactor

Chapter 1

Introduction

Contents

1.1 Introduction

The first four-stroke internal combustion engine (ICE) that constitutes the base for the modern vehicle engine was created by Nikolaus Otto in 1876. However, it was not until 1908 when Ford sold the Model T as the first mass-produced vehicle. This was the first model designed to be affordable for the average costumer. The first year of production, the number of cars produced were just over 10000 but 10 years later the car production exceeded the million units already. This trend continued over the years increasing the car production and sales until today. The number of cars has increased drastically over the last 30 years and it is expected that by 2040 the number of cars on the road will be nearly doubled (see Fig. 1.1), specially in developing countries like China or India. This growth directly affects the worldwide pollution, therefore the emission levels of the vehicles is a topic that has been extensively discussed in recent years.

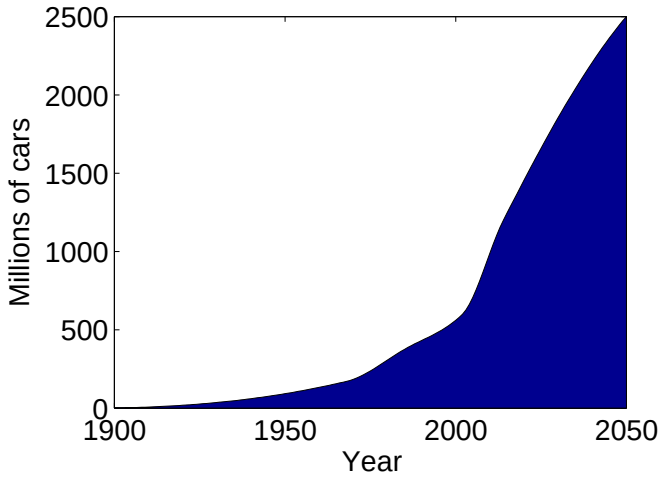

Figure 1.1. *Evolution of number of cars on road. Adapted from [1, 2].*

Nowadays the engines are already really optimized and can offer higher efficiency and lower emission levels than 30 years ago. However, that improvement is insufficient to control the increase in pollutant levels because the vehicles sales increase at a faster rate than the emission levels are decreased [2]. In order to control the pollution, the emission standards are becoming more and more restrictive. Although the new generation engines are able to offer emission levels many times lower that their predecessors, the target emission levels are becoming difficult to achieve and that hinders the design of future generation engines. Fig. 1.2 shows the evolution of the emission standards since 30 years ago and it can be seen how nowadays the engines are allowed to pollute significantly less than compared to 30 years ago.

Another aspect that is gaining a lot of attention in recent years is the engine efficiency. It is driven by the concerns over greenhouse gas (GHG) emissions and long term energy supplies, specially CO_2 that is directly related to the use of fossil fuels. This is particularly relevant in transport applications because they represent the second sector that produces the most CO_2 (see Fig. 1.3) and the main sector that produces environmental pollution and climate change. This forces new generation engines to not only accomplish the new emissions standards but also offer higher efficiencies and lower fuel consumption.

The researchers are following two main paths to offer higher efficiency and lower emissions:

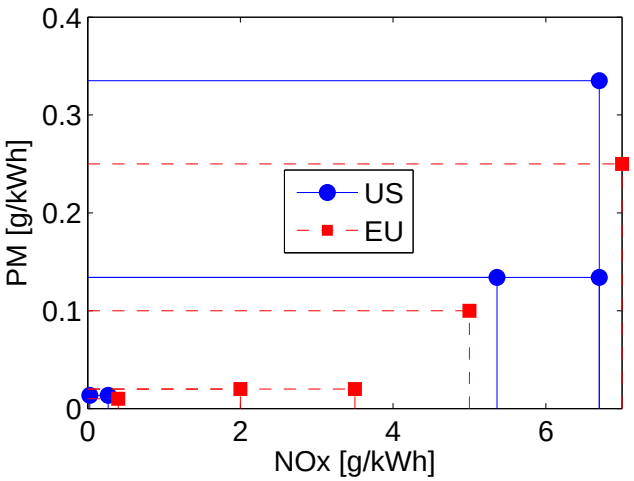

Figure 1.2. *Emission standards for the last 30 years. Adapted from [3].*

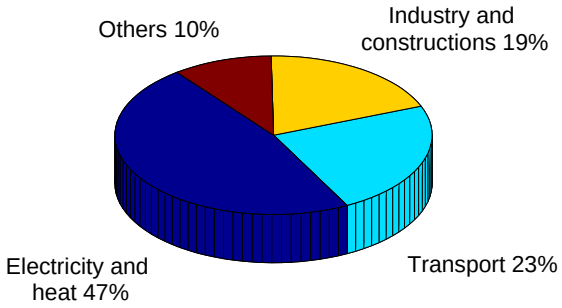

Figure 1.3. *Global CO_2 production per sector. Adapted from [4].*

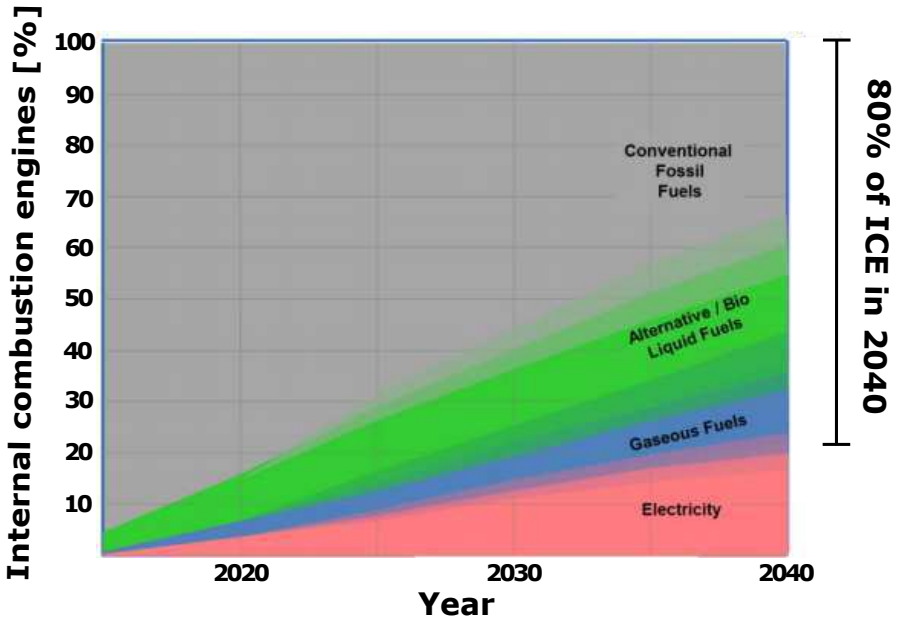

Figure 1.4. *Evolution of transport energy towards 2040. Adapted from [5].*

- Improve the existent ICE to be cleaner and more efficient. This path not only considers improving the current combustion concepts but also developing and optimizing advanced combustion systems.
- Substitute the ICE with electric motors and provide the customers with robust and fast charging networks.

The electric motors have been suggested as the alternative to the ICE for a long time but in recent years that idea is building strength. Nevertheless, it is expected that by 2040 the 80% of vehicles will still depend on an ICE (see Fig. 1.4).

In big cities where the distances are short and the limited capacity of the batteries are less problematic, the electric motors will dominate in the future. However, this plug-in electrification will be less relevant in non-city heavy-duty (HD) vehicles due to the high energetic requirements. For that reason in HD (also medium duty (MD)) applications the electrification of the engines is not a short term option and the optimization of the current ICE to improve efficiency is the way to go [5].

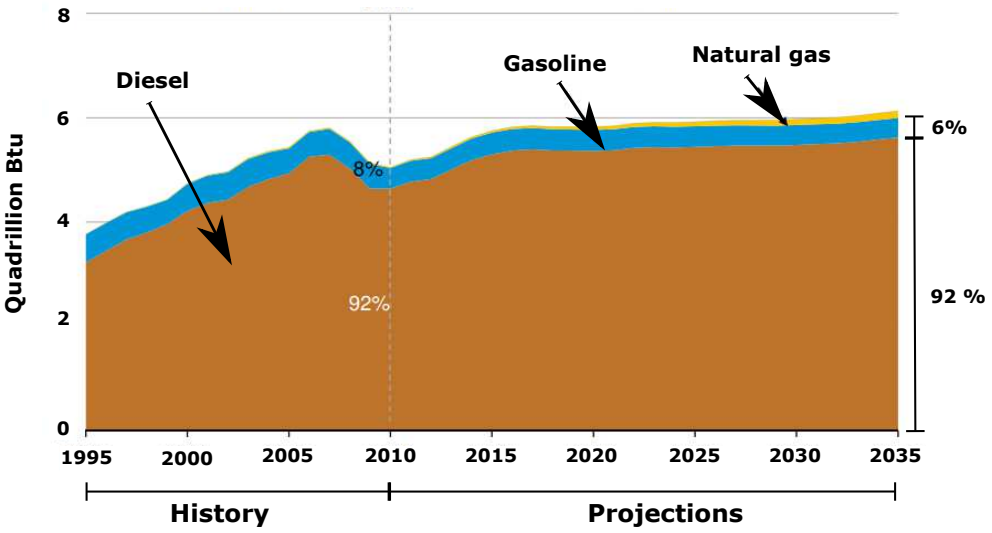

Figure 1.5. *Evolution of fuel usage in heavy-duty engines. Adapted from [6].*

The HD applications are mainly dominated by diesel engines (see Fig. 1.5). Even though there are some alternatives, the robustness and efficiency of the diesel engines ensures that the transport vehicles are at their destination on time with a minimal cost. Additionally, emission controlling strategies that can not be used for small vehicles due to overcost (i.e. SCR) are widely used in HD vehicles allowing them to achieve low emission levels without punishing efficiency.

Diesel HD engines have suffered several changes over the years, most of them focused on reducing their pollutant levels to achieve more stringent emission standards. Most of these changes have been focused on improving the flexibility of the subsystems coupled with the diesel engine like fuel multi-injection or variable valve timing. Fig. 1.6 represents the subsystems that have been applied to diesel engines in chronological order. Some of these systems have been crucial to control the pollutant emissions. For example, the exhaust gas recirculation (EGR) system is compulsory nowadays in every conventional diesel combustion (CDC) engine. At reasonable levels, EGR allows to control NOx emissions with minimal degradation of the engine efficiency. In the same manner, the after-treatment systems like diesel particle filter (DPF) allows

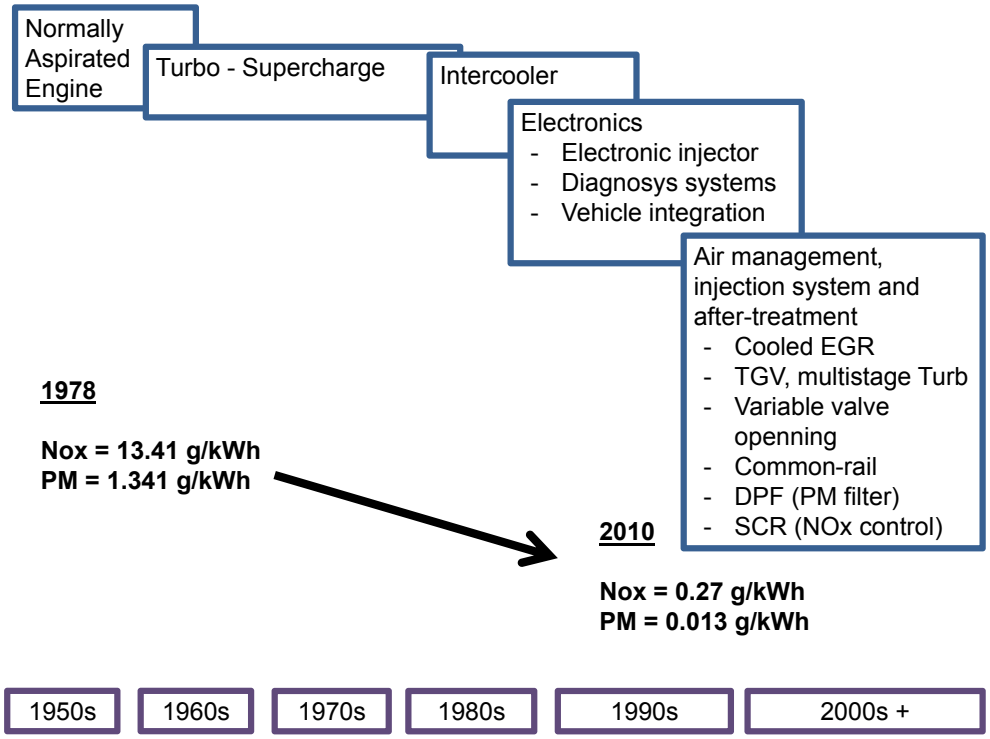

Figure 1.6. *Technological evolution of the flexibilitation trend in diesel engines. Adapted from [7].*

the vehicle to emit really low particle levels and are present in most of the vehicles nowadays. Even though these techniques allowed the evolution of the engines to meet the current standards, those emission levels are becoming more a more stringent at a really fast rate, therefore a bigger step in the field of engine optimization is needed to meed future regulations.

The exponential increase in the engine system flexibility increases at the same time the complexity of designing and optimizing an engine. This task has been done experimentally in the past but due to the increasing difficulty, doing a parametric study experimentally is no longer enough and optimization methods coupled with Computational Fluid Dynamics (CFD) are gaining interest. These methods are becoming more and more accurate and robust, and are a lot cheaper than the experimental version in terms of time and resources cost. Additionally, they permit the study of situations that can not happen with the current technology or are just dangerous to

test experimentally. Nevertheless, experimental testing would never dissapear because all the optimizations end up being validated experimentally.

In this context, the research work presented in this Thesis is focused on applying optimization methods to design and analyze the combustion system of medium and heavy-duty engines aiming to show their potential to meet current and future emissions standards. Due to the long journey that MD and HD engines have and the increasing potential of the CFD optimization methods, this Thesis will provide useful information and tools for future engine designs.

1.2 Objectives and methodology

This section presents the main objectives of this research work and the main working path followed to accomplish them. It will be seen how the methodology presented in this section is directly related to the structure of the Thesis.

1.2.1 Objectives

The final objective of this Thesis is to optimize a mixing-controlled compression ignition (MCCI)[1] combustion system to show its potential for future generation engines. This implies improving efficiency to keep the CO_2 under control while keeping the NOx and soot levels under current and future emission standards. Due to the long life expected for diesel engines, the first steps will be focused on CDC engines. Then, Dimethyl ether (DME) will be introduced as a diesel substitute and its potential will be analyzed. However, in order to achieve the main objective it is necessary to complete some extra objectives that are directly related to the main one:

- Create an automatic system capable of optimizing a complete combustion system with a reasonable time cost. This implies creating a system that can generate, simulate and post-process CFD cases of a complete combustion system coupled with an optimization method. This is necessary because the combustion systems have become really complex with too many variables to be handled by a person so an automatic

[1] The term MCCI is used to represent the type of engines that are going to be studied in this Thesis because it is considered the most suitable term, however, the term diesel is often used as a synonym.

system capable of performing and controlling the whole process is compulsory.

- Create a new methodology to analyze and understand the cause/effect relations of the input and output variables considered in the optimizations. This objective is of big interest because the optimization process usually gives the optimum configuration, however, the reasons behind that configuration being the optimum are not usually fully understood. Moreover, the methodology should be able to identify correlated effects that can not be considered with simpler analysis like parametric studies. Therefore, developing a method that provides the reasons behind each change on each input variable to reach the optimum configuration is necessary.

- Perform an experimental validation of the results obtained from the optimization process (only when it is possible).

1.2.2 Methodology

A detailed methodology was followed to achieve the objectives presented in the previous section. That methodology is summarized in Fig. 1.7. It can be divided in 3 clear steps that are directly related with the main work structure.

1. **Literature review.** The main objective of the literature review is to summarize the state-of-the-art knowledge related to the subject of this Thesis. It was divided in two blocks to make it clearer and easier to understand:

    - **Engine optimization strategies.** This first block is developed in Chapter 2. The initial part of the chapter presents the main advanced and conventional combustion concepts and their advantages and disadvantages are compared. The objective of this initial part is to justify why the CDC concept is chosen as the starting point for this Thesis. Then this combustion concept is described in detail and the state-of-the-art strategies used to improve efficiency and control emissions on these engines are described. Those strategies are divided in 5 sections, combustion chamber geometry, air management settings, injection settings, after-treatment and alternative fuels. This block is essential for this Thesis because it presents the tools that the optimization systems

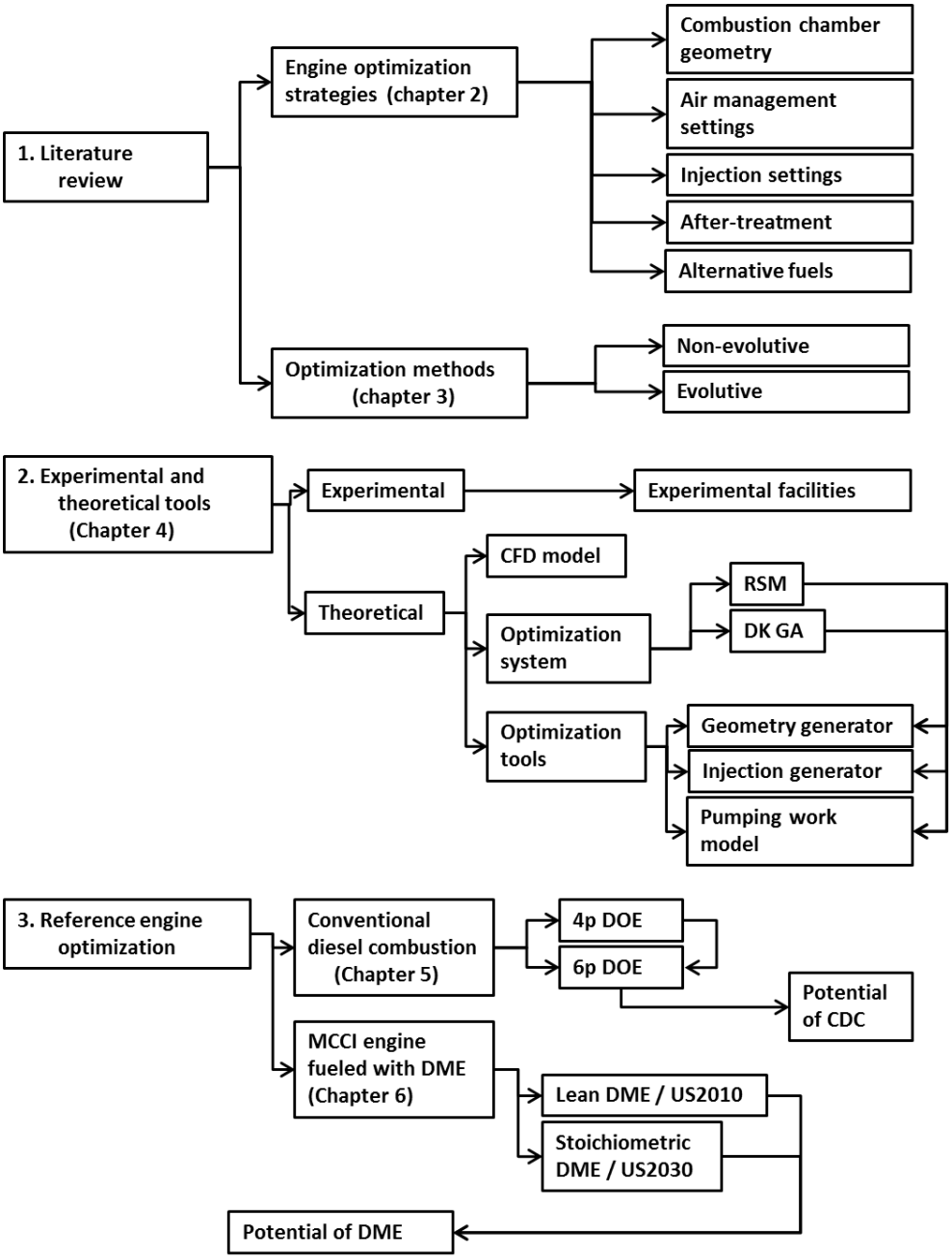

Figure 1.7. *Thesis methodology.*

will use to improve the reference engine and achieve current and future emission standards.

- **Optimization methods.** This second block is developed in Chapter 3. It describes the optimization methods used in this work highlighting the differences between evolutionary and non-evolutionary methods. These differences between both methods will justify what method should be used for each optimization in order to get the best and more accurate result with the least cost possible.

2. **Experimental and theoretical tools.** This part of the methodology is presented in Chapter 4 and is focused on describing the main tools integrated to create and validate the automatic optimization system used in this work. It starts presenting the experimental facilities where the experimental data used to calibrate the CFD model was obtained. Then the CFD model is presented together with all the tools coupled with it to create the optimization system, this is, the optimization method, geometry generator, injection generator and pumping work model. Additionally, examples of the geometry generator capabilities or the genetic algorithm working with different populations is shown to prove the potential of the system and decide the best initial configuration.

3. **Reference engine optimization.** This part of the methodology is presented in chapters 5 and 6.

   - **Chapter 5.** It summarizes the results from the optimization of a CDC engine optimized with non-evolutionary optimization methods. The process is divided in two main blocks, the first one is a simpler optimization where only 4 parameters are optimized and the results are used to complement the second and more complete optimization where 6 parameters are optimized. Then these results are used to conclude if the combustion concept has potential for future generation engines.
   - **Chapter 6.** In this chapter the results from a DME fueled MCCI engine optimized with evolutionary methods are summarized. Two different optimizations are performed but, unlike chapter 5, both optimizations are independent and used to show the flexibility and potential of the DME for achieving current and future emission standards.

References

[1] "Automobile Production 1900 - 2003". *http://www.carhistory4u.com/the-last-100-years/car-production*.

[2] Sperling C and Gordon D. "Two billion cars, transforming a culture". *http://onlinepubs.trb.org/onlinepubs/trnews/trnews259billioncars.pdf*.

[3] DieselNet. "Emission standards". *https://www.dieselnet.com/standards*.

[4] Birol F. "CO2 highlights 2016". *http://www.iea.org/publications/freepublications/publication/co2-emissions-from-fuel-combustion-highlights-2016.html*.

[5] ERTRAC. "Future light and heavy duty ICE powertrain technologies". *http://www.ertrac.org*, 2016.

[6] information administration U.S. Energy. "Annual energy outlook". *https://www.eia.gov/outlooks/aeo/pdf/0383(2012).pdf*, 2012.

[7] Novella R. "Influencia de los ciclos Atkinson y Miller sobre el proceso de combstión y las emisones contaminantes de un motor diesel". *Editorial Reverté*, 2012.

Chapter 2

Literature review: mixing-controlled compression ignition engine

Contents

2.1 Introduction

The use of ICE engines allowed the industry and global transportation to become what it is nowadays. These engines have been modified for decades but

the core of the combustion concepts has been kept almost unmodified and most of the engines can be classified as compression ignition (CI) or spark ignition (SI). Spark ignition engines operate with a premixed mixture whose ignition is controlled by the spark timing. The mixture is usually stoichiometric to allow the use of cost-efficient after-treatment equipment. Since the mixture is stoichiometric, the load of the engine is controlled by the total mass flow. This type of combustion offers soot emission levels that are orders of magnitude lower than these of CI engines but suffer a reduction in efficiency compared to them. Additionally, they are forced to use low compression ratio (CR) to avoid knock and that produces low efficiency and cold start problems. CI engines usually work with higher compression ratios. They inject the fuel in the cylinder and the mixture autoignites due to the piston compression, this is, no spark is needed. Between the injection and the ignition of the fuel there is a really complex process where the fuel is evaporated and mixed with the in-cylinder flow. The speed of the combustion is controlled by this process. During the combustion the fuel mixes generating rich regions, where the soot is formed, and lean regions. In addition, the gas temperature during a CI engine combustion is usually really high, what promotes the formation of NOx. Both NOx and soot emissions are higher than in SI and have become the main drawback of these engines, therefore further research must be done in this topic [1]. On the contrary, CI engines are able to provide higher efficiency and lower fuel consumption than SI engines. The problems attached with CI emissions can be controlled by after-treatment, that is expensive and not used very often in the past in high-speed direct injection (HDSI) engines but has been used for years in MD and HD engines with impressive results. For that reason, as noted in Chapter 1, most of the off road transportation is equipped with CI engines, therefore it is compulsory to keep researching in this topic.

The NOx-soot trade-off is not easy to break in CI engines. Researchers have paid attention to this topic during the last decades and new advanced combustion concepts have been developed like premixed low temperature combustion (LTC) or mixing-controlled LTC. Both concepts follow the same strategy, to reduce NOx and soot emissions by lowering the combustion temperature.

Premixed LTC concept tries to lower the combustion temperature by extending the ignition delay period coupled with early injection timings so the mixture is almost homogeneous when the ignition occurs [2]. This strategy is able to simultaneously reduce soot and NOx emissions. The mixture is almost homogeneous, therefore there are no rich regions and the soot formation is drastically reduced. At the same time the in-cylinder temperature is more uniform, there are no local peak temperatures and due to the low global

equivalence ratio the flame temperature is lower, thus the NOx formation is sharply reduced. However, premixed LTC has some drawbacks that need further research. Premixed LTC engines usually lack of control on the ignition timing and combustion rate over a range of speeds and loads, specially at high loads where they also suffer from noise and higher NOx emissions. Additionally, LTC is really sensitive to the intake temperature and further research is needed in LTC cold start [3].

Mixing-controlled LTC follows the same objective than the premixed version, to reduce emissions though low temperature combustion. However, the objective is achieved with a different strategy. The main idea is to reduce the flame temperature by reducing the intake temperature, the nozzle hole diameter or the O_2 concentration. A reduction of the intake temperature directly reduces the in-cylinder temperature but the margin is really limited using this technique. The O_2 concentration is easily reduced by increasing the EGR rate and offers high flexibility, therefore high EGR rate and small nozzle hole diameter are usually used to achieve mixing-controlled LTC. The implementation of this LTC strategy worsens the mixing capacity of the in-cylinder gas resulting in a smoother heat release rate and a lower adiabatic flame temperature. As a result, the soot and NOx emissions are significantly reduced, however, the HC/CO emissions are increased and the engine efficiency worsened [4].

The LTC concepts have shown significant advantages over the conventional MCCI engines. However, at its current state, the advantages of these strategies do not compensate the lack of control at high loads for premixed LTC or the worsening of efficiency and HC/CO emissions for mixing-controlled LTC. For that reason, this Thesis and literature review will be focused on MCCI concepts for MD and HD engines, specially in optimization strategies used to improve them trying to achieve future emission standards with low fuel consumption.

2.2 MCCI combustion process

This section focuses on describing the main physical processes that occur in a combustion chamber of a MCCI engine. The main objective of this description is to introduce the main concepts that will be used in the section 2.3 and the rest of this Thesis. This section is structured in a first description of the main phases of a combustion process and a second part with a detailed explanation of the main phenomena that happen in each phase.

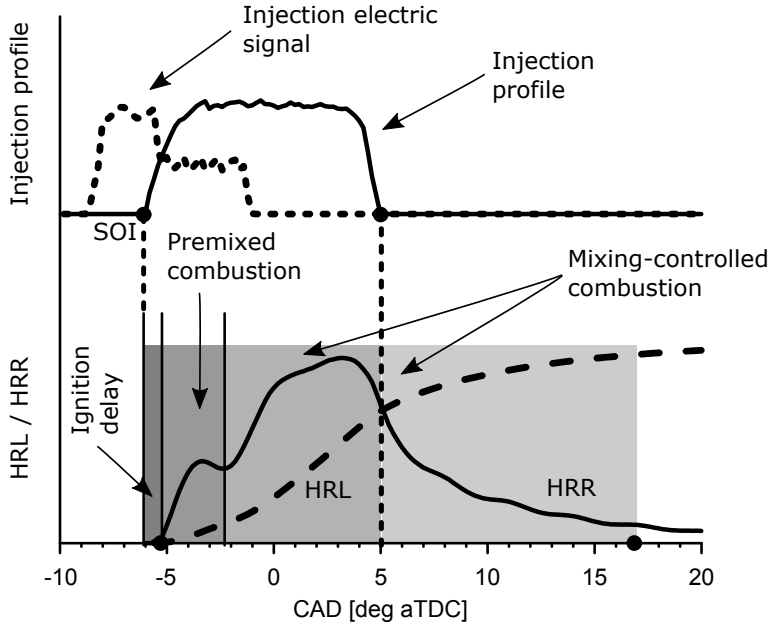

Figure 2.1. *Combustion process phases defined by the heat release rate and injection profile. Adapted from [7].*

2.2.1 Combustion process

The heat release rate (HRR) is one of the most important parameters used to describe a combustion process. It is calculated from the evolution of the in-cylinder pressure applying a zero-dimensional model based on the first law of thermodynamics [5]. Comparing the HRR and the fuel injection profile, it is possible to perform a chronological description of the phases that take place in a combustion process. Fig. 2.1 shows a comparison of a fuel injection profile and the related HRR, and the main phases can be distinguished [6]:

- **Ignition delay.** This phase occurs between the start of the injection and the start of the combustion process. When the fuel is injected in the combustion process, it mixes with the air due to several physical phenomena like the atomization of the liquid fuel, evaporation of the fuel and air entrainment. Since the in-cylinder mass contains oxygen, the mixture air-fuel is unstable and produces several low intensity chemical pre-reactions that end up with the autoignition of the mixture, generating a sudden increase in the heat release.

- **Premixed combustion.** Once the combustion process has started, the fuel mixed during the ignition delay phase is oxidized. This fuel is inside the inflammability limit but did not autoignite because it did not reach the autoignition condition. In this phase, the HRR shows a sharp increase until a maximum value that decreases until a local minimum. The duration of this phase is usually defined as the period between the start of the combustion and the first local minimum in HRR.
- **Mixing-controlled phase.** This phase starts when the fuel mixed during the ignition delay phase is completely burned. In this phase it is assumed that the heat is released at the same rate that the fuel and air are mixed. During the injection phase, the mixing process is controlled by the momentum introduced by the spray in the combustion chamber. In this phase, the flame reaches a quasi stationary state while the injection process continues. Once the fuel injection stops, it can be observed a reduction in HRR because of the absence of momentum introduced by the spray. Then the flame shows random shapes and the HRR reduces intensity until the process ends, usually during the expansion stroke.

The phases of the combustion process described above are further described in the following subsections ordered chronologically.

2.2.1.1 Ignition delay

After the start of the injection, during the ignition delay phase, several physical and chemical phenomena guide the process until the start of the ignition. That moment when the ignition starts has been related to the moment when an increase in pressure or temperature due to the combustion process is detected, or when the heat release rate starts to increase or when a visible flame due to the smoke oxidation process appears.

The first phenomena related to the start of ignition that can be detected is a weak emission related to a phenomena called chemiluminescence [8]. This phenomenon of chemiluminescence is not an isolated case and it has to be considered as a continuous process that can be studied in terms of time and space [9]. Then, a summary of the phenomena that happen during the continuous process of chemiluminescence is described below following the phases proposed by Higgins et al. [10].

- **Physical induction period.** This phase starts with the start of injection and lasts until a pressure increase or an emission related to

the chemiluminescence is detected. During this phase the fuel starts to penetrate the chamber following the physical processes of atomization, vaporization and air entrainment. It is the evaporation of the fuel what lowers the temperature of the mixture near the liquid fuel inhibiting the autoignition chemical reactions. As time goes by, the fuel penetration and air entrainment continues and at some point a certain region of the jet reaches the optimal conditions to develop the first ignition stage; however, the physical processes of evaporation and mixing keep being equally important.

- **First stage ignition period.** This phase exists between the first detected pressure increase or chemiluminescence emission until the beginning of the rapid heat release. In this phase the reactions develop on the downstream region of the jet in a rich region with equivalence ratios between 2 and 4 [11]. The origin of the chemiluminescence that appear in this phase is mainly due to the presence of formaldehyde (CH_2O) and radicals CH [12]. However, as temperature increase continues due to mixing and heat release, the dissociation reactions of intermediate products reduce the chain branching, explaining the reduction in heat release at the beginning of the next phase.

- **Second stage ignition/premixed-burn period.** This stage corresponds to the what we called premixed combustion phase so in this Thesis we will keep the classic structure described in section 2.2.1.

2.2.1.2 Premixed combustion

The premixed combustion has been extensively studied by different authors [8, 9] but only a brief summary will be presented in this Thesis. Firstly, the chemical reactions during the ignition delay phase produce a temperature increase in the region between the liquid length and the tip of the jet. In this region reacts all the fuel that has been mixed during the ignition delay phase and has the proper conditions to be inflammable. This generates a sharp increase in temperature and pressure as shown in Fig. 2.1. The premixed combustion is mainly controlled by the injection profile, injection rate and ignition delay [13], and is fast compared to the combustion controlled by the diffusion phenomena.

In terms of pollutants formation, it is important to consider the location of the premixed combustion and the equivalence ratio of that region. Smoke and NOx emissions depend mainly on two variables, the local equivalence ratio

and temperature of the zone. The premixed combustion happens in the region between the tip of the jet and the lift-off, if the fuel injection continues after the premixed phase. This region presents high equivalence ratios with values between 2 and 4 [14].

Under those conditions, the premixed combustion is too rich to produce significant amounts of NO and therefore NOx [15]. However, for operating conditions where the ignition delay is long enough, there are regions where the mixture has low equivalence ratios and can generate significant amounts of NO [16]. In terms of Smoke, the premixed combustion region presents high equivalence ratios. This promotes the formation of small soot particles that covers the whole region. The soot starts forming when the maximum heat release rate is reached because it is needed some time to increase the temperature and reduce the oxygen to match the conditions that the soot reaction mechanisms require.

2.2.1.3 Mixing-controlled phase

Finally the process enters the phase called mixing-controlled combustion that extends until the injected fuel is burned. During this phase, the flame front generated in previous phases is consolidated and fed by the convective and diffusive contribution of the fuel and oxygen. The convective input from the fuel is crucial because it acts like the engine that moves the mixing process by the momentum introduced with the jet. Therefore, at the end of the injection there is one last important change in the structure of the flame and the process is then dominated by the diffusion between the oxygen and the fuel. Some authors [17] even consider this last phase as an independent phase and call it "late combustion phase". This section is going to be focused on the phenomena that happen until the end of the injection.

The most extended model about the flame generated at the beginning of the mixing-controlled phase is the model from Dec [14] that was then extended by Flynn et al. [18], that is shown in Fig. 2.2.

According to this model, there is a first zone between the injector nozzle hole and the position where the diffusive flame starts, which is called Zone I. In this zone the physical phenomena atomization, air entrainment and evaporation happen similar than in a non reactive and evaporative jet. However, this processes are influenced by the presence of a diffusive flame downstream Zone I. The length of this zone is known as lift-off. After the lift-off (Zone II), the jet faces reactive conditions and downstream the lift-off there is a premixed reaction zone that consumes all the oxygen mixed

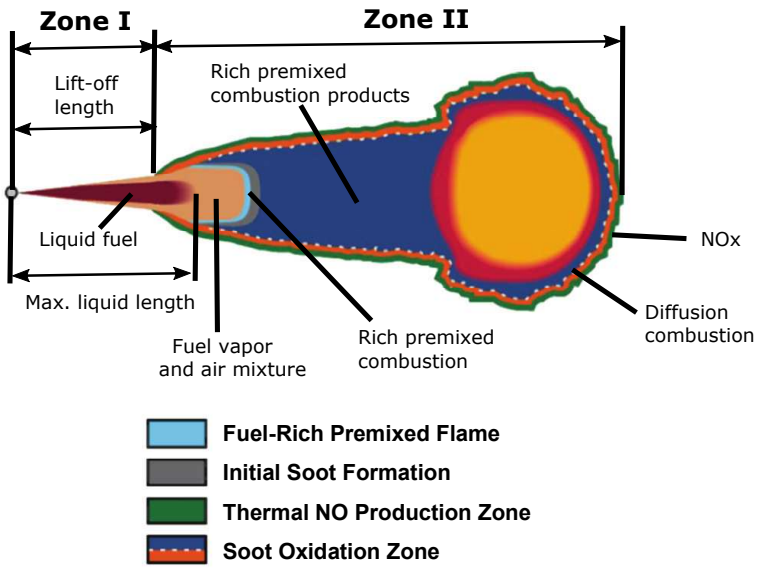

Figure 2.2. *Diffusive flame structure during the quasi stationary phase according to the conceptual model proposed by Dec. Adapted from [18].*

with the jet during Zone I [19]. As a consequence it can be assumed that inside the diffusive flame there is no oxygen concentration. The products from this premixed combustion are generated in a rich region and contain partially oxidized hydrocarbons that will act as precursors for soot formation.

After the premixed combustion region, the flame adopts a structure of a diffusive flame. The basic structure is an internal zone composed by the partially oxidized unburned fuel and the soot. This region is surrounded by the reaction surface where the fuel is oxidized to CO_2 and water. Even though the formation of soot precursors depend mainly on the conditions of the premixed reaction, the formation and growth of the soot particles is produced in the internal zone of the diffusive flame. Moreover, as seen in Fig. 2.3, the soot proportion reaches its maximum at the low velocity vortex that is produced at the front part of the flame, where both the soot formation and growth are enhanced. When the soot finally reaches the reaction zone, it is almost completely oxidized by the effect of OH radicals generated in the diffusion flame. In terms of NO formation, the species NO is mainly formed in the external zone of the diffusion combustion, where the conditions of high temperature and high presence of oxygen are met [15]. However, in the

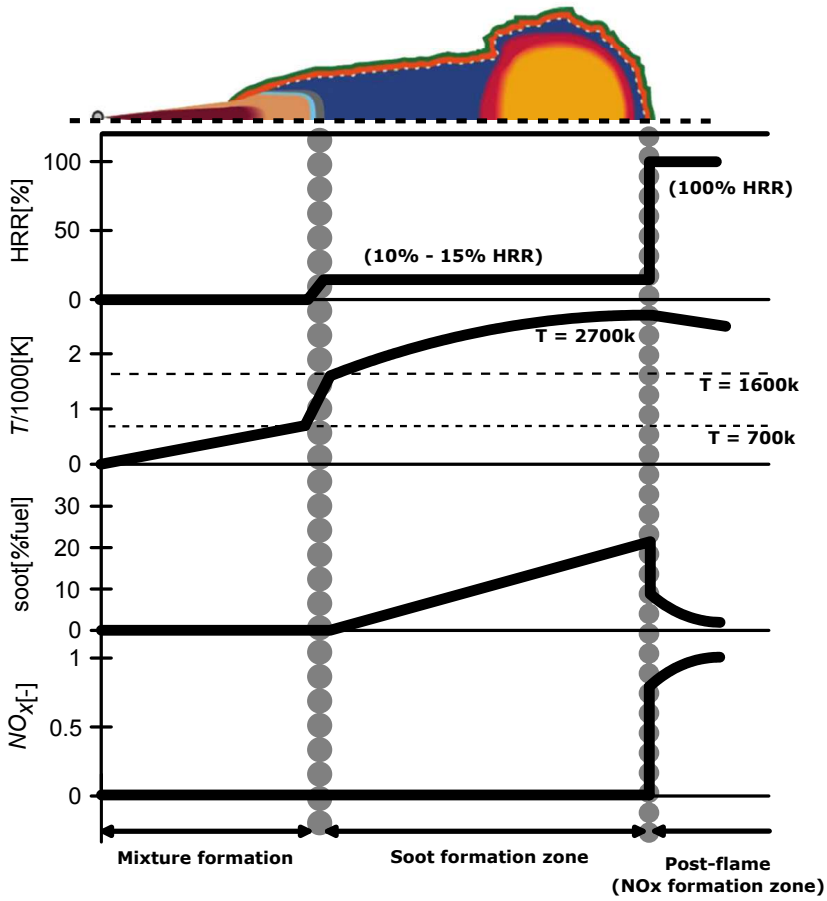

Figure 2.3. *Diffusive flame structure during the quasi stationary phase according to the conceptual model proposed by Dec. Adapted from [20].*

internal zone of the flame there is no presence of the necessary oxygen to form NO.

This conceptual model can be extended with a qualitative description of the temporal-spatial evolution of a fuel mass that passes and evolves through the different zones. Fig. 2.3 represents that temporal-spatial evolution adapted from Molina [20].

The injected fuel mass is first atomized and mixed with the high temperature air that finds in the combustion chamber. As a consequence, the liquid fuel temperature increases and is evaporated progressively until

the liquid phase completely dissapears. The fuel mass keeps mixing with the air and advancing until reaching the premixed reaction zone when the temperature has increased to 700 K and the average equivalence ratio is rich, about 4. While advancing through the premixed reaction zone the 10% - 15% of the fuel energy is released increasing its temperature to 1600 K. During this premixed combustion the oxygen concentration is too low to form NO but the conditions are suitable to form soot precursors.

Then, the fuel keeps advancing and reaches the diffusive flame zone. In this first region there is no oxygen input because it is consumed in the outer region where the reactive zone of the diffusion combustion zone is located. Since there is no oxygen, there is no significant heat release in the internal zone of the flame. While advancing towards the reactive zone of the flame, the temperature of the fuel mass keeps increasing and the soot particles grow until reaching its maximum at the flame front. Finally, the fuel mass passes through the reaction zone that is a thin surface where the equivalence ratio is stoichiometric and the temperatures are close to the adiabatic flame temperature. In this surface, the mass is burned with the oxygen added by diffusion, releasing the rest of the remaining energy (85% - 90%) in the fuel.

While in the flame front, the soot concentration is reduced to near zero, the NO formation rate is significantly increased in the outer part of the diffusion flame. Then, the combustion products are mixed with the rest of gases in the combustion chamber.

2.3 Optimization strategies for MCCI

The combustion process is the most important stage of the cycle of a MCCI engine, it is the moment when the fuel is converted into heat. For that reason a lot of research has been done around this topic and many strategies and subsystems have been developed aiming to improve that combustion efficiency and emissions. These strategies have been classified in 5 groups for this Thesis, geometry of the combustion chamber, air management, injection settings, after-treatment or alternative fuels. These strategies are well known and allow the current MCCI engines to provide high efficiency with emission levels under the emission standards.

2.3.1 Strategies based on geometric parameters

The main strategies based on geometric parameters used for engine design are the geometry of the combustion chamber shape, the spray angle and CR.

These type of strategies are usually costly to test experimentally because any hardware modification requires the manufacture of new components. However, until the CFD's birth, any geometric optimization and test was done experimentally. Nowadays there are still hardware optimization studies performed experimentally that offer very interesting results but the amount of different combustion chamber or injection geometries tested is limited due to related costs [21, 22].

The CR is the ratio between the maximum volume (volume at BDC) and the minimum volume of the combustion chamber (volume at TDC). Nowadays the CR is used as a design variable due to its influence over the engine efficiency and pollutant emissions. Theoretically, increasing the compression (or expansion) ratio increases the thermal efficiency of the engine [23], however, there are some drawbacks that limit the maximum CR of the current engines:

- **Peak pressure (PP).** An increase in CR keeping the same heat released results in an increase in compression pressure and PP. This increment in pressure increases the noise and, when it is too high, can overcome the mechanical PP limit of the engine.
- **NOx emissions.** A high CR not only improves efficiency but also increases the NOx emissions due to higher in-cylinder temperature. In some cases, the NOx increase is significant and further engine adjustments are required to keep the NOx emissions under control [24].
- **Surface/volume ratio.** The surface/volume ratio increases for higher CR, what increases the heat losses on the piston and cylinder head [25].

When the first ICE were born, the values of the CR were related to the type of combustion, in SI the value should be low enough to avoid autoignition and in CI should be high enough to let the autoignition happen [26]. Nowadays, in order to control pollutant emissions and PP, CR is becoming lower. However, the CR has a key roll in the CI engine cold start, specially in extreme low temperatures (i.e. -20 °C), therefore low CR applications are currently being studied [27].

The shape of the combustion chamber in a CI engine is also one of the most important and discussed topics because it plays an important role in generating the gas motion in the cylinder. It is really difficult to obtain general conclusions about the effect of the geometry on a combustion system because the combustion chamber geometry interacts with the in-cylinder flow

and spray, therefore, the design rules are usually case specific. However, there are four main criteria followed when designing a new combustion chamber [24]:

- **Improve mixing.** The combustion chamber is the container where all the fuel/air admission, mixing and combustion occurs. Therefore the swirl, injector and combustion chamber shape are the main tools that control the mixing process so a well design chamber can improve the in-cylinder turbulent level resulting in a better mixing process, faster combustion and higher efficiency.
- **Reduce pollutant emissions.** Following the previous point, the combustion chamber has a significant effect over the mixing process of the combustion. This means that it has an indirect effect over the combustion speed, temperature and equivalence ratio distribution resulting in a noticeable influence over the pollutant formation.
- **Reduce surface/volume ratio.** The main reason behind reducing the surface/volume ratio is to reduce the heat losses. Heat losses are energy directly taken from the in-cylinder fluid during the expansion stroke that is transferred to the environment as heat, thus a reduction in heat losses becomes a direct reduction of the engine losses and an efficiency improvement. In MCCI engines the losses generated by heat transfer (HT) represents between 16% and 35% of the total injected energy [17], therefore, a surface reduction would result in a significant efficiency improvement, even overcoming some mixing worsening in certain cases.
- **Improve volumetric efficiency.** The size and shape of the piston and cylinder head affects the valves design, which directly affects the cylinder filling process and the volumetric efficiency [26]. The volumetric efficiency is the main parameter to characterize the cylinder filling process and is defined as the ratio between the mass flow rate of the engine and the maximum mass flow rate that the engine would have at the considered reference conditions. Higher volumetric efficiency provides higher power density, therefore high volumetric efficiency is required.

In the course of the history many piston bowl geometries have been developed, however, nowadays most of the conventional CI engines can be included in any of these 3 types of geometries (see Fig. 2.4).

Fig. 2.4 (top) represents a reentrant piston shape. This type of geometry is considered an improvement for soot emissions allowing higher EGR levels

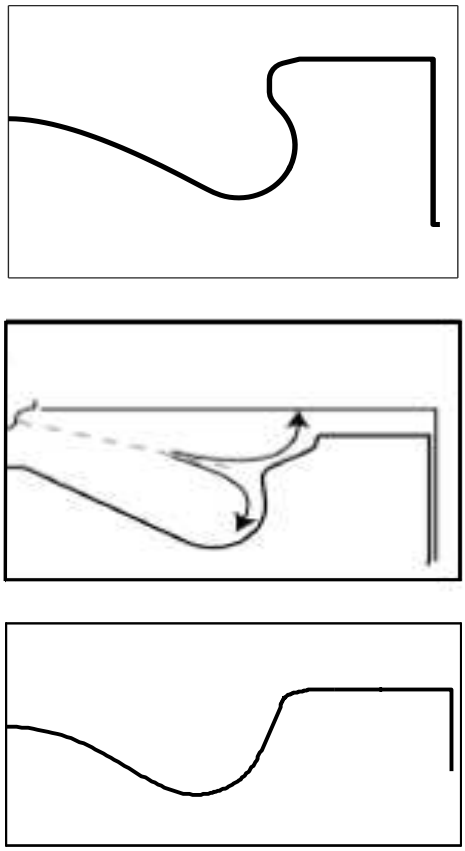

Figure 2.4. *CI engine piston bowl geometries. Adapted from [28].*

to further control NOx emissions [24]. The fuel spray usually interacts with the lower lip shape affecting the overall in-cylinder fluid motion resulting in a impact over the efficiency and pollutant emissions [29]. Fig. 2.4 (middle) represents a stepped-lip bowl geometry. These type of bowls are mainly designed to reduce soot-in-oil. By redirecting the spray towards the head of the engine, the spray penetration in the squish region is reduced and the soot formed during the combustion is separated from the cylinder walls, directly reducing the soot-in-oil [30]. Additionally, stepped bowls are expected to reduce heat losses through the liner and the piston bowl due to surface/volume ratio reduction. Finally, Fig. 2.4 (bottom) represents a bathtub shape. This

geometry is focused on reducing the surface area to reduce the HT losses and improve engine efficiency and fuel consumption. Even though this type of shapes are penalized in terms of emissions compared to the other two shapes, they still manage to keep the emissions under the current standards while offering higher efficiency [31].

Finally, the included nozzle angle (NA) or spray angle is the design parameter that controls the angle between two opposite sprays. The optimal value of the spray angle strongly depends on the combustion chamber geometry since for a certain geometry the NA would determine the air/fuel, geometry/fuel and spray/spray interaction. Accordingly, an absolute optimum of nozzle angle exists for every combustion chamber design that usually is able to simultaneously improve efficiency and emissions [32, 33].

2.3.2 Strategies based on air management parameters

The main air management strategies are based on air intake pressure, swirl and exhaust gas recirculation (EGR). This type of parameters are used to control the quality, quantity and velocity of the air admitted in the engine. Due to the engine evolution and the introduction of electronic devices, the current engines have different air intake pressure, swirl and EGR for each operating point aiming to provide maximum efficiency and low emissions for every operating condition. This is possible because, contrary to the hardware related parameters, the air management settings are easily modified and can be optimized for different environmental and operating conditions.

The swirl is defined as the rotational motion of the air around the cylinder axis. It is generated due to the initial momentum of the admission air created by the intake ports. The intensity of the rotational motion is defined by the ports and piston geometry. After the valve closing, the swirl level during the compression and expansion strokes is only controlled by the piston geometry and the losses due to friction [26]. The swirl level has a noticeable effect over the combustion process, higher swirl improves the air/fuel mixing and facilitates the available oxygen usage which allows to provide higher efficiency and lower soot emissions [33]. In addition, higher swirl levels imply higher in-cylinder air velocities resulting in higher convective HT coefficient and higher heat losses [34], and can reduce the sprays penetration if the swirl level is too high resulting in a degradation in air utilization [24].

The air intake pressure is defined as the pressure of the fresh air introduced in the cylinder through the intake port. In current engines the intake pressure is higher than the external environment pressure, therefore a turbocharger

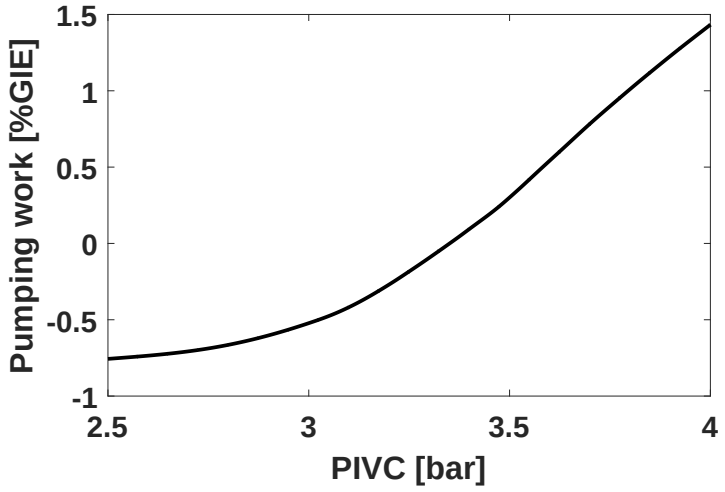

Figure 2.5. *Pumping work required for each PIVC value.*

system is needed to accomplish the desired intake pressure values. An increase in air intake pressure generates an increase in in-cylinder density and O_2 mass that enhances the air/fuel mixing. This results in higher in-cylinder PP, increased NOx emissions and improved soot levels [35]. In terms of engine efficiency, the indicated efficiency improves but the effect on the brake specific fuel consumption (BSFC) is case specific. Higher air intake pressure implies higher pumping work (see Fig. 2.5, note that pressure at intake valve closing (PIVC) is presented instead of air intake pressure), therefore, the increase in indicated efficiency has to compensate the increase in pumping work, which strongly depends on the turbo system efficiency and operating condition.

The EGR is the most common technique used in current MCCI engines to control the NOx emissions. It consists on recirculating a portion of the engine exhaust gases to the engine admission. EGR is defined as the ratio between the gas mass coming from the recirculation and the total in-cylinder mass, see equation 2.1.

$$EGR = \frac{m_{EGR}}{m_{EGR} + m_{air}} \tag{2.1}$$

This process adds inert substances to the cylinder that displaces a portion of the intake oxygen and increases the heat capacity of the mixture [36]. This results in a reduction of combustion rate, instant temperature and peak

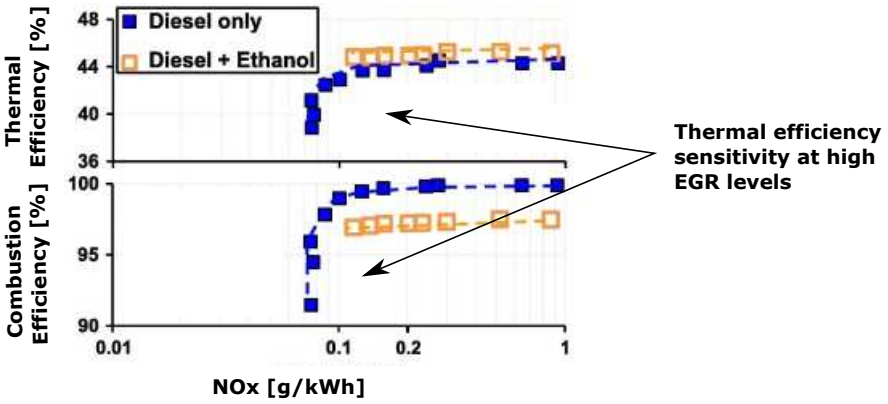

Figure 2.6. *Engine efficiency and NOx emissions trade-off for increasing EGR levels. Adapted from [28].*

temperature, which is considered the main reason behind the NOx reduction [37]. However, increasing EGR not only affects NOx emissions but also tend to increase soot, HC, CO emissions and reduce the engine efficiency [38]. The effect of the EGR over the NOx emission is more relevant than the effect over the efficiency for low EGR levels, however, for high EGR levels the combustion efficiency starts to decrease exponentially. Fig. 2.6 shows the NOx emissions and combustion efficiency trends for increasing EGR levels and at some point the NOx levels become unchanged while the combustion efficiency drops drastically.

2.3.3 Strategies based on injection parameters

In MCCI engines, the mixing and combustion processes are strictly related because they happen simultaneously; accordingly, the fuel injection law has a significant impact on the engine performance. The design strategies based on injection parameters aim to improve that injection law modifying the injection profile and timing [26]. The main parameters are injection pressure (IP), start of injection (SOI) and nozzle hole diameter (Dnoz).

The IP is the pressure of the fuel when it is injected in the cylinder. It is known that higher IP offers many advantages to DI engines but there has always been limitations in the maximum IP offered by the available injectors. That limitation has been overcome over the years, specially after 1967 when

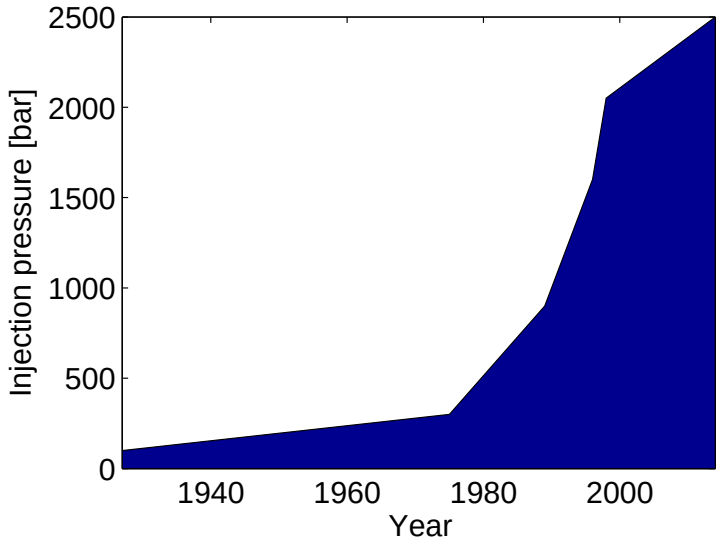

Figure 2.7. *Evolution of IP since 1930. Adapted from [40].*

Bosch introduced the first mass-produced electronic injector that allowed faster and more accurate injections [39]. Nowadays, the modern common-rail systems offer up to 2500 bar of IP.

Higher IP improves the fuel atomization and evaporation, this is, improves the mixing process, shortens the ignition delay and shortens the combustion duration [35]. As a result, the engine efficiency and emissions are strongly affected by IP variations. Higher IP improves the engine efficiency and soot emissions, however, it also has a negative effect over the NOx emissions that is usually very significant and has to be controlled by other means [41].

The second parameter that, for a given fuel mass and nozzle hole number, defines the shape of the injection profile is Dnoz. At constant IP, Dnoz defines the nozzle flow capacity, thus defines the injection duration. In addition, lower Dnoz not only reduces the nozzle flow capacity but it also influences how the fuel spray interacts with the piston bowl geometry and the flow [24], resulting in an improvement in fuel consumption and an increase in NOx emissions [42].

Finally, SOI or injection timing is defined as the crank angle at which the fuel starts to be injected in the cylinder. Advancing SOI leads to longer ignition delays, this is, the time gap between the fuel injection and the fuel burn increases and that promotes premixed combustion. This results in higher

peak heat release rate (HRR), therefore higher PP [43]. In addition, in-cylinder temperature increases for advanced SOI, thus NOx emissions increase significantly. Finally, the soot emissions are also affected, advanced SOI results in lower soot emissions [44].

2.3.4 Strategies based on after-treatment

The increasingly stringent emission standards (i.e. US2030 or EURO VI) become a real challenge for new generation engines. The already presented techniques are not enough to fulfill the requirements because the current engines are already optimized in terms of injection/air management settings and new strategies have to be applied to control emissions. The after-treatment strategies, contrary to the previously presented strategies, do not modify the combustion process because they treat the exhaust gas in order to achieve lower emission levels. This kind of strategies are used in HD engines but they were not very common in small vehicles due to the high cost involved, however, due to the new emission standards, the after-treatment equipments are becoming more and more common. Specially in CI engines, soot emissions are difficult to control and most vehicles wear a Diesel Particulate Filter (DPF). In addition, other after-treatment techniques are used to limit the NOx emissions like Urea Selective Catalytic Reduction (SCR), Lean NOx Trap (LNT) or Three Way Catalyst (TWC).

The DPF is the most commonly used after-treatment technique in CI engines to meet the soot emission standards. It is composed of a porous substrate wall-flow where the diesel particulates are deposited, specially the solid particles. The DPF has been developed since 1970 and now can offer a soot reduction efficiency of nearly 95%. In addition, certain DPF also reduce CO emissions with 50%-90% efficiency and HC emissions with 85%-95% efficiency. However, these filters often produce an engine efficiency degradation when the accumulation of particulates becomes significant and creates a back pressure that increases pumping loses, worsens the combustion process and increases the fuel consumption. For that reason, the engines that are equipped with DPF have to regenerate the filter by oxidizing the trapped particles [45, 46].

The LNT is a widely used technique to control NOx emissions. This method reduces the pollutants in 2 cycles, a lean and a rich cycle. During the lean cycle, the NOx is stored, then, once the capacity of the absorber is overcome, the stored NOx is released and reduced to N_2 during the rich cycle [47]. LNT systems offer up to 90% NOx reduction efficiency [48] but

they struggle to reach the high NOx conversion efficiencies required to meet current and future regulations over the wide range of conditions experienced during engine operation [49]. Additionally, LNT systems often increase fuel consumption due to periodic rich operation required for regeneration.

Urea SCR is a direct competitor of LNT as a NOx reducer, it injects urea that is transformed into NH_3 and then reacts with the exhaust gases to transform NOx into nitrogen [47]. They were introduced in the market in 2003 with a modest 75% NOx conversion efficiency, since then it has been developed to have much higher NOx conversion efficiency [50] (conversion efficiencies can be in the range of 90% to 95%); however, diesel exhaust fluid (DEF) dosing required for NOx reduction may increase the overall operational cost compared to a non-SCR equipped engine. Additionally, SCR systems struggle to achieve high NOx conversion efficiencies at temperatures below 200 °C due to deposit formation from DEF dosing [51] and poor catalyst activity [52]. Currently, SCR equipped HD CI engines are capable of meeting current regulated NOx emissions limits on the order of 0.268 g/kWh. However, the California Air Resources Board (CARB) has proposed future NOx targets of 0.0268 g/kWh [53]. Reaching this level of tailpipe NOx with a urea SCR or LNT system will likely be challenging. That is, NOx conversion efficiencies would need to be on the order of 99%.

An alternative approach to enable low NOx emissions is the use of stoichiometric operation coupled with a TWC. The TWC is a widely used technique, is low cost, and can simultaneously reduce CO and HC while reaching NOx reductions over 99% [54]. It is based on a 2 stage conversion, a first stage where a reduction catalyst transforms NOx into N_2 and O_2 and a second stage where a oxidation catalyst converts CO and HC into CO_2 and H_2O. The drawback is that, because stoichiometric operation is required, its use with fueled CI engines results in extremely high soot emissions [55–57]; however, further research has been done with near-stoichiometric CI combustion combining DPF and TWC with very encouraging results [58].

2.3.5 Strategies based on alternative fuels

Compression ignition engines have been developed for decades and its performance, efficiency and emission levels have been improved to levels that were not even dreamed when the first CI engine was produced. Thanks to the optimization strategies presented in this chapter, CI engines fueled with diesel are able to meet the current emission standards and still manage to be extremely efficient. However, pollutant standards keep being more a more

restrictive at a fast rate and the CI engine improvement is not able to follow the same rate just with the already presented strategies. A new path that is being followed is the use of new fuels with improved characteristics that are able to offer similar performance and efficiency but with unique characteristics to overcome the emission issues of the diesel fuel. Diesel fuel offers high efficiencies but can not avoid the NOx-soot trade-off, which is the main reason behind its pollutant level problems.

An alternative that has been considered is the use of biodiesels. Biodiesels are fuels obtained from vegetable oils or animal fat, they are non-toxic, renewable, have combustion properties similar to the conventional diesel and reduces most of the pollutant emissions (except NOx). Additionally, biodiesels are easily obtainable and that would permit the energy independence from diesel fuels. However, there are a number of reasons why the biodiesels have not substituted the conventional diesel. Biodiesel deteriorate some component of the injector, what forces to modify the injection system, it is oxidized when in contact with the environment, has lower heating value and generates higher NOx emissions. On top of that, biodiesels are more expensive than fossil fuels [59].

An improved alternative for diesel and biodiesel is a new oxygenated fuel similar to diesel. Dimethyl ether (DME) is a liquefied gas with good thermal and chemical properties which is considered an excellent substitute for conventional diesel and liquefied petroleum gas (LPG) fuels [60, 61]. DME can be produced from crude oil or residual oil but also from other sources such as natural gas, coal or waste products [62].

DME is a colorless, non-toxic, highly flammable gas under ambient conditions with physical properties similar to those of LPG, high cetane number (55-60) and good evaporation characteristics in the combustion chamber; therefore, it is a suitable fuel for MCCI engines. DME is the simplest ether with the chemical formula CH3-O-CH3, gaseous at room temperature that becomes liquid at 6 atm or -25°C and less viscous and lubricating than diesel fuel. This means that it has to be liquefied in the storage and some additives are needed to improve the viscosity and lubricity such as Lubrizol, biodiesel or other hydrocarbon fuels [62–65].

The combustion properties of DME are quite comparable to those of diesel fuel. The lower heating value of DME (28.8 kJ/kg) is less than that of diesel fuel (42.5 kJ/kg). Accordingly, the amount of fuel injected has to be increased leading to longer injection durations. However, the stoichiometric air/fuel ratio of the DME is 8.99 kg-air/kg-DME while that of diesel fuel is equal to 14.6 kg-air/kg-diesel, what means that, for a given mass of fuel, DME combustion

needs less air than diesel fuel. After combining the differences in lower heating value and stoichiometric air/fuel ratio, around 10% less air is required by DME at iso-injected energy conditions, resulting in a positive impact on pumping losses. In addition, the ignition delay of DME was observed to be shorter than that of diesel due to the difference in cetane number, its better evaporation characteristics, and its oxygenated chemical structure [66].

Controlling emission levels below the current standards is one of the main research challenges in the field of ICE for road and rail transport applications. Due to the increasingly stringent emissions regulations, current engines are often operated away from the peak efficiency point to control NOx emissions. This often results in an increase in soot or particulate matter (PM) emissions, requiring the addition of post-treatment of both NOx and soot. A primary benefit of the use of DME is its non-sooting nature [67]. Soot precursors do not form easily during DME combustion because the oxygen content of DME is 34.8% and there are no direct carbon-to-carbon bonds [68, 69]. As a result, DME combustion has almost zero-soot emission characteristics, however, very small soot emissions are detected due to the additives used to improve lubrication [70, 71]. Regarding NOx emissions, due to DME chemical properties, its adiabatic flame temperature is lower compared to that of diesel, which is reflected in lower NOx emissions [61]. However, there is controversy about this topic in the literature since some studies using DME in compression ignition engines reported an increase in NOx emissions compared to the reference levels using diesel in the same operating conditions, while the opposite trend is also found [63]. These opposite trends arise from the differences in how the experimental activities have been carried out since NOx emissions are strongly dependent on engine architecture and settings. Nevertheless, this increase in NOx can be easily controlled with state-of-the-art strategies such as EGR. This technique has some drawbacks operating with diesel, such as the increase in soot emissions, but there are no significant problems using DME as fuel because it avoids soot formation even operating with high equivalence ratio and low oxygen concentration. In terms of combustion efficiency, higher EGR value extends combustion duration but the combustion efficiency is weakly affected until EGR levels over 30% where the effect starts to be more noticeable [72]. Therefore, DME is extremely compatible with EGR to control simultaneously NOx and soot emissions [73].

HC emissions are usually lower with DME than with diesel [74, 75]. The most relevant sources of HC emissions are the liquid wall impingement onto the combustion chamber walls together with the over-lean and the over-rich mixtures remaining along the combustion process. DME evaporates faster than diesel, so the liquid wall impingement onto the combustion chamber

walls is largely reduced. The shorter ignition delay of DME decreases the presence of over-lean mixtures before the onset of combustion. DME's low stoichiometric air/fuel ratio is also favorable to avoid over-rich mixtures along the combustion. CO emissions are also an output of an incomplete combustion, located where fuel concentration is too lean or too rich [17]. Then, the same reasons previously discussed, particularly the reduction of the over-lean and over-rich mixtures along the combustion, explain the benefits of DME in terms of CO emissions compared to diesel combustion [76].

2.4 Summary and conclusions

In this chapter, a review of the main optimization strategies used to improve efficiency and emission levels in MCCI engines was discussed in detail. In addition, advanced combustion concepts were presented as alternatives for the conventional MCCI concept. However, even though they offer many advantages over the conventional MCCI, they have to be further developed to be able to compete with MCCI engines in on-road situations. For that reason the literature review and the main work in this Thesis was focused on optimizing MCCI engines using the strategies presented in this chapter.

Geometry, injection and air management based strategies modify the combustion process itself. They modify the mixing process, HT or burning rate resulting in efficiency and emission levels variations. These strategies were born with the increasing engine flexibility and the addition of engine subsystems but they are struggling to reach future emission levels standards and extra strategies are needed for future generation engines.

Nowadays, after-treatment systems are widely used to complement the geometry, injection and air management based strategies. They do not affect the combustion process but they treat the exhaust gases aiming to control the emission levels, which are usually too high in the exhaust flow and do not satisfy the emission standards. The DPF is the main after-treatment used to control soot emissions, it is necessary and affordable, therefore most of the MCCI engines use it. The SCR is the equivalent for NOx emissions, however, it is expensive and requires reductants, therefore it is usually only used in MD and HD duty engines. Finally, the TWC is presented as a good option to simultaneously control NOx, CO and HC but working in stoichiometric conditions has proven to be a difficult task with MCCI engines fueled with diesel.

The previously discussed strategies allowed to improve MCCI engines for decades but they are no longer enough to achieve future emission standards. A

new path that is followed is the use of new fuels with improved characteristics that are able to offer similar performance and efficiency but with unique characteristics to overcome the emission issues of the diesel fuel. Biodiesels have been extensively studied but they produce higher NOx emissions, lower efficiency and are more expensive. DME is an improved alternative for diesel and biodiesel. It has similar combustion properties than that of diesel and offers lower NOx and HC, no soot emissions, lower pumping losses and higher efficiency. In addition it is extremely easy to obtain from different sources.

From the detailed analysis performed, it can be highlighted that MCCI engines have many tools to keep improving and offering high efficiency and low emissions standards. Therefore a conventional combustion system will be optimized aiming to find the maximum potential that they can offer and find if they are able to satisfy future emission levels. Additionally, new fuels clearly offer advantages that are not reachable by conventional diesel fuels, even after an optimization with the already mentioned strategies, like the non-sooting nature of the DME. For that reason the study will be extended to MCCI engines fueled with DME. It does not only offer better properties than diesel, but those properties permit stoichiometric combustion conditions with non-soot emissions, therefore a TWC can be used to reduce NOx, CO and HC. However, these differences between DME and diesel fuels in terms of combustion and emissions imply that it is likely that the optimum combustion chamber for a DME fueled engine would be different from the combustion chamber optimized for a diesel fueled engine. The design of the combustion chamber geometry of MCCI engines has a significant impact on the combustion process and it is nowadays critical to control pollutant emissions keeping competitive efficiency levels (as seen in previous sections). Thus, an extreme optimization of the combustion chamber and the injection nozzle designs coupled with a set of the most relevant air management and injection settings would be critical for designing a combustion system fueled with DME [77].

More engine flexibility has also a drawback, it is harder to optimize all the subsystems simultaneously. For that reason, the next chapter will be focused on optimization methodologies and tools that can be used for that purpose. It provides information about evolutionary and non-evolutionary algorithms together with information about the CFD software that will be used in this Thesis.

References

[1] Yao M., Zheng Z. and Liu H. "Progress and recent trends in homogeneous charge compression ignition (HCCI) engines". *Progress in Energy and Combustion Science*, Vol. 35 n^o 5, pp. 398–437, 2009.

[2] Han S., Kim J. and Bae C. "Effect of air-fuel mixing quality on characteristics of conventional and low temperature diesel combustion". *Applied Energy*, Vol. 119, pp. 454–466, 2014.

[3] Agarwal A.K., Singh A.P. and Maurya R.K. "Evolution, challenges and path forward for low temperature combustion engines". *Progress in Energy and Combustion Science*, Vol. 61, pp. 1–56, 2017.

[4] Benajes J., Molina S., Novella R. and Belarte E. "Evaluation of massive exhaust gas recirculation and Miller cycle strategies for mixing-controlled low temperature combustion in a heavy duty diesel engine". *Energy*, Vol. 71, pp. 355–366, 2014.

[5] Armas O. "Diagnostico experimental del proceso de combustion en motores Diesel de inyeccion directa". *PhD Thesis*, 1998.

[6] C.F. Taylor. "The Internal Combustion Engine in Theory and Practice". *The MIT Press*, Vol. 2, 1985.

[7] Novella R. "Influencia de los ciclos Atkinson y Miller sobre el proceso de combstión y las emisones contaminantes de un motor diesel". *Editorial Reverté*, 2012.

[8] Dec J.E. and Espey C. "Ignition adn early soot formation in a D.I. diesel engine using multiple 2-D imaging diagnostics". *SAE Paper*, Vol. 24 n^o 950456, 1995.

[9] Dec J.E. and Espey C. "Chemiluminescence imaging of autoignition in a DI diesel engine". *SAE Paper*, n^o 982685, 1998.

[10] Higgins B, Siebers D and Aradi A. "Diesel spray ignition and premixed-burn behavior". *SAE paper*, 2000.

[11] Bruneaux G. "Study of the correlation between mixing and auto-ignition processes in high pressure Diesel jets". *SAE Paper*, n^o 2007-01-0650, 2007.

[12] Kosaka H., Drewes V.H., Catalfamo L., Aradi A.A., Iida N. and Kamimoto T. "Two-dimensional imaging of formadehyde formed during the ignition process of a diesel fuel spray". *SAE Paper*, n^o 2000-01-0236, 2000.

[13] Plee S.L. and Ahmad T. "Relative roles of premixed and diffusion burning in DIisel combustion". *SAE Paper*, n^o 831733, 1983.

[14] Dec J.E. "A conceptual model of DI diesel combustion based on laser-sheet imaging". *SAE Paper*, n^o 970873, 1997.

[15] Dec J.E. and R.E. Canaan. "PLIF imaging of NO formation in a DI diesel engine". *SAE Paper*, n^o 980147.

[16] Musculus M.P.B. "On the correlation between NOx emissions and the diesel premixed burn". *SAE Paper*, n^o 2004-01-1401, 2004.

[17] Heywood J.B. "Internal combustion engine fundamentals". *McGraw Hill Inc.*, 1988.

[18] Flynn P.F., Durrett R.P., Hunter G.L., zur Loye A.O., Akinyemi O.C. and Dec J.E. "Diesel combustion: An integrated view combining laser diagnostics, chemical kinetics and empirical validation". *SAE Paper*, n^o 1999-01-0509, 1999.

[19] Idicheria C.A. and Pickett L.M. "Formaldehyde visualization near lift-off location in a Diesel jet". *SAE Paper*, n^o 2006-01-3434, 2006.

[20] Molina S.A. "Influencia de los parametrod de inyeccion y la recirculacion de gases de escape sobre el proceso de combustion en un motor diesel". *PhD Thesis*, 2003.

[21] Choi S, Shin SH, Lee J, Min K and Choi H. "The effects of the combustion chamber geometry and a double-row nozzle on the diesel engine emissions". *Proceedings of the Institution of Mechanical Engineers, Part D: Journal of Automobile Engineering*, Vol. 229 n^o 5, pp. 590–598, 2015.

[22] Benajes J, Pastor JV, GarcÃa A and Monsalve-Serrano J. "An experimental investigation on the influence of piston bowl geometry on RCCI performance and emissions in a heavy-duty engine". *Energy Conversion and Management*, Vol. 103, pp. 1019–1030, 2015.

[23] Reddy A., Pratap N, Kolluri R.V., Priyedarshi A. and Singh S.N. "Effect Of Compression Ratio On The Performance Of Diesel Engine At Different Loads". *International Journal of Engineering Research and Applications*, Vol. 5, 2015.

[24] Miles P.C. and Andersson O. "A review of design considerations for light-duty diesel combustion systems". *International Journal of Engine Research*, Vol. 17 n^o 1, pp. 6–15, 2016.

[25] Funayama Y., Nakajima H. and Shimokawa K. "A Study on the Effects of a Higher Compression Ratio in the Combustion Chamber on Diesel Engine Performance". *SAE Technical Paper*, n^o 2016-01-0722, 2016.

[26] Payri F and Desantes J.M. "Motores de combustión interna alternativos". *Editorial Reverté*, 2011.

[27] Pacaud P., Perrin H. and Laget O. "Cold start on diesel engine: is low compression ratio compatible with cold start requirements?". *SAE International Journal of Engines*, Vol. 1 n^o 2008-01-1310, pp. 831–849, 2008.

[28] Divekar P.S., Chen X., Tjing J. and Zheng M. "Energy efficiency impact of EGR on organizing clean combustion in diesel engines". *Energy Conversion and Management*, Vol. 112, pp. 369–381, 2016.

[29] Diwakar R. and Singh S. "Importance of spray-bowl interaction in a DI diesel engine operating under PCCI combustion mode". *SAE Technical Paper*, n^o 2009-01-0711, 2009.

[30] Dreisbach R., Graf G., Kreuzig G., Theissl H. and Pfahl U. "HD base engine development to meet future emission and power density challenges of a DDI engine". *SAE Technical Paper*, n^o 2007-01-4225, 2007.

[31] Benajes J., Pastor J.V., GarcÃa A. and Monsalve-Serrano J. "An experimental investigation on the influence of piston bowl geometry on RCCI performance and emissions in a heavy-duty engine". *Energy Conversion and Management*, Vol. 103, pp. 1019–1030, 2015.

[32] Shi Y and Reitz RD. "Assessment of optimization methodologies to study the effects of bowl geometry, spray targeting and swirl ratio for a heavy-duty diesel engine operated at high-load". *SAE International Journal of Engines*, Vol. 1 n^o 2008-01-0949, pp. 537–557, 2008.

[33] Genzale C. L., Reitz R.D. and Wickman D.D. "A computational investigation into the effects of spray targeting, bowl geometry and swirl ratio for low-temperature combustion in a heavy-duty diesel engine". *SAE Technical paper*, n^o 2007-01-0119, 2007.

[34] Broatch A., Olmeda P., GarcÃa A., Salvador-Iborra J. and Warey A. "Impact of swirl on in-cylinder heat transfer in a light-duty diesel engine". *Energy*, Vol. 119, pp. 1010–1023, 2017.

[35] Han S. and Bae C. "The influence of fuel injection pressure and intake pressure on conventional and low temperature diesel combustion". *SAE Technical Paper*, n^o 2012-01-1721, 2012.

[36] Thangaraja C. and Kannan C. "Effect of the exhaust gas recirculation on advanced diesel combustion and alternate fuels - A review". *Applied Energy*, Vol. 180, pp. 169–184, 2016.

[37] Lázaro L., Aparecida C. and Lacava P.T. "Strategies for emission control in diesel engine to meet Euro VI". *Fuel*, Vol. 104, pp. 183–193, 2013.

[38] Sher E. "Handbook of air pollution from internal combustion engines". *USA Academic press*, 1998.

[39] Amstrong J. "Electronic fuel injection: A history lesson". *http://www.autonews.com/article/20040823/SUB/408230807/electronic-fuel-injection:-a-history-lesson*, 2004.

[40] Bosch. "Pressure in diesel engines". *http://www.bosch-presse.de/pressportal/de/en/pressure-in-diesel-engines-42396.html*, 2013.

[41] Hountalas D.T., Kouremenos D.A., Binder K.B., Schwarz V. and Mavropoulos G.C. "Effect of injection pressure on the performance and exhaust emissions of a heavy duty DI diesel engine". *SAE Technical Paper*, n^o 2003-01-0340, 2003.

[42] Kim B.S., Yoon W.H., Ryu S.H. and Ha J.S. "Effect of the injector nozzle hole diameter and number on the spray characteristics and the combustion performance in medium-speed diesel marine engines". *SAE Technical Paper*, n^o 2005-01-3853, 2005.

[43] Agarwal A.K., Srivastava D.K., Dhar A., Maurya R.K., Shukla P.C. and Singh A.P. "Effect of fuel injection timing and pressure on combustion, emissions and performance characteristics of a single cylinder diesel engine". *Fuel*, Vol. 111, pp. 374–383, 2013.

[44] Kweon C.B., Okada S., Stetter J.C., Christenson C.G., Shafer M.M., Schauer J.J. and Foster D.E. "Effect of injection timing on detailed chemical composition and particulate size distributions of diesel exhaust". *SAE Technical Paper*, n^o 2003-01-1794, 2003.

[45] Guan B., Zhan R., Lin H. and Huang Z. "Review of the state-of-the-art of exhaust particulate filter technology in internal combustion engines". *Journal of environmental management*, Vol. 154, pp. 225–258, 2015.

[46] Stamatellou A.M. and Stamatelos A. "Overview of Diesel Particulate Filter Systems sizing approaches". *Applied Thermal Engineering*, 2017.

[47] Praveena V. and Martin M.L.J. "A Review on Various After Treatment Techniques to Reduce NOx emissions in a CI Engine". *Journal of the Energy Institute*, 2017.

[48] Alimin A.J., Benjamin S.F. and Roberts C.A. "Lean NO x trap study on a light-duty diesel engine using fast-response emission analysers". *Journal of Engine Research*, Vol. 10 n^o 3, pp. 149–164, 2009.

[49] DiGiulio C.D., Pihl J.A., Choi J.S., Parks J.E., Lance M.J., Toops T.J. and Amiridis M.D. "NH 3 formation over a lean NO X trap (LNT) system: Effects of lean/rich cycle timing and temperature". *Applied Catalysis B: Environmental*, Vol. 147, pp. 698–710, 2014.

[50] Guan B., Zhan R., Lin H. and Huang Z. "Review of state of the art technologies of selective catalytic reduction of NO x from diesel engine exhaust". *Applied Thermal Engineering*, 2014.

[51] Prabhu S.S., Nayak N.S., Kapilan N. and Hindasageri V. "An experimental and numerical study on effects of exhaust gas temperature and flow rate on deposit formation in Urea-Selective Catalytic Reduction (SCR) system of modern automobiles". *Applied Thermal Engineering*, Vol. 111, pp. 1211–1231, 2017.

[52] Liu C., Shi J.W., Gao C. and Niu C. "Manganese oxide-based catalysts for low-temperature selective catalytic reduction of NO x with NH 3: A review". *Applied Catalysis A: General*, Vol. 522, pp. 54–69, 2016.

[53] Agency California Environmental Protection. "Heavy-Duty Technology and Fuels Assessment: Overview, Air resources board". *C.E.P. Agency*, 2015.

[54] Einewall P., Tunestal P. and Johansson B. "Lean burn natural gas operation vs. stoichiometric operation with EGR and a three way catalyst". *SAE Technical Paper*, n^o 2005-01-0250, 2005.

[55] Lee S. and Reitz R.D. "Stoichiometric combustion in a HSDI diesel engine to allow use of a three-way exhaust catalyst". *SAE Technical Paper*, n^o 2006-01-1148, 2006.

[56] Lee S. and Reitz R.D. "Effects of engine operating parameters on near stoichiometric diesel combustion characteristics". *SAE Technical Paper*, n^o 2007-01-0121, 2007.

[57] Chase S., Nevin R., Winsor R. and Baumgard K. "Stoichiometric compression ignition (SCI) engine". *SAE Technical Paper*, n^o 2007-01-4224, 2007.

[58] Sung K., Kim J. and Reitz R.D. "Experimental study of pollutant emission reduction for near-stoichiometric diesel combustion in a three-way catalyst". *International Journal of Engine Research*, Vol. 10, pp. 349–357, 2009.

[59] Saluja R.K., Kumar V. and Sham R. "Stability of biodiesel - A review". *Renewable and Sustainable Energy Reviews*, Vol. 62, pp. 866–881, 2016.

[60] Yoon E.S. and Han C. "A review of sustainable energy recent development and future prospects of dimethyl ether (DME)". *Computer aided chemical engineering*, Vol. 27, pp. 169–175, 2009.

[61] Thomas G., Feng B., Veeraragavan A., Cleary M.J. and Drinnan N. "Emissions from DME combustion in diesel engines and their implications on meeting future emission norms: A review". *Fuel processing technology*, Vol. 119, pp. 286–304, 2014.

[62] Park S.H. and Lee C.S. "Applicability of dimethyl ether (DME) in a compression ignition engine as an alternative fuel". *Energy Conversion and Management*, Vol. 86, pp. 848–863, 2014.

[63] Arcoumanis C, Bae C, Crookes R and Kinoshita E. "The potential of di-methyl ether (DME) as an alternative fuel for compression-ignition engines: A review". *Fuel*, Vol. 87 n^o 7, pp. 1014–1030, 2008.

[64] Kapus P. and Ofner H. "Development of fuel injection equipment and combustion systems for DI diesels operated on dimethyl ether". *SAE Technical Paper*, n^o 950062, 1995.

[65] Zhao X., Ren M. and Liu Z. "Critical solubility of dimethyl ether (DME)+ diesel fuel and dimethyl carbonate (DMC)+ diesel fuel". *Fuel*, Vol. 84 n^o 18, pp. 2380–2383, 2005.

[66] Goto S., Oguma M. and Suzuki S. "Research and development of a medium duty DME truck". *SAE Technical Paper*, n^o 2005-01-2194, 2005.

[67] Youn I.M., Park S.H., Roh H.G. and Lee C.S. "Investigation on the fuel spray and emission reduction characteristics for dimethyl ether (DME) fueled multi-cylinder diesel engine with common-rail injection system". *Fuel processing technology*, Vol. 92 n^o 7, pp. 1280–1287, 2011.

[68] Teng H, McCandless JC and Schneyer JB. "Thermochemical characteristics of dimethyl ether-An alternative fuel for compression-ignition engines". *SAE Technical Paper*, 2001.

[69] Curran HJ, Pitz WJ, Westbrook CK, Callahan GV and Dryer FL. "Oxidation of automotive primary reference fuels at elevated pressures". *Elsevier*, Vol. 27, pp. 379–387, 1998.

[70] Curran HJ, Fisher EM, Glaude PA, Marinov NM, Pitz WJ, Westbrook CK, Layton DW, Flynn PF, Durrett RP and Zur Loye AO. "Detailed chemical kinetic modeling of diesel combustion with oxygenated fuels". *SAE Technical Paper*, 2001.

[71] Jung H., Kittelson D.B. and Zachariah M.R. "The influence of engine lubricating oil on diesel nanoparticle emissions and kinetics of oxidation". *SAE Technical Paper*, n^o 2003-01-3179, 2003.

[72] Sidhu S., Graham J. and Striebich R. "Semi-volatile and particulate emissions from the combustion of alternative diesel fuels". *Chemosphere*, Vol. 42 n^o 5, pp. 681–690, 2001.

[73] Jang J., Lee Y., Cho C., Woo Y. and Bae C. "Improvement of DME HCCI engine combustion by direct injection and EGR". *Fuel*, Vol. 113, pp. 617–624, 2013.

[74] Fleisch T., McCarthy C., Basu A., Udovich C., Charbonneau P., Slodowske W., A.E. Mikkelsen and McCandless J. "A new clean diesel technology: demonstration of ULEV emissions on a Navistar diesel engine fueled with dimethyl ether". *SAE Technical Paper*, n^o 950061, 1995.

[75] Egnell R. "Comparison of heat release and NOx formation in a DI diesel engine running on DME and diesel fuel". *SAE Technical Paper*, n^o 2001-01-0651, 2001.

[76] Park SH and Lee CS. "Combustion performance and emission reduction characteristics of automotive DME engine system". *Progress in Energy and Combustion Science*, Vol. 39 n^o 1, pp. 147–168, 2013.

[77] Benajes J, Novella R, Pastor JM, Hernández-López A, Hasegawa M, Tsuji N, Emi M, Uehara I, Martorell J and Alonso M. "Optimization of the combustion system of a medium duty direct injection diesel engine by combining CFD modeling with experimental validation". *Energy Conversion and Management*, Vol. 110, pp. 212–229, 2016.

Chapter 3

Literature review: optimization methods

Contents

3.1 Introduction

The engine design and optimization strategies have evolved during the past decades forced by the increasingly stringent regulations. To counter the more a more difficult task of designing a future generation engine with improved efficiency and emissions, the amount of subsystems attached to a modern

engine has grown to improve flexibility and provide more tools to the research community. However, the number of parameters that have to be studied in order to optimize an engine is increasing exponentially, accordingly new and improved optimization methods are needed.

Parametric studies have been the preferred optimization method for a long time and there are still occasions where this method is of interest and still used. A parametric study is a non-systematic method that is based on calculating the effect of an isolated variable over the objective output variable. It is a straightforward method that provides robust and accurate results. However, the intuition and experience of the designers are fundamental to success in this type of methods. Additionally, parametric studies are not designed to study coupled effects. Furthermore, this method is used to optimize a limited number of inputs because the number of iterations increases significantly with the number of inputs and that limits its use with complex problems [1]. Different alternatives are available for engine optimization methods. All of them can be included in two main groups, evolutionary and non-evolutionary methods. These methods are really efficient with a large number of variables because they substitute the human intelligence with automated optimization systems.

In the past, optimizations have been done experimentally but with the significant amount of iterations that non-evolutionary and specially evolutionary methods require, optimizing an engine experimentally has become a hard task. These problems are more noticeable when hardware components are included in the optimization and due to the importance of these components in engine design (see section 2.3.1), experimental testing has become a validation step in the field of engine combustion system optimization. The alternative to experimental testing is CFD modeling since nowadays it has gained reliability in predicting emissions and combustion characteristics by using properly calibrated and validated models. Additionally, CFD methods can be coupled with evolutionary and non-evolutionary methods to create a completely automated system to be able to work more and better. These automated systems are the reason behind the significant development of the optimization methods presented in this chapter.

3.2 Non-evolutionary optimization methods

Non-evolutionary methods are statistical methods that use a predefined population of input combinations to obtain the wanted information. These methods rely heavily on spatial information to find the optimum, such as

a mathematical response surface generated from the initial population. In general, these methods are extremely efficient for a moderate number of optimization variables but rapidly become costly to use with increasing amount of inputs. In addition, when applied to really non-linear problems the approaches followed by non-evolutionary methods lack accuracy and are not always applicable [1]. For that reason, this kind of methods are often used for cases where previous experience on the topic helps to define the optimization inputs and ranges. That way the non-evolutionary algorithms can be applied with reasonable time cost. In this section two different non-evolutionary methods are presented, the 2^k factorial design method and the response surface method.

3.2.1 The 2^k factorial design

Factorial designs are commonly applied to experiments with numerous factors when the coupled effect of the factors over a response is of interest. A special case of factorial design is the 2^k factorial design. It has been widely used in research studies because it requires the minimum amount of runs to study k factors in a complete factorial design. Accordingly, they are commonly used in factor screening experiments at early stages of the experiments [2].

The 2^k factorial design only considers two levels for each factor. These levels can be quantitative (i.e. pressure or temperature values), qualitative (i.e. high or low) or simply the existence and absence of the value. Due to having only two levels per factor, it is assumed that the factor effect is linear. This assumption is considered acceptable when the region of interest is small enough.

The main objective of this kind of technique is to find the magnitude and direction of the effect of each independent variable over the response variable to be able to determine which factors are more relevant to the study. In order to specify how are they calculated in 2^k factorial designs, an example of a 2 factor design is presented (example obtained from [2]). Then the methodology used in this example can be extrapolated to k factors. Imagine we want to study the yield of an experiment, which is the objective of the study, and two factors, reactant concentration (A) and amount of catalyst (B) that affect the yield of the experiment. Since we are doing a 2^k factorial design, only 2 levels for each factor are considered. The values of each factor level and the yield value are presented in Fig. 3.1. It can be seen in the figure that the high level of the factor is represented by the lowcase letter that represents the

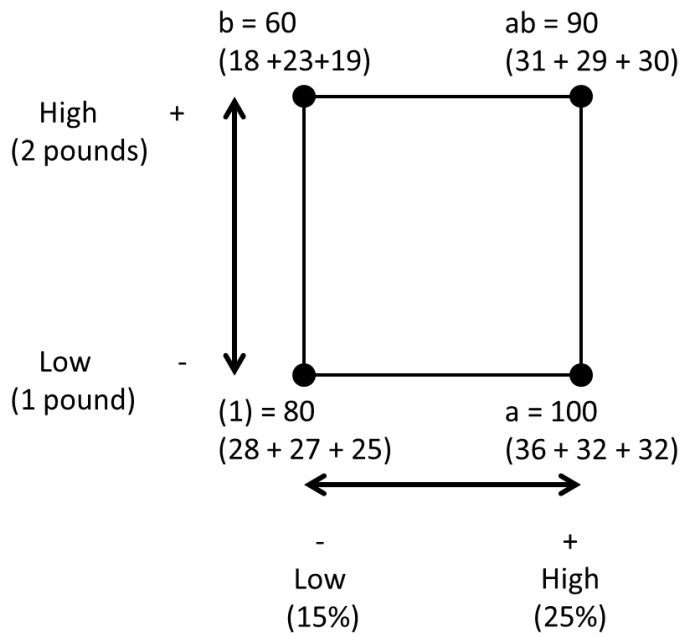

Figure 3.1. *Example of a 2^k factorial design. Adapted from [2].*

factor and the low value is represented as the absence of it ((1) represents the combination of the lower value of both factors).

Once the 2^k factorial design is defined, the main objective is to obtain the main effect of each factor. The main effect of factor A would be the average between the effect of A at the low level of B and the effect of A at he high level of B, this is

$$A = \frac{1}{2n}(ab + a - b - (1)) \tag{3.1}$$

where n is the number of replicates, in this case each value was measured 3 times. In the same manner, the main effect of B is described as

$$B = \frac{1}{2n}(ab + b - a - (1)) \tag{3.2}$$

The correlated effect of both factors is defined as the average difference of B at high and low level of A (average difference of A at high and low level of B also works), this is,

$$AB = \frac{1}{2n}(ab + (1) - a - b) \tag{3.3}$$

After applying the equations, the main effects of the factors of this design would be A = 8.33, B = -5 and AB = 1.67. These results suggest that the effect of A is positive (increasing A increases the yield), the effect of B is negative (increasing B decreases the yield) and the joint effect of AB is not relevant compared to that of A and B. These results and the relevance of certain factors can be supported by the application of an ANOVA study.

This method is a powerful tool but has a significant limitation when working with non-linear systems. Then, due to the highly non-linear behavior of the combustion engines, this technique has its use limited in this field.

3.2.2 Response surface methods

The RSM method is a set of statistical and mathematical tools used to analyze and model problems where the main objective is to optimize a response that is affected by numerous variables [2]. This is, if it is wanted to improve the engine efficiency (ef) by finding the optimum values of intake flow temperature (T) and pressure (P), then the engine efficiency would be a function of intake temperature and pressure, this is,

$$ef = f(T, P) + err \tag{3.4}$$

where *err* is the error observed in the response (ef). If the expected response is noted as E(ef) = f(T,P) = RS, the response surface is represented by

$$RS = f(T, P) \tag{3.5}$$

In most cases the real shape of the response surface is unknown, therefore the first step when optimizing with RSM is to find a reasonable approximation for the response surface. First a low-order approximating function is used to model the relationship between the response and independent variables. If the behavior is properly modeled, then a first order model is used to approximate the response.

$$y = \beta_0 + \beta_1 x_1 + \beta_2 x_2 + ... + \beta_k x_k + err \tag{3.6}$$

where y is the response variable, x are the independent variables (factors), k is the number factors and β are the coefficients that define the response surface. If this approximation is not good enough because there is curvature in the real behavior of the response, then a higher degree polynomial is required, like a second order model.

$$y = \beta_0 + \sum_{i=1}^{k} \beta_i x_i + \sum_{i=1}^{k} \beta_{ii} x_i^2 + \sum \sum_{i<j} \beta_{ij} x_i x_j + err \tag{3.7}$$

For most of the problems, high order polynomials are used to create the response surface. Even then, it is expected that the response surface is not a perfect approximation of the real response behavior. However, if the ranges taken into account to build the response surface are small enough, a second order model or even a first order model is considered accurate.

The coefficients of eq. 3.6 and 3.7 are approximated with the method of least squares, then the surface can be analyzed and the optimum can be found. The accuracy of the results not only depend on the polynomial used to generate the surface but also on the data used to estimate the coefficients and adjust the model, which is usually called response surface design. The central composite design (CCD) is the response surface design chosen for this Thesis. It offers a proper distribution of the data over the experimental region, requires reasonable number of runs and independent variables levels, is robust with incomplete data and is rotational and orthogonal.

The CCD is a 2^k factorial with n_c center points and 2^k axial points. In order to keep the rotatibility, the value of α (see Fig. 3.2 for α definition) has to be calculated as in eq. 3.8. A sketch of a CCD with 2 and 3 factors can be found in Fig. 3.2.

$$\alpha = (2^k)^{\frac{1}{4}} \tag{3.8}$$

This optimization methods have been applied in the past to engine optimizations, mostly to experimental approaches. Atmanli et al [3] used RSM methods on an experimental optimization for finding the optimum diesel-n-butanol-cotton oil ternary blend ratios for controlling emissions. Saravanan et al [4] performed an statistical experimental engine optimization using RSM methods to analyze the effects of IP, injection timing and EGR aiming to improve efficiency and emissions. Then, it can be seen that RSM methods can be used to optimize many different aspects of an engine but they are always limited to a small number of parameters.

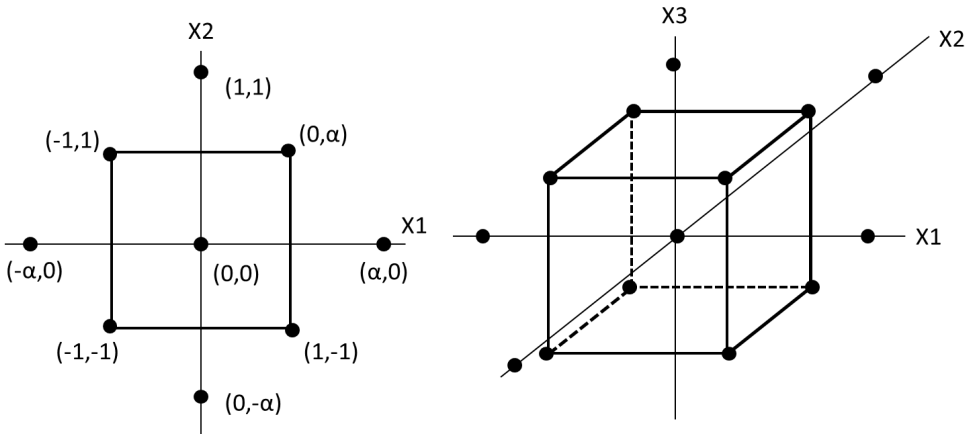

Figure 3.2. *Central composite designs for $k = 2$ and $K = 3$. Adapted from [2].*

3.3 Evolutionary optimization methods

Evolutionary methods are very different but the core idea behind them is common. They are based on an initial population of individuals that evolves due to environmental pressure aiming to improve the fitness of the individuals of the population. Every iteration the initial population is controlled and classified by certain external requirements imposed to the problem and the fittest individuals (parents) will be chosen to have a strong influence on the new generation (children) while the weaker ones will not, just like natural selection does in the nature, this is called 'survival of the fittest'. The process stops once a child with enough quality is found or after certain generations [5]. The process is presented in Fig. 3.3.

Most of these methods are based on natural mechanisms from cells or animals but at the end the only difference is how the initial population evolves and finds the final optimum. In this section three evolutionary methods are presented: particle swarm algorithms, genetic algorithms (GA) and artificial neural networks. They have been widely used and have proven to behave well against real non-linear problems. Contrary to the non-evolutionary algorithms, these methods have proven their potential when optimizing unknown problems with several input parameters but they are only be coupled with modeling approaches due to the high number of iterations required [7].

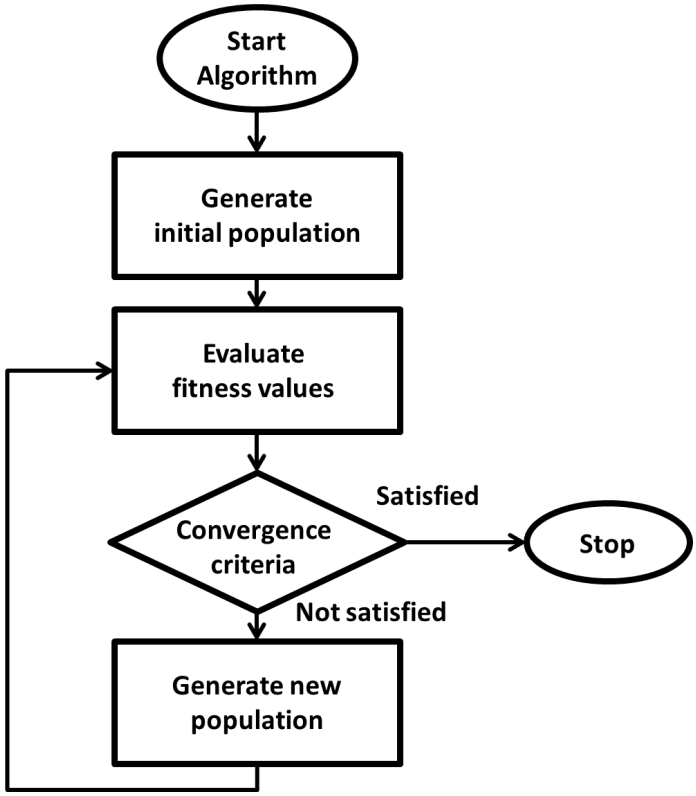

Figure 3.3. *Sketch of an evolutionary algorithm process. Adapted from [6].*

3.3.1 Genetic algorithm

Genetic algorithms were first introduced in the literature by John Henry Holland in 1975. They are evolutionary methods that try to mimic the mechanisms of natural selection and evolution, this is, genetic evolution. Like any other evolutionary algorithm, an initial population is generated and the fittest individuals are chosen to become the parents of the new generation but the mechanisms used to exchange information between the parents and generate the new population is what characterizes all the GAs, this is, selection, mutation and crossover [8]. A sketch of the process followed by a GA is summarized in Fig. 3.4.

In GAs, the first step is to generate a random initial population. Each individual is represented as a chromosome, which is a combination of several

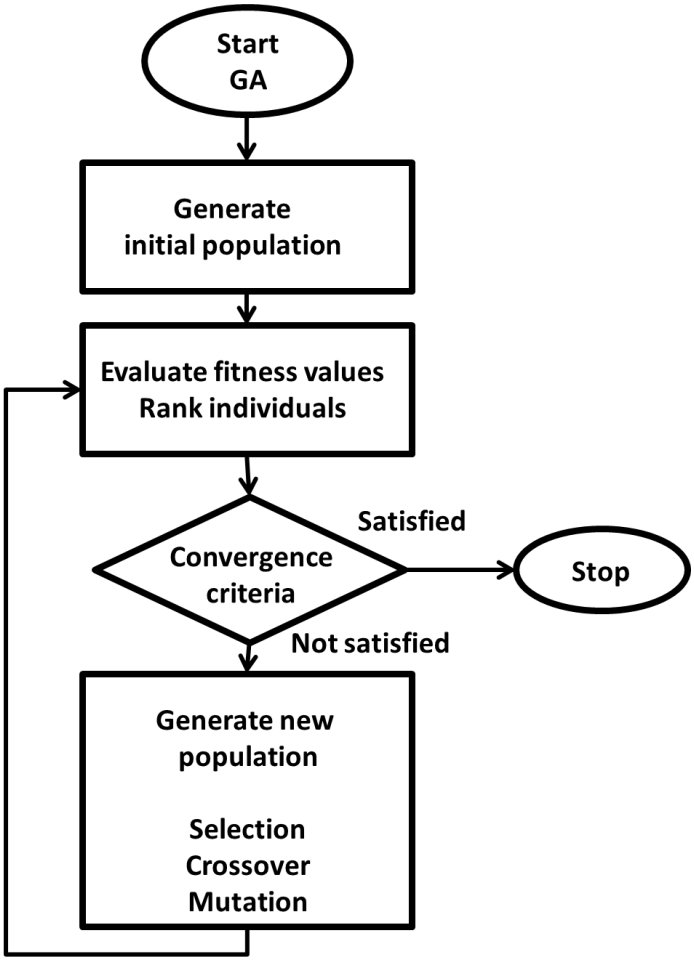

Figure 3.4. *Sketch of a generic genetic algorithm. Adapted from [6].*

genes, and the genes represent the values of the input variables that are going to be optimized. The individuals of this initial population, just like any other future generation, are evaluated and ranked in terms of its fitness value. Then a new generation is created by applying the 3 genetic operators to the current population. The genetic operators are [6, 9]:

- **Selection.** This operator selects the individuals that become parents for the next generation. Based on the 'survival of the fittest' theory,

the fittest individuals that were ranked better have more chances of becoming the future generation parents.

- **Crossover.** This operator combines the chromosomes of the parents to create new individuals. The fittest individuals are used as parents more often than the rest, therefore, after applying the crossover operator, the average fitness of the new population increases. Additionally, this operator tends to generate very similar individuals after several generations, reducing diversity and leading to population stagnation.

- **Mutation.** This operator is in charge of increasing the diversity of the population to compensate the tendency of the crossover operator to population stagnation.

Once the new population is generated, it is ranked and used as parents for the next generation until a convergence criteria is reached. Although all GAs follow this steps, there are several variants of GA that use different methods to perform selection, crossover and mutation. In this section 3 of the most used GAs are presented, micro genetic algorithm (micro-GA), nondominated sorting genetic algorithm (NSGA-II) and DKGA. They have been widely used in several research topics but specially in the engine optimization field proving its potential to be used as an optimization methodology for engine design. Kim et al. [10] used a micro-GA on a HD engine optimization. Fuel fraction,PIVC, EGR,SOI and delay between first an second injection were used as inputs for the algorithm and the results presented an optimum configuration with improvements in both soot and NOx emissions. Ge et al. [11] used a NSGA-II algorithm to preform a HSDI engine optimization. They optimized the engine configuration in 2 steps, a first optimization focused on the piston bowl and injector geometry and a second step using the optimum configuration from step 1 as baseline case while optimizing the SOI, PIVC, swirl and IP. The result was an optimum configuration able to simultaneously improve emission levels and performance.

3.3.1.1 Micro genetic algorithm

Krishnakumar developed the micro-GA in 1989 [12] and it has been further developed by other researchers like Coello et al. [13] and Senecal [14]. The motivation behind this GA was to modify the existing algorithms to be applicable to computationally expensive problems. The micro-GA has the population size limited to a maximum of 5. Due to this characteristic, it

is suitable for problems where expensive simulations are required and a large number of parallel cases can not be run due to lack of resources.

An algorithm with such a very small population needs additional mechanisms to offer robust results. It uses a reinitialization procedure with an external memory to save the pareto front optimums. The algorithm has four main step presented below that are repeated until a maximum number of iterations is reached [15].

1. An initial population of 5 individuals is generated (one is the present baseline case and the rest are generated randomly).
2. The population is evaluated and the fittest individual is kept for the next generation (elitist strategy).
3. A tournament selection strategy is used to determine the parents for the remaining 4 individuals for next generation. Then the new generation is created using uniform crossover.
4. If the convergence criteria is not satisfied, go to step 2 to evaluate the new population. If the population is considered converged, then go to step 1 and generate a new initial population keeping the current best optimum case (new cycle).

3.3.1.2 NGSA-II algorithm

The NSGA-II [16] is based on the original nondominated sorting genetic algorithm with improved aspects that makes it one of the most popular GA due to its robustness and efficiency. The main improvement from its predecessor is the fast nondominated sorting approach, a fast crowded distance estimation procedure and a simple crowded comparison operator. The description of the algorithm is summarized in the following steps [17]:

1. Create initial population
2. Rank the individuals based on their nondomination level (apply the nondomination sorting approach).
3. Estimate the crowding distance of each individual. Then the population individuals can be selected based on their crowding distance and rank (nondomination). This is necessary because the number of individuals is higher than the population size so crowding distance decides which individuals are chosen from individuals with the same rank.

4. The chosen individuals are used to generate the new population by applying the genetic operators, this is, selection, crossover and mutation. To perform the selection process, a tournament selection strategy is used. The crowding comparison procedure is used in the selection process to introduce diversity.

5. If convergence is reached, keep the optimum pareto solution. If the solution is not converged then go to step 2.

3.3.1.3 DKGA algorithm

The DKGA algorithm [18] was developed as an alternative for the previously presented GAs because it was thought that there was room for improvement. This algorithm has two main differences compared to the previously mentioned GAs, the chromosomes are represented in decimal format and the initial mutations are large but decrease while the optimization progresses to force convergence. The description of the algorithm is summarized in the following 7 steps:

1. Create initial population
2. Rank the individuals based on fitness.
3. Choose the best individuals to be the parents for the next generation.
4. Create a new generation using the Punnett square technique (discussed below) to cross breed the parents.
5. Mutate the chromosomes of each child of the new generation.
6. Evaluate the new generation.
7. Penalize the children that does not meet the constraints.
8. Classify the generation from best to worst.
9. Repeat steps 2 to 8 until the maximum number of generations is reached.

Four coefficients are required to configure the GA : initial time constant ($\tau_{GA,0}$), convergence constant (σ), number of parents and number of generations. The length of the optimization is controlled by the number of generations because there is no other convergence criteria and the optimization continues until the maximum number of generations is reached.

	A	B	C	D	E
A	AA	AB	AC	AD	AE
B	BA	BB	BC	BD	BE
C	CA	CB	CC	CD	CE
D	DA	DB	DC	DD	DE
E	EA	EB	EC	ED	EE

Figure 3.5. *Example of Punnet Square technique for 5 parents. Adapted from [18].*

The number of parents controls the selection of children that become parents for the next generation and the population. As noted in step 4, the DKGA uses a Punnet square to do the mating selection, this is, the best nd designs are chosen from the previous generation to become the parents of the new generation. With this technique, each parent has two children with every other parent and one with himself, generating a total of nd^2 children for the next generation. An example of a Punnett square mating selection is shown in Fig. 3.5 for 5 parents.

After applying the Punnet square technique, a new generation is created and each chromosome of each child is mutated. The mutated values are a random number from a normal distribution with its mean set to the non-mutated value and the standard deviation controlled by the DKGA. The standard deviation decreases as the optimization progresses, being large for initial generations to completely explore the design space and small at the later generations to help the process to converge. The behavior of the standard deviation is described in equation 3.9.

$$\tau_{GA,i} = \tau_{GA,0} * exp(-\sigma \frac{i}{MaxGen}) \tag{3.9}$$

where i is the number of generation, $\tau_{GA,i}$ is the current standard deviation for generation i, the coefficient $\tau_{GA,0}$ represents the initial time constant and MaxGen is the maximum number of generations.

3.3.2 Particle swarm algorithm

The particle swarm algorithm (PSA) was developed by Kennedy and Eberhart in the 1995 [19]. It is based on the natural behavior of the flocks of birds and the collective intelligence. The main idea is that past experiences and knowledge of the individuals of a flock can affect positively the rest of the birds and influence their behavior, like regrouping and synchronously changing direction. This has been observed in the nature and is considered as an evolutive advantage, and this hypothesis is the base of the algorithm. A sketch of the PSA structure is presented in Fig. 3.6

In PSA, a swarm is a group of particles dispersed over the N-dimensional space, where N is the number of inputs to optimize. This particles are initialized randomly with a position and a velocity (just like if they were birds flying). Then that position is evaluated and all the particles are ranked in terms of their fitness value. The individual position for each particle and the global best position are stored every iteration. If the converge criteria is not satisfied, a new generation of particles is created with the position and velocity of each particle assuming a certain time step. This loop is repeated until the convergence criteria is satisfied [6].

The step where the search direction or current velocity is calculated is where the 'collective intelligence' is implemented. The formula that updates the velocity of each particle is influenced by two factors, the global best position and the position of the particle with the best average fitness value. This assures that the particles have their own path but end up going towards the optimal region of the space. The formula used to calculate the search direction is presented in eq. 3.10.

$$NSD = IW * LIV + 2 * rand() * (PBP - CP) + 2 * rand() * (GBP - CP) \quad (3.10)$$

The new search direction is represented as NSD, inertia weight as IW, last iteration velocity as LIV, personal best position as PBP, current position as CP and global best position as GBP.

3.3.3 Artificial Neural Network

Artificial neural networks (ANN) try to mimic the behavior of biological nervous systems. ANN are a combination of interconnected neurons that are able to learn, process inputs and respond without a mathematical relationship

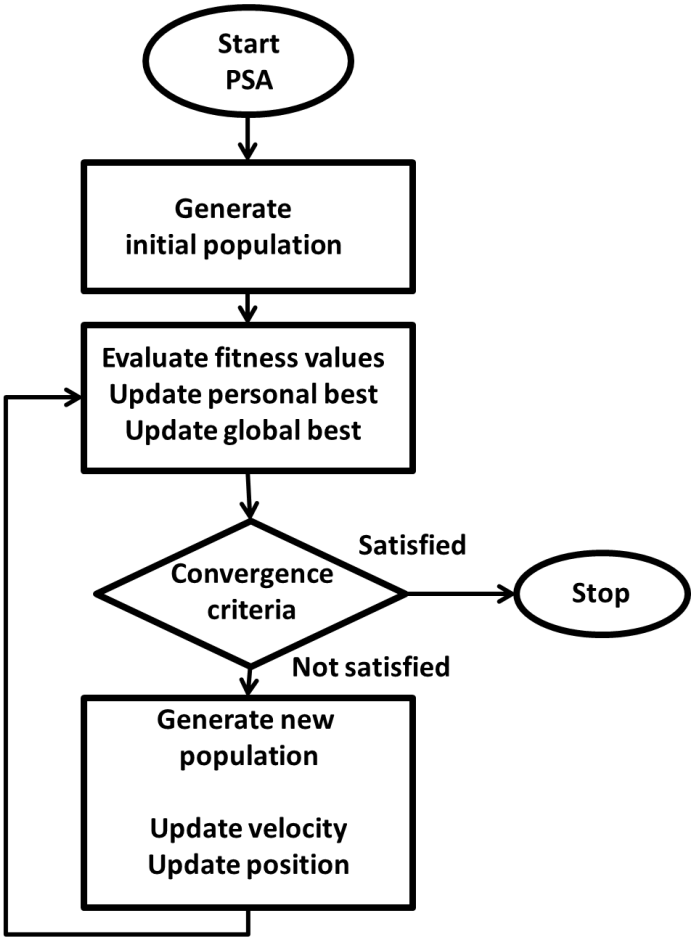

Figure 3.6. *Sketch of a particle swarm algorithm. Adapted from [6].*

between the inputs and outputs. Even though it can not be strictly classified in the evolutionary methods definition provided, it learns and evolves during the process, simulating the behavior of a human brain.

Warren S. McCulloch and Walter Pits presented the first ANN concept [20]. They described the idea of an artificial neuron able to process information that is usually a really easy task for humans but incredibly difficult for machines. The model of an artificial neuron (this is the simplest neural network possible) was invented by Frank Rosenblatt in 1957 [21] and was called a perceptron. A sketch of a single perceptron is presented in Fig. 3.7.

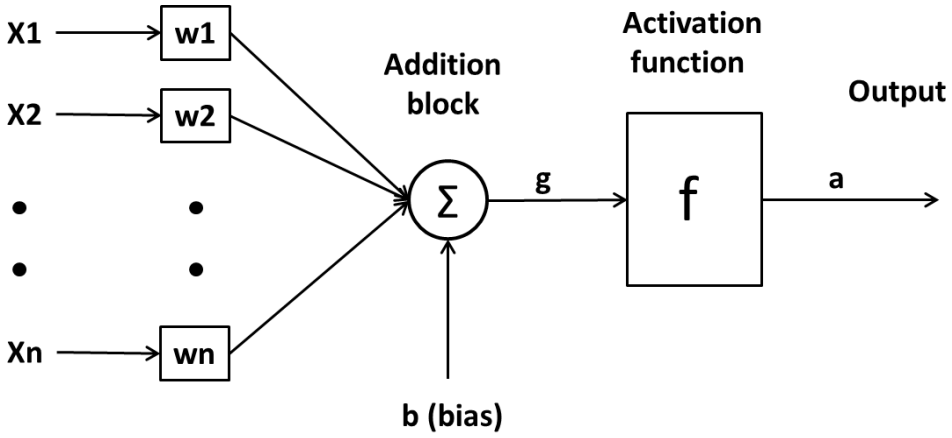

Figure 3.7. *Sketch of a perceptron model. Adapted from [22].*

The perceptron model is considered as a construction block used to build the ANN system. In this block the inputs (x_1, x_2...x_j) are weighted by applying coefficients (w_1, w_2...w_j) to obtain the output response. In addition to the weight coefficients there are extra features to control the neuron response. The activation function is used to limit the value of the output signal, usually within a range of [-1,1] or [0,1], and the bias that is represented as b in the sketch [22].

Equations 3.11 and 3.12 describe the behavior of a perceptron.

$$t_k = \sum_{i=1}^{j} x_i w_{ik} \tag{3.11}$$

$$a = f(t_k + b) \tag{3.12}$$

where x_i represents the inputs and w_{ik} the weights. Then t_k represents the summation of the weighted inputs and f is the activation function. The activation function is the last step of the perceptron model and simplifying its role in the process, it decides the answer of the neuron based on the sum of the weighted inputs obtained. It has a wide variety of shapes but it is usually described by Heaviside, Piecewise-linear, Log-sigmoid and Tangent-sigmoid functions [22].

A key aspect of ANN is that they are able to learn, this is, it is not a rigid system but adaptative that can evolve depending on the information received. This learning process is performed by adjusting the weights and it is usually guided by how good or bad was the answer from the neuron. There are many strategies developed for ANN learning like supervised learning or unsupervised learning. The main difference is that the supervised learning has a smarter teacher that provides the ANN with inputs and outputs and the neural network has to readjust its weights to obtain better results in those specific cases, while in the unsupervised learning there is not a predefined set of values to train the ANN.

ANN are useful for many situations, but just like human brain, not all humans are good for the same situations. Depending on how this building blocks (neurons, perceptrons) are combined and connected, the ANN can be classified in two main classes, feedfoward and recurrent neural networks. The main difference is that feedfoward networks are a one-way process (like perceptrons) while the recurrent network reintroduce the output of the model as a new input. This variety of ANN allows them to be very efficient in several problems like pattern recognition, time series prediction or signal processing [21].

These methods have been also used in the automotive field. Costa et al. [23] developed a methodology to reduce the computational cost of the optimizations of combustion engines combining CFD with neural networks. The main objective is to reduce computational cost related to 3D CFD simulations. To achieve that the author proposes to couple genetic algorithms with CFD simulation to generate a training set to later train a neural network. Then, this network can be used to predict optimum configurations avoiding the high cost of running 3D CFD simulations. Other authors like Channapattana et al. [24] adapted the method using experimental data to train the network. Then this network was used to find the optimal combination of injection settings and fuel blend to obtain a more efficient and clean engine.

3.4 Summary and conclusions

In this chapter a review of the most common optimization methods has been presented. In the past, simple parametric studies were powerful enough to perform engine calibration and optimization. However, nowadays the number of inputs available for engine design is overwhelming and optimizing all of them at the same time has become a hard task. The optimization methodologies have been categorized in two groups, evolutionary and non-evolutionary.

Non-evolutionary methods are statistical methods that use a predefined population of input combinations to obtain the wanted information. They rely on spacial information to find the optimum and are extremely efficient for a moderate number of optimization variables. However, they lack accuracy when applied to highly non-linear problems. RSM based on CCD designs are robust non-evolutionary methods able to capture curvatures and coupled effects. They have been used in real engine optimizations [25, 26] with promising results, therefore they were chosen as the best option for this Thesis. It is known that for significant number of inputs the amount of simulations required increases exponentially and for that reason they were chosen to perform only the CDC engine optimization where previous experience on CDC engines permits the reduction of optimization inputs and ranges.

Evolutionary methods are based on the evolution of an initial population of individuals aiming to improve its fitness. In every iteration, the initial population is checked to ensure that only the strong individuals keep growing. Even though there are many evolutionary algorithms, they are all based on the same evolution concept. These methods, contrary the non-evolutionary, are more flexible and perform better with higher number of inputs and bigger ranges. Therefore they are often used with less known problems where the previous experience on the topic is insufficient or nonexistent. For that reason, an evolutionary method is used in the DME fueled engine optimization. The GAs were chosen as the best approach for this problems because they have been widely used in the field of engine optimization with encouraging results. As pointed out in the review and literature, there are several GAs with different properties, thus the election of the best GA for the DME optimization will be done in the next chapter.

References

[1] Shi Y., Ge H.W. and Reitz R.D. "Computational Optimization of Internal Combustion Engines". *Springer Science and Business Media*, 2011.

[2] Montgomery D.C. "Design and Analysis of Experiments". *John Wiley and Sons*, 2013.

[3] Armanli A., Yuksel B., Ileri E. and Karaoglan a.D. "Response surface methodology based optimization of a diesel-n-butanol-cotton oil ternary blend ratios to improve engine performance and exhaust emission characteristics". *Energy Conversion and Management*, Vol. 90, pp. 383–394, 2015.

[4] Saravanan S., Rajesh K.B., Varadharajan A., Rana D., Balaji A and Lakshmi N.G. "Optimization of DI diesel engine parameters fieled with iso-butanol/diesel blends - Response surface methodology approach". *Fuel*, Vol. 203, pp. 658–670, 2017.

[5] Eiben A.E. and Smith J.E. "Introduction to Evolutionary Computing". *Springer*, 2003.

[6] Kachitvichyanukul V. "Comparison of three evolutionary algorithms: GA, PSO, and DE". *Industrial Engineering and Management Systems*, Vol. 11 n^o 3, pp. 215–223, 2012.

[7] Shi Y. and Reitz R.D. "Assessment of optimization methodologies to study the effects of bowl geometry, spray targeting and swirl ratio for a heavy-duty diesel engine operated at high-load". *SAE International Journal of Engines*, Vol. 1 n^o 2008-01-0949, pp. 537–557, 2008.

[8] Clow B. and White T. "An evolutionary race: a comparison of genetic algorithms and particle swarm optimization used for training neural networks". *Proc. of International Conference on Artificial Intelligence*, pp. 582–588, 2004.

[9] Hassan R., Cohanim B., De Weck O. and Venter G. "A comparison of particle swarm optimization and the genetic algorithm". *Proceedings of the 1st AIAA multidisciplinary design optimization specialist conference*, Vol. 18 n^o 21, pp. 2005.

[10] Kim M., Liechty M.P. and Reitz R.D. "Application of micro-genetic algorithms for the optimization of injection strategies in a heavy-duty diesel engine". *SAE Technical Paper*, n^o 2005-01-0219, 2005.

[11] Ge H, Shi Y, Reitz RD, Wickman D and Willems W. "Engine development using multi-dimensional CFD and computer optimization". *SAE Technical Paper*, 2010.

[12] Krishnakumar K. "Micro-genetic algorithms for stationary and non-stationary function optimization". *Symposium on Visual Communications, Image Processing, and Intelligent Robotics Systems*, pp. 289–296, 1990.

[13] Coello C.A.C. and Pulido G.T. "A micro-genetic algorithm for multiobjective optimization". *EMO*, Vol. 1, pp. 126–140, 2001.

[14] Senecal P.K. "Development of a methodology for internal combustion engine design using multi-dimensional modeling with validation through experiments". *University of Wisconsin*, 2001.

[15] Kim M, Liechty MP and Reitz RD. "Application of micro-genetic algorithms for the optimization of injection strategies in a heavy-duty diesel engine". *SAE Technical Paper*, 2005.

[16] Deb K, Pratap A, Agarwal S and Meyarivan T. "A fast and elitist multiobjective genetic algorithm: NSGA-II". *IEEE transactions on evolutionary computation*, Vol. 6 n^o 2, pp. 182–197, 2002.

[17] Yusoff Y., Ngadiman M.S. and Zain A.M. "Overview of NSGA-II for optimizing machining process parameters". *Procedia Engineering*, Vol. 15, pp. 3978–3983, 2011.

[18] Klos DT. "Investigations of low temperature combustion (LTC) engine design and combustion instability". *University of Wisconsin*, 2015.

[19] Kennedy J. and Eberhart R. "Particle Swarm Optimization". *Proceedings of the IEEE International Conference on Neural Networks*, pp. 1942–1945, 1995.

[20] McCulloch W.S. and Pitts W. "A logical calculus of the ideas immanent in nervous activity". *The bulletin of mathematical biophysics*, pp. 115–133, 1943.

[21] Shiffman D. "The nature of code". *http://natureofcode.com/book/index*, 2012.

[22] Turkson R.F., Yan F., Ali M.K.A. and Hu J. "Artificial neural network applications in the calibration of spark-ignition engines: An overview". *Engineering Science and Technology, an International Journal*, Vol. 19 n^o 3, pp. 1346–1359, 2016.

[23] Costa M., Bianchi G.M., Forte C. and Cazzoli G. "A numerical methodology for the multi-objective optimization of the DI diesel engine combustion". *Energy Procedia*, Vol. 45, pp. 711–720, 2014.

[24] Channapattana S.V., Pawar A.A. and Kamble P.G. "Optimization of operating parameters of DI-CI engine fueled with second generation Bio-fuel and development if ANN based prediction model". *Applied Energy*, Vol. 187, pp. 84–95, 2017.

[25] Hajireza S., Regner G., Christie A., Egert M. and Mittermaier H. "Application of CFD modeling in combustion bowl assessment of diesel engines using DoE methodology". *SAE Technical Paper*, n^o 2006-01-3330, 2006.

[26] Yuan Y, Li G, Yu Y, Zhao P and Li H. "Multi-parameter and multi-object optimization on combustion system of high power diesel engine based on response surface method". *Chinese Internal Combustion Engine Engineering*, Vol. 5, pp. 005, 2012.

Chapter 4

Experimental and theoretical tools

Contents

4.1 Introduction

Computational optimizations usually involve many simulations, up to thousands for GAs, that have to be supported by a number of softwares to be able to be automatically configure, simulate and post-process. Those softwares have to be validated with experimental data to ensure the accuracy and robustness of the models. This chapter focuses on describing the experimental and computational tools used in this Thesis.

The work presented in this Thesis is divided in two main blocks, non-evolutionary optimization of a CDC system and evolutionary optimization of a DME fueled system. The tools used for both processes are mostly different except for the injection profile generator and geometry generator. Fig. 4.1 sums up the tools used for each optimization.

4.2 Experimental tools

This section presents the experimental tools used in this Thesis, this is, the reference engine used to obtain the experimental data necessary for the CFD software validation and the experimental facilities where the data was generated. As seen in Fig. 4.1, the experimental facilities and reference engine are different for both main activities carried out in the Thesis, for that reason this section is divided into non-evolutionary optimization experimental tools and evolutionary optimization experimental tools.

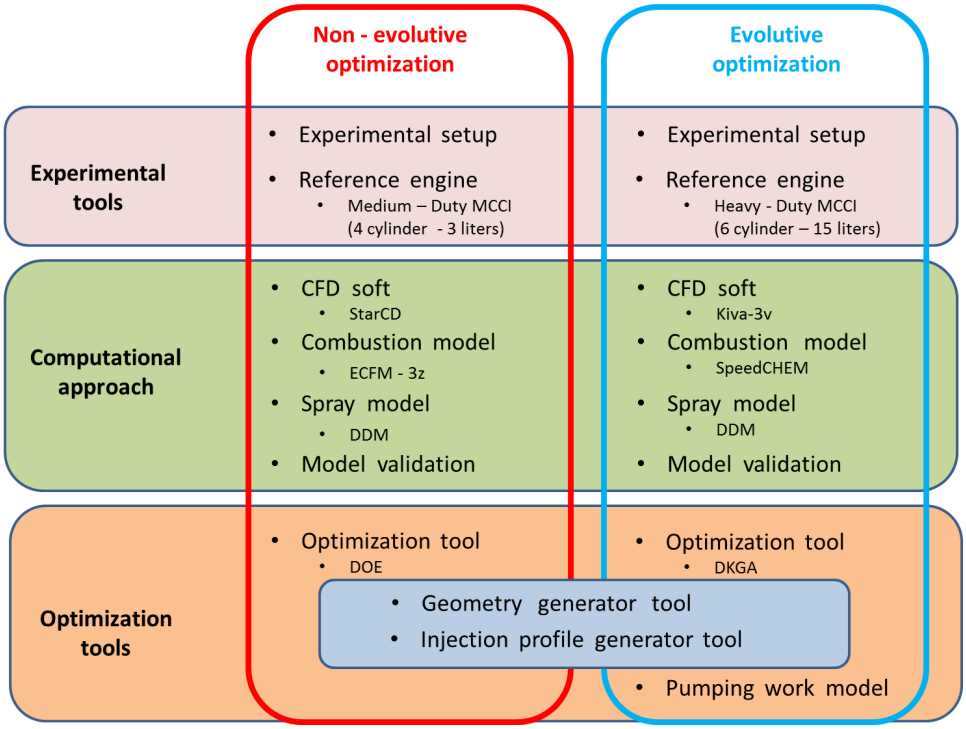

Figure 4.1. *Sketch of the tools used in this Thesis.*

4.2.1 Non-evolutionary optimization experimental tools

4.2.1.1 Experimental facilities

The engine is assembled into a fully instrumented test cell. An external compressor provides the intake air (oil and water-free) required to simulate boost conditions, while the exhaust backpressure is reproduced and controlled by means of a throttle valve placed in the exhaust line after the exhaust settling chamber. The experimental facility also includes a high pressure EGR system, designed to provide arbitrary levels of cooled EGR.

The test cell is equipped with a dedicated air and fuel flow meters, and a set of temperature and pressure sensors to assure the proper operation of the system. Data of O2, CO, CO2, HC, NOx, N2O and EGR is measured with a state-of-the-art exhaust gas analyzer, while Smoke emissions in Filter Smoke Number (FSN) units are measured by a Smokemeter connected to the

exhaust line. Instantaneous high frequency signals such as cylinder pressure, pressures at the intake and exhaust ports and energizing current of the injector are sampled with a resolution of 0.2 crank angle degree (degree to top dead center). Cylinder pressure is measured using a state-of-the-art piezoelectric sensor. The most important combustion parameters like indicated mean effective pressure (IMEP), maximum cylinder pressure (Pmax), pressure gradient (dP/da), combustion noise, combustion phasing angles and heat release rate (HRR); as well as the initial thermodynamic conditions and wall temperatures required for performing the setup of the CFD model, are calculated from the experimental cylinder pressure signal by means of the in-house combustion analysis software (CALMEC) [1, 2]. This 0-Dimensional model simplifies the phenomena occurring inside the engine cylinder, so it does not provide any information related to local thermochemical conditions. However, the instantaneous evolution of the energy released by the progress of the combustion can be obtained with accuracy by resolving the first law of thermodynamics taking the combustion chamber as the control volume independently from the local conditions where this energy is being released. [1]

Measurements of injection rate were carried out with an Injection Discharge Rate Curve Indicator (IRDCI) commercial system. The device makes it possible to display and record the data that describe the chronological sequence of an individual fuel injection event. The measuring principle used is the Bosch method [3], which consists of a fuel injector that injects into a fuel-filled measuring tube.

The fuel discharge produces a pressure increase inside the tube, which is proportional to the increase in fuel mass. The rate of this pressure increase corresponds to the injection rate. A pressure sensor detects this pressure increase, and an acquisition and display system further processes the recorded data for further use.

4.2.1.2 Engine characteristics

The experimental data required for the calibration and validation of the CFD model was obtained from a 4-cylinder 4-stroke Medium Duty Direct Injection CI engine, equipped with a common-rail injection system. Table 4.1 contains the main engine characteristic, while Table 4.2 shows the key settings for the reference engine operating at three different operating conditions.

Table 4.1. *Engine main characteristics.*

Engine data	
Max Torque [Nm]	550 (1400rpm –2200 rpm)
Max Power [kW]	128 (2200 rpm)
Unitary Displacement [cm3]	738.3
Bore x stroke [mm]	96 x 102
Connecting rod length [mm]	154.5
Geometric compression ratio [-]	15.5
IVC [deg aTDC]	-113.8
EVO [deg aTDC]	103
Nozzle hole number	9
Included Spray Angle [deg]	74
Nozzle Hole Diameter [μm]	126

Table 4.2. *Engine operating conditions.*

Operating conditions			
Speed [rpm]	1200	1600	1800
Fuel mass [mg/cc]	26.8	70.2	100.5
IMEP [bar]	6.5	16.2	24.9
EGR [%]	17.7	13	11.3
Intake temperature [K]	324.9	313.15	318.9
Boost pressure [bar]	1.15	2.28	3
Swirl number [-]	2	2	2

4.2.2 Evolutionary optimization experimental tools

4.2.2.1 Experimental facilities

A compressor and drier located outside the lab supplies dry intake air to the test cell. PID controlled intake air heaters precisely control the temperature of the charge entering the engine. Large (265 L) surge tanks ensure stable intake

and exhaust pressure. PID controlled valves control the intake and exhaust pressure and EGR rate. A Fourier Transform Infrared (FTIR) spectrometer (Nicolet Model CQ1319-100) is used to measure the asymmetric species in both the intake and exhaust. The EGR rate is calculated from measurements of carbon dioxide in the intake and exhaust stream. Soot is measured using an AVL 415 SE Smoke meter. A magnetopneumatic oxygen analyzer (Horiba Model MPA-220) and Bosch LSU4.9 oxygen sensors provide measurements of intake and exhaust oxygen concentration. A Coriolis-type mass flow meter (Emerson Coriolis Elite Model CMFS100M) measures the intake air flow rate and positive displacement flow meters (Max Machinery Model 213) measure the volumetric fuel flow rates. The fuel temperature was maintained constant at 20 °C using a high efficiency heat exchanger with process water and the fuels density at 20 °C was used to convert the fuel flow rates from a volumetric to mass basis.

4.2.2.2 Engine characteristics

The engine used is a single cylinder version of a Caterpillar C-15, 15-L six-cylinder engine. Table 4.3 contains the main engine characteristic. For the validation tests carried out using diesel fuel, the engine was operated at 1800 rev/min and a nominal load of 18 bar gross IMEP, the fueling was held constant and the SOI timing was swept from -18 deg aTDC to -3 deg aTDC. The EGR rate, intake pressure, and intake temperature were held constant and its related settings are included in Table 4.4.

4.3 Computational approach

The calculations involved in the evolutionary and non-evolutionary optimizations were done with different CFD softwares. The non-evolutionary optimization was performed by the commercial software Star-CD because it proved to be a robust and accurate software in previous projects performed by our research team. However, when working with genetic algorithms it was decided that it was a good opportunity to test the capabilities of the open-source code Kiva-3v. The description of all the models used in this Thesis are presented in this section.

Table 4.3. *Engine main characteristics.*

Engine data	
Unitary Displacement [cm3]	2500
Bore x stroke [mm]	137 x 171
Connecting rod length [mm]	270.6
Geometric compression ratio [-]	17
IVC [deg aTDC]	-154
EVO [deg aTDC]	113
Nozzle hole number	6
Included Spray Angle [deg]	65
Nozzle Hole Diameter [μm]	214

Table 4.4. *Engine operating conditions.*

Operating conditions	
Speed [rpm]	1800
Fuel mass [mg/cc]	252
IMEP [bar]	18
EGR [%]	25
Intake temperature [K]	333
Boost pressure [bar]	3.1
Swirl number [-]	0.7
SOI [deg aTDC]	-18 to -3
Injection Pressure [bar]	1800

4.3.1 Non-evolutionary optimization computational approach

4.3.1.1 CFD software and models

The StarCD code version 4.18 [4] was used to perform the CFD simulations of the engine combustion system. The combustion model was the ECFM-3z developed by IFP [5]. Concerning pollutants, NOx were calculated using the

extended Zeldovich (thermal) mechanism, where source terms were obtained from a flamelet library [6]. A two-step Hiroyasu-like model was used for soot formation and oxidation [7].

Concerning the physical sub-models, the diesel spray was simulated with the standard Droplet Discrete Model available in StarCD. Spray atomization and break-up were simulated by means of the Huh-Gosman [8] and Reitz-Diwakar [9] models, respectively. Diesel fuel physical properties were given by the DF1 fuel surrogate [10]. In these simulations, turbulent flow was modeled by means of the RNG k-ϵ model [11], with wall functions based on the model from Angelberger [12] in order to account for wall HT. An implicit scheme was used for time discretization, while divergence terms used the second order Monotone Advection and Reconstruction Scheme (MARS) [4]. Velocity-pressure coupling was solved by means of a Pressure-Implicit with Splitting of Operators (PISO) algorithm [13].

4.3.1.2 Model validation

This section presents the validation and calibration of the models used in the non-evolutionary optimization. The axisymmetry of the combustion chamber allowed to consider a sector of the combustion chamber representing a single nozzle hole to reduce computational time. Additionally, the simulations are restricted to the closed engine cycle, from intake valve closure (IVC) to exhaust valve opening (EVO). The sector mesh contained a total of 131360 cells at BDC with periodic boundary conditions after performing a grid convergence study. The simulations were calculated with 12 cores with an average time cost of 36 hours per simulation.

The CFD model was thoroughly validated by simulating the three operating conditions under investigation described in Table 4.2. The results of the CFD model compared to the experimental data in terms of HRR and in-cylinder pressure (Pcyl) are included in Fig. 4.2. Results related to performance and pollutants after calibrating the sub-model constants, specially those related to the soot model, are shown in table 4.5. Those figures show a fair agreement in terms of performance (IMEP), indicated specific fuel consumption (ISFC) and combustion characteristics (HRR). In addition, the final soot levels were close to the experimental data after adjusting the constants of the soot formation model. An over-prediction of NOx emissions is observed for the high load condition, probably related with the faster rise of the HRR compared to experimental data, however, the quality of the CFD model was considered suitable for carrying out the optimization activities.

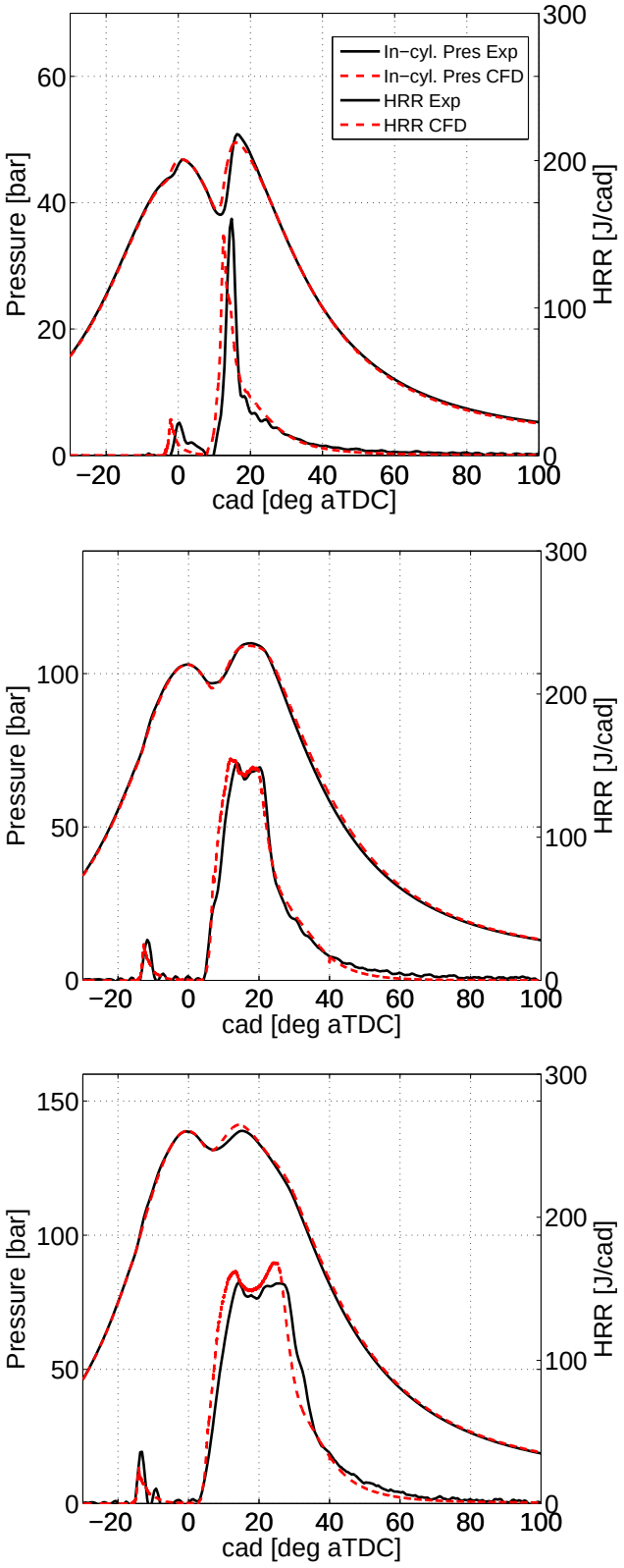

Figure 4.2. *Experimental vs CFD results with the reference combustion system at (top) 1200 rpm, (middle) 1600 rpm and (bottom) 1800 rpm .*

Table 4.5. *Experimental vs CFD results with the reference combustion system for the three operating conditions of the engine performance and emissions.*

Case		ISFC	IMEP	NOx	Soot
		[g/kWh]	[bar]	[g/h]	[FSN]
1200 rpm	**Exp**	201.5	6.5	28.6	0.29
	Diesel CFD	203.1	6.2	27.6	0.24
1600rpm	**Exp**	188.8	17.7	213.3	0.078
	Diesel CFD	186.3	18.3	218.6	0.08
1800 rpm	**Exp**	194.3	24.7	249.16	0.4
	Diesel CFD	193.7	24.96	368.4	0.42

4.3.2 Evolutionary optimization computational approach

4.3.2.1 CFD software and models

Computations were performed using an in-house CFD code based on the KIVA-3v release 2 platform [14] with improvements to many physical and chemistry models developed at the Engine Research Center (ERC) [15], [16], [17].

The KIVA-3v code is coupled with the SpeedCHEM [18] solver for detailed chemistry calculations. The RNG k-ϵ model [19] is used for the turbulence calculations; however, sub grid turbulence chemistry interactions are not considered. That is, the current implementation of the SpeedCHEM solver considers every computational cell to be a Well Stirred Reactor (WSR) and the cell average species production rates are assumed to be equal to the species production rates evaluated at the average cell conditions. At each time step, species concentrations and thermodynamic conditions are passed to the chemistry solver for each computational cell. The chemistry solver then integrates the mass and energy equations at constant volume over a period of time equal to the computational time step. Although, sub grid scale turbulent chemistry interactions are not considered, by coupling the chemistry solver with the CFD code, the effects of turbulence on combustion are accounted by modeling the effects of turbulence on property transport, heat flux, and mixture formation. Justification for this modeling approach has also been discussed by Kokjohn and Reitz [20].

The chemistry of DME was simulated using a reduced reaction mechanism consisting of 29 species and 66 reactions [21]. Validation simulations of CDC were carried out using n-heptane as surrogate and describing its oxidation by a reduced reaction mechanism made up of 45 species and 142 reactions [16].

The spray model employed in this study uses the Lagrangian-Drop and Eulerian-Fluid (LDEF) approach. Because a detailed chemistry model is used, it is desirable to use a relatively coarse computational mesh; however, severe grid size dependency has been observed in LDEF spray models. The problem is most severe in the near nozzle region where the droplets are very close together and occupy only small portions of the Eulerian mesh cell. Abraham [22] showed that accurate modeling of the near nozzle region required grid resolution on the order of the orifice diameter. However, it is not feasible from a computational time standpoint to solve engine problems on such a fine mesh. Furthermore, a fundamental assumption of the LDEF approach is that the volume fraction of droplets in each cell is small, that is, the void fraction is near unity. Thus, this assumption may be violated if the mesh size is overly refined up to a mesh size of the order of the droplet size. In order to reduce the grid size dependency of the LDEF spray model and allow accurate spray simulation on a relatively coarse grid, the Gasjet model of Abani et al. [17, 23] is employed to model the relative velocity between the droplets and gas phase in the near nozzle region.

Droplet breakup is modeled using the hybrid Kelvin Helmholtz (KH) - Rayleigh Taylor (RT) model described by Beale and Reitz [15]. The droplet collision model is based on O'Rourke's model; however, a radius of influence method is used to determine the possible collision partners to further reduce mesh dependency [24]. In addition, the collision model was expanded by Munnannur [24] to include a more comprehensive range of collision outcomes. The current implementation of the droplet collision model considers the effects of bounce, coalescence, and fragmenting and non-fragmenting separations. Droplet interactions with the wall are considered through a wall film submodel [25], which includes the effects associated with splash, film spreading, and motion due to inertia.

4.3.2.2 Model validation

Experimental data for the engine fueled with DME was not available. Accordingly, the CFD code was validated by first comparing to engine data from Allen [26] where the same engine was operated at the condition of interest (18 bar IMEP and 1800 rev/min) using diesel fuel over a range of SOI timings.

Next, DME fueled simulations were performed to verify that the model is able to qualitatively capture the changes in combustion characteristics expected when diesel fuel is replaced with DME (i.e., shorter ignition delay and shorter combustion duration). The justification for using this approach is

- The operating range considered in this study is expected to be mixing controlled. Accordingly, validation using diesel fueled combustion in a mixing controlled combustion regime provides validation that the CFD model adequately captures the mixing characteristics.
- The DME chemical kinetics mechanism and spray model have been validated in previous work (see Pan et al. [21]). The reaction mechanism has been shown to accurately capture the ignition delay from shock tube basic configuration to ICE applications. The spray model has been shown to capture DME spray penetration accurately.

To reduce computing time, simulations consider a sector of the combustion chamber, representing a single nozzle hole of the six hole fuel injector. Additionally, the simulations are restricted to the closed engine cycle, from IVC to EVO. The simulations were initialized using solid body rotation to specify the azimuthal velocity flow field at IVC. Prior to performing model validation, a grid convergence study was performed to identify the necessary grid resolution. The CFD results for axial cell sizes (dS) between 2 mm and 4 mm are shown in Fig. 4.3. It can be seen that the effect of the cell size starts to minimize at dS 3 mm showing almost negligible differences between dS 3 mm and 2 mm in terms of NOx emissions and very little variations in terms of HRR. Accordingly, cell sizes of 3 mm or lower were considered to generate grid independent results. The final setup used a cell size of 2 mm to minimize CR discrepancies between cases. The typical cell count was 30,000 to 40,000 cells at BDC, depending on the shape of the piston , and each case took approximately 20 h to complete with a single processor.

Fig. 4.4 shows the comparison between the experimental and CFD Pcyl and HRR profiles for the baseline diesel case with 3 different SOI values. Although several cases show a slight over prediction of the PP value resulting from a more intense premixed combustion stage, in general, the simulations accurately reproduce the combustion characteristics under mixing controlled operation.

Table 4.6 compares the experimental and modeling results in terms of gross indicated efficiency (GIE), maximum pressure rise rate (maxPRR), NOx emissions and PP. In general, it is shown that the experimental results

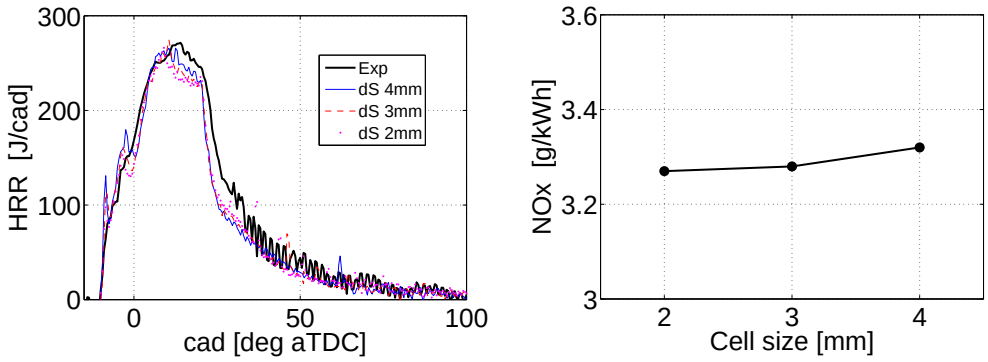

Figure 4.3. *Effect of cell size on (Left) HRR and (Right) NOx emissions .*

Table 4.6. *Comparison of the selected key parameters between experiments and CFD results with diesel.*

Case		GIE	maxPRR	NOx	PP
		[%]	[bar/deg]	[g/kWh]	[bar]
SOI -13	**Exp**	44.43	5.88	2.9	188.12
	Diesel CFD	42.48	6.19	3.28	188.16
SOI -10	**Exp**	43.31	4.72	2.05	173.27
	Diesel CFD	42.37	5.16	2.58	174.2
SOI -8	**Exp**	42.3	4.7	1.66	164.75
	Diesel CFD	42.37	4.71	2.13	166.95

agree with the simulations adequately. The NOx emissions are slightly over predicted by the simulations; however, since the trends are captured accurately, the results are deemed acceptable. Additionally, the CFD results show lower IMEP and GIE values mainly due to the pressure evolution during the expansion stroke, where it is underpredicted in all 3 cases. This drop in the cylinder pressure results from the differences in HRR observed in all 3 cases around 27 deg. After Top Dead Center (aTDC), as the CFD results show a sudden HRR decrease while the experimental results do not show this effect.

After performing the CFD model validation with diesel fuel, the same model setup was then used to carry out simulations with DME. The quantity of fuel injected was increased by adjusting the Dnoz (from 214μm to 300μm)

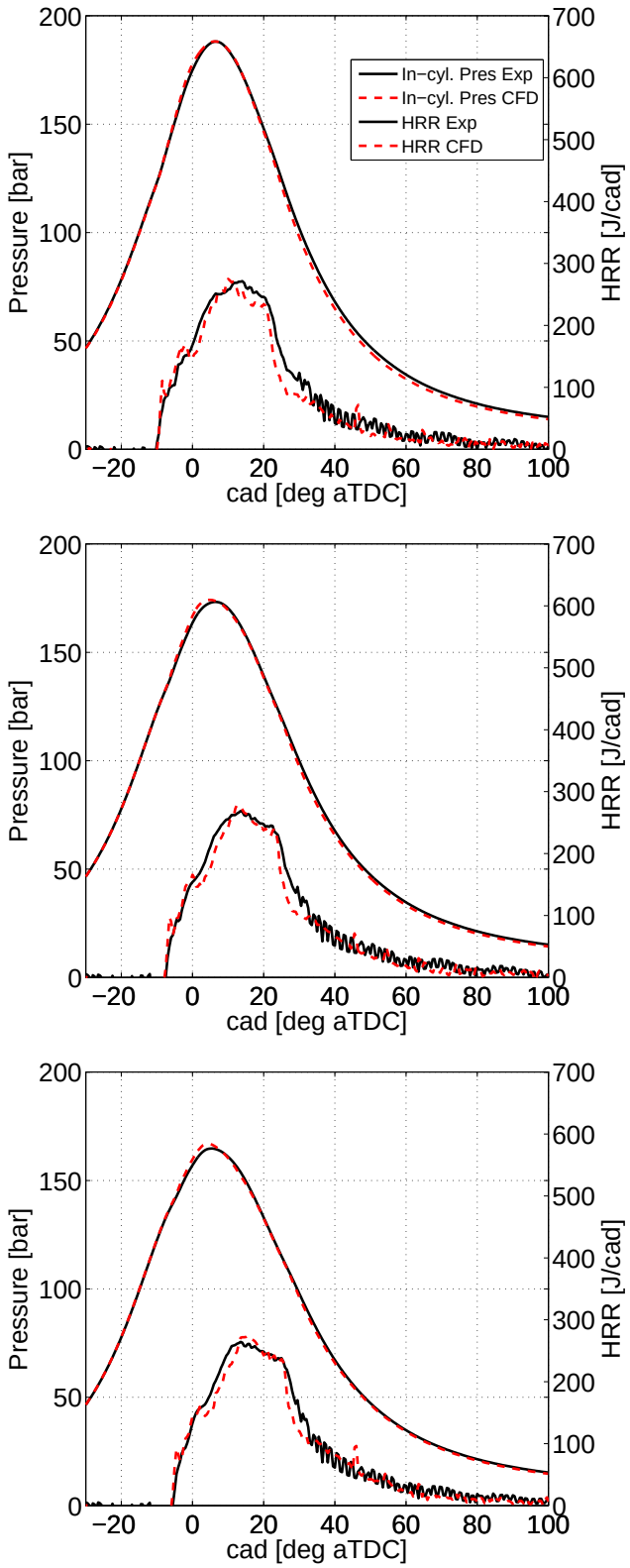

Figure 4.4. *Comparison of Pcyl and HRR between CFD and experiments at (up) SOI -13 cad, (middle) SOI -10 cad and (bottom) SOI -8 cad .*

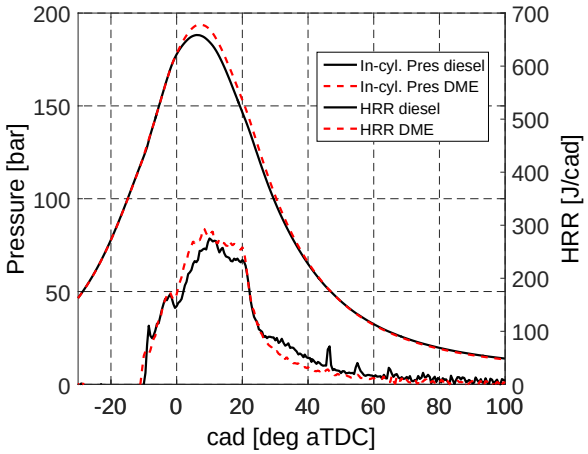

Figure 4.5. *CFD results of Pcyl and HRR using diesel and DME as fuels.*

to match the energy injected in the diesel case keeping the injection length and pressure constant. The comparison of the pressure and HRR profiles of the CFD results with diesel fuel and DME is shown in Fig. 4.5.

Despite not having experimental results operating with DME to compare directly with the modeling results, the main differences between diesel fuel and DME are consistent with those found in the literature. Fig. 4.5 shows a faster HRR for DME leading to higher PP and higher GIE, as seen in Table 4.7. The higher PP and GIE is due to the shorter ignition delay of DME and increased mixing energy resulting from the higher fuel quantity. In relation to NOx emissions, there is some uncertainty since it is not clear if DME levels should be higher or lower than those operating with diesel since there are multiple competing effects [27] [28]; however, the general trends of the model working with DME are similar to the diesel cases, as seen in Table 4.7. In addition, as reported in the literature carbon monoxide (CO), unburnt hydrocarbons (UHC) and soot emissions generated by DME combustion systems are noticeably lower than the diesel values [29], and for this reason they are not considered as restrictions for the optimization so they are not taken into account in the validation process.

To summarize, the KIVA-3v CFD code was validated against experimental data for diesel fuel and found to yield acceptable results. The previously validated DME reaction mechanism and spray model was used to simulate

Table 4.7. *Comparison of the restricted parameters and performance between diesel and DME fuels.*

Case		GIE	GIW	maxPRR	NOx	PP
		[%]	[kJ]	[bar/deg]	[g/kWh]	[bar]
SOI -13	**Diesel CFD**	42.48	4790	6.19	3.28	188.16
	DME CFD	42.82	4854	6.14	2.81	193.88
SOI -10	**Diesel CFD**	42.37	4760	5.16	2.58	174.2
	DME CFD	42.55	4808	5.13	2.1	177.72
SOI -8	**Diesel CFD**	42.37	4760	4.71	2.13	166.95
	DME CFD	42.38	4778	4.71	1.74	168.85

DME combustion and was shown to follow the general trends discussed in the literature review. Accordingly, it is concluded that the integrated CFD model setup is suitable for performing the optimization of the engine combustion system operating with DME.

4.4 Optimization tools

4.4.1 Injector profile generator

The injection rate profile has a critical effect on the combustion process so in order to be consistent with the experimental data, an in-house 0D model code capable of reproducing any injection rate profile was developed. Due to its high flexibility, any profile can be adjusted and then modified to fit the required values. The required inputs to make the model work depend on the case, for both optimizations the fuel mass was kept constant so only the IP was modified.

The 0D model needs experimental data from the same injector in order to generate new consistent results. The original shape is adjusted using Bezier curves so a continuous set of data is available and then modified to fit the required IP and mass. Fig. 4.6 shows the experimental injection profiles and the curves obtained from the software, which used the 1200 bar case to be trained and then predict the other profiles.

A critical aspect of the injection is the slope of the injection rate when the injector receives the electric signal and when the signal ends. It can be seen in

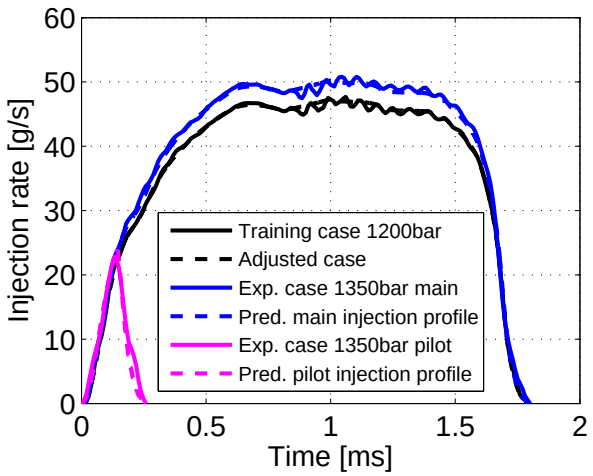

Figure 4.6. *Reference injection profile, 2 new generated profiles with the 0D model and the adjusted profiles with Bezier curves.*

Fig. 4.6 how the injection profile generator keeps the original slopes, even for the pilot injection, what ensures the consistency with the experimental data.

4.4.2 Bowl geometry generator

The generation of the combustion chamber geometry is one of the most time consuming steps in an optimization, specially when coupled with an evolutionary optimization method with a large population. For that reason, a code capable of generating an arbitrarily shaped axisymmetric piston bowl geometry and automatically producing a block structured mesh suitable for KIVA-3v and StarCD was developed. The code generates the new piston shape and adjusts the clearance height to achieve a target CR. The bowl shape is parametrized by five control points, as shown by p1 to p5 in Fig. 4.7. Each control point is connected by a Bezier spline that is controlled by another 8 offline control points (Bezier control points that are not part of the piston shape), which are represented as arrows in Fig. 4.7.

Since the control points of a Bezier curve are compulsory tracks for the curve, they determine the depth of the bowl and if it is going to be reentrant or not, giving a general idea of the shape of the combustion chamber. The control points need 2 coordinates to completely define them (X and Y position) so a

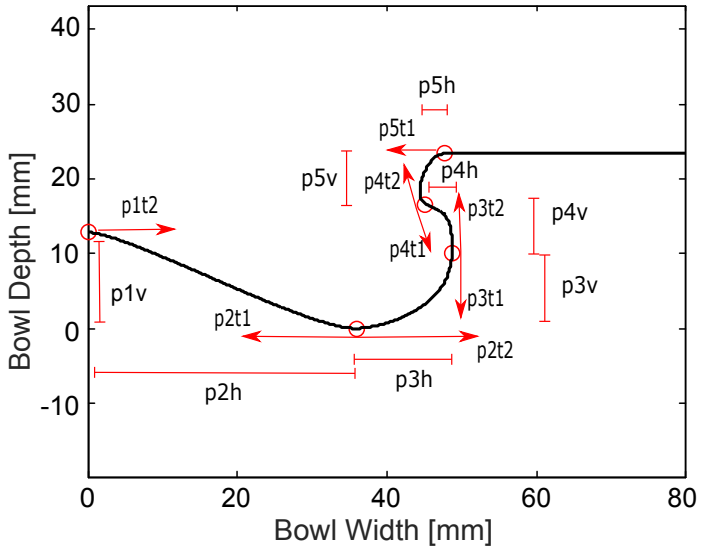

Figure 4.7. *Distribution of Bezier parameters in the geometry generator tool. The circles are the control points p1 - p5.*

total of 26 parameters are needed to complete define the final spline generated by the code. However, 26 inputs are not acceptable due to the required size of the population that would be needed to optimize an engine with that flexibility. In order to reduce the inputs of the geometry tool several hypothesis were assumed.

- The bowl chamber geometry is symmetric, so the slope of the spline in the symmetric axis is 0 and only 1 parameter is need to define the arrow of the Bezier point 1 (p1t2h).
- The piston shape defined by the 5 bezier points will always connect to a horizontal line so the slope of the curve in the last Bezier point is also 0 and the arrow of the last Bezier point can be defined only by 1 parameter (p5t1h)
- The connection between 2 curves defined by Bezier points should be smooth so the slope of both of the arrows for each Bezier point should have the same value. This means that only 3 parameters are needed to define both arrows on each bezier point.
- The X coordinate of the first Bezier point is always 0.

- The Y coordinate of the second Bezier point is 0, being always the point with maximum depth. The derivative on this point is also 0.

Taking into account all the hypothesis only 15 input parameters are needed. The Bezier points function of the 15 input parameters are defined in equation 4.1 to 4.27, where the bowl maximum width is defined as maxW, the bowl maximum depth is defined as maxD, cell size is defined as dS and G1-G15 are the 15 input parameters optimized in the evolutionary optimization.

$$p1h = 0 \tag{4.1}$$

$$p1v = G1 * (maxD - 3 * dS) \tag{4.2}$$

The coordinate p1v can not have the value maxD in order to avoid interactions between the bowl central protrusion and the injector so the maximum value that p1v can reach is limited.

$$p2h = G2 * maxW \tag{4.3}$$

$$p2v = 0 \tag{4.4}$$

$$p3h = p2h + G3 * (maxW - p2h) \tag{4.5}$$

$$p3v = G4 * maxD \tag{4.6}$$

The parameter G5 is the only parameter that goes from -1 to 1 because it has to define if the geometry is reentrant or non-reentrant. If G5 is positive and the geometry is non-reentrant, the code uses equation 4.7 to define p4h.

$$p4h = p3h + G5 * (maxW - p3h) \tag{4.7}$$

However, if the geometry is reentrant, the code uses equation 4.8 to define p4h.

$$p4h = p3h + G5 * (p3h - p2h) \tag{4.8}$$

$$p4v = p3v + G6 * (maxD - p3v) \tag{4.9}$$

$$p5h = p4h + G7 * (maxW - p4h) \tag{4.10}$$

$$p5v = p4v + G8 * (maxD - p4v) \tag{4.11}$$

$$p1t2h = G9 * (p2h - p1h) \tag{4.12}$$

$$p1t2v = 0 \tag{4.13}$$

$$p2t1h = G10 * (p2h - p1h) \tag{4.14}$$

$$p2t2h = G10 * (p3h - p2h) \tag{4.15}$$

$$p2t1v = p2t2v = 0 \tag{4.16}$$

$$p3t1h = G11 * (p3h - p2h) \tag{4.17}$$

$$p3t1v = G12 * (p3v - p2v) \tag{4.18}$$

$$p3t2h = G12(maxW - p3h) \tag{4.19}$$

$$p3t2v = p3t2h * \frac{p3t1v}{p3t1h} \tag{4.20}$$

$$p4t1h = G13 * (p4h - p3h) \tag{4.21}$$

$$p4t1v = G14 * (p4v - p3v) \tag{4.22}$$

Similar to equation 4.7 and 4.8, if the bowl has a non-reentrant shape equation 4.23 is used.

$$p4t2h = G14 * (p5h - p4h) \tag{4.23}$$

if the bowl has a reentrant shape equation 4.24 is used.

$$p4t1h = G14 * (p2h - p4h) \tag{4.24}$$

$$p4t2v = p4t2h * \frac{p4t1v}{p4t1h} \tag{4.25}$$

$$p5t1h = G15 * (p5h - p4h) \tag{4.26}$$

$$p5t1v = 0 \tag{4.27}$$

In order to have a better understanding of the influence of each geometric parameter on each dimension of the bowl, Fig. 4.8 represents the 15 parameters.

To illustrate the flexibility of the code, a test was performed to the in-house geometry code with the most common bowl geometries until date and results are shown in Fig. 4.9.

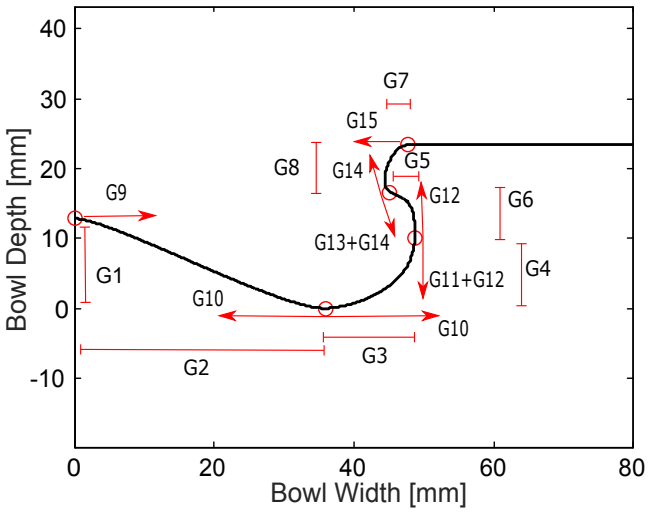

Figure 4.8. *Optimization parameters related to Bezier geometric points used in the geometry tool.*

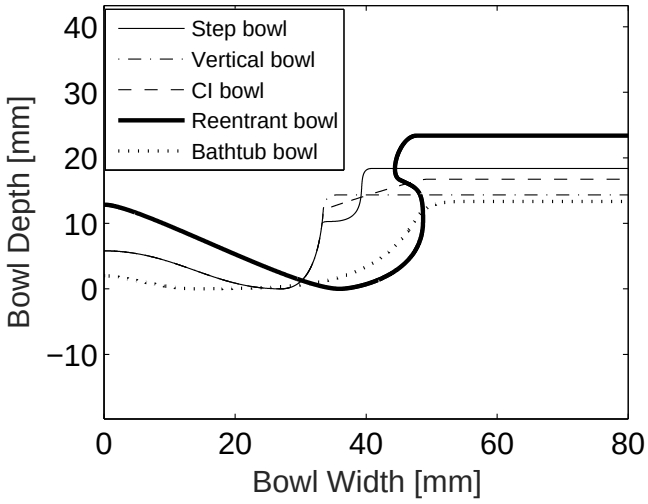

Figure 4.9. *Example of geometries generated with the geometry generator tool..*

4.4.3 Pumping work model

An in-house code is used to estimate the pumping work needed to achieve the required intake boost to estimate the net indicated work (NIE). The model is based on basic thermodynamic calculations supported by the hypothesis marked below.

- Compressor and turbine work are considered equal so no mechanical losses are taken into account.
- The compressor and turbine efficiencies are considered constant.
- A constant pressure drop is considered between the compressor and the engine intake valve to simulate the effect of the aftercooler.

The target of this Thesis is to optimize an engine and not a turbocharger. Accordingly, it is assumed that, for every case simulated, the turbocharger has been chosen to have a compressor and turbine efficiency of 70% and 80%, respectively. The aftercooler pressure drop is set to 0.15 bar. These assumptions have been previously accepted in other studies with successful results [26].

4.4.4 Genetic algorithm

In this section the selection of the best GA for this Thesis and the optimal calibration for that algorithm is performed. Note that this approach is not performed for the non-evolutionary optimization methods because in the literature it was concluded that the RSM coupled with a CCD was the best option due to its capability of predicting non-linear shapes and coupled effects.

4.4.4.1 Genetic algorithm benchmarking

The genetic algorithms presented in section 3.3.1 were written in Matlab and their performance was compared. The fitness function used for the performance test is described in equation 4.28, where s is the number of variables.

$$FitnessFunc = \prod_{i=1}^{s} |15 * X_i * (1 - X_i) * sin(n * \pi * X_i)| \tag{4.28}$$

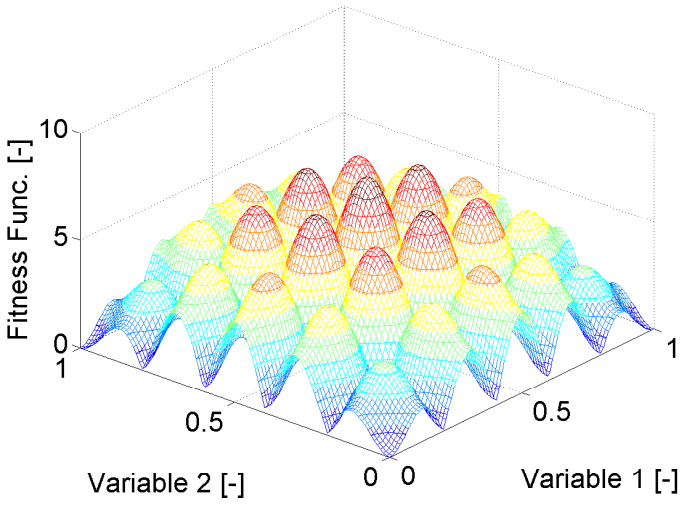

Figure 4.10. *Fitness function output for s=2 and n=5.*

When n is odd, the function has its maximum at 0.5 and many peaks with local optimums to make it difficult to find the absolute solution. Fig. 4.10 shows the fitness function output for s=2 and n=5. All three algorithms were tested with this function starting from the same initial point [0.1 , 0.1 , 0.1] and the results are shown in Fig. 4.11. The optimizations were run until 2000 function evaluations were performed or the optimum was reached. Additionally, all the optimizations were repeated 100 times because they are not guaranteed to reach the same optimum every time due to the randomness involved in the mutations. The plotted line represents the average results every 100 function evaluations and the gray shade represents the dispersion of the 100 repetitions. It can be seen that, even though all three genetic algorithm are able to reach the optimum after 500 function evaluations, the DKGA algorithm is able to always find the absolute optimum after 800 evaluations while the NSGA-II needs 1300 evaluations and the micro-GA can not assure a 100% success rate with 2000 function evaluations.

The difficulty of the test was increased to s=2 and n=25, Fig. 4.12 shows the output of the benchmark function. Following the same criteria, 100 repetitions of the optimization were performed and the results are shown in Fig. 4.13. Similar to the previous test, DKGA, NSGA-II and micro-GA are able to find the absolute optimum, however, the differences between the algorithms seem to increase with the increasing difficulty. After 2000 function

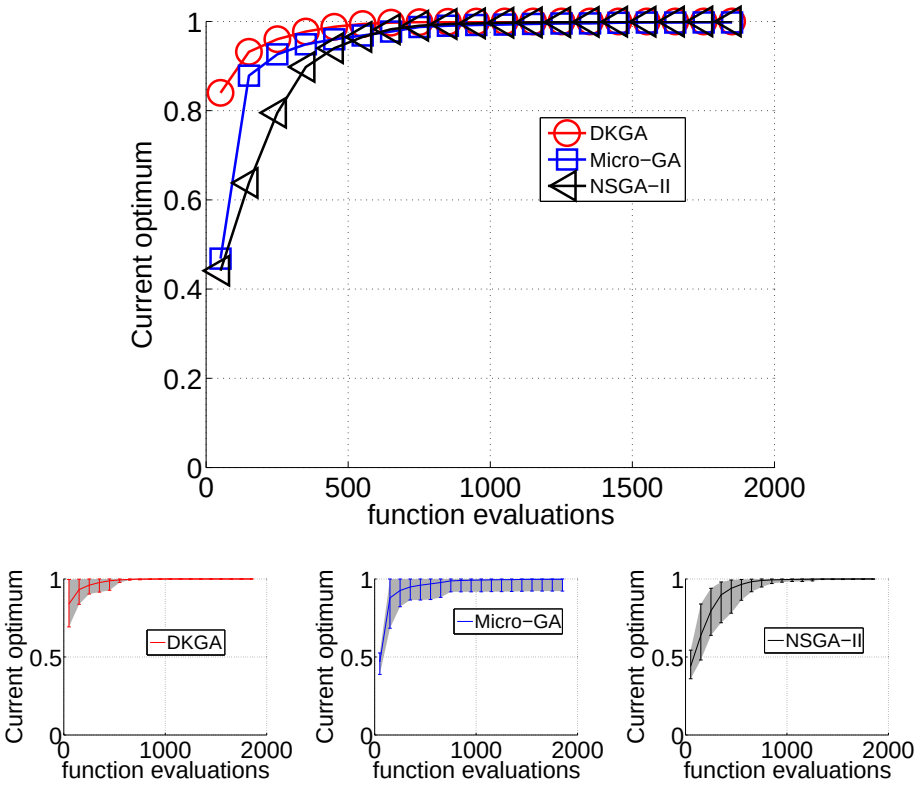

Figure 4.11. *Optimization results for the benchmark function with 2 variables and n=5 with DKGA algorithm, micro-GA and NSGA II. Top figure compares the average result for 100 repetitions with the three optimization algorithms. The bottom figures show the average result of 100 optimizations with a line and the dispersion with a gray shade.*

evaluations the DKGA algorithm is the only one that guarantees to find the absolute optimum. This means that the DKGA is able to avoid local optimums and keep searching for the absolute optimum better than the other two algorithms, which is a key aspect of this type of optimizations.

A third difficulty was tested with s=22 and n=25. The number of variables chosen was based on the number of inputs optimized in the evolutionary optimization chapter aiming to simulate a problem with equivalent difficulty. Additionally, 2000 function evaluations were not considered enough to give an accurate result of the performance of the algorithm with this problem so it was

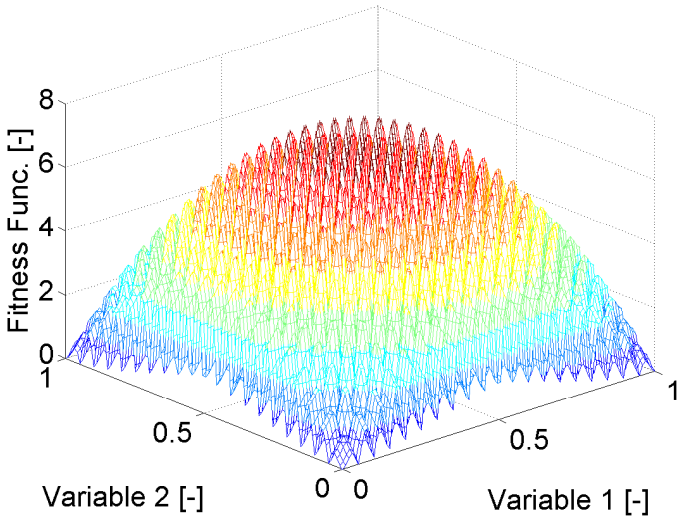

Figure 4.12. *Fitness function output for s=2 and n=25.*

increased to 15000 function evaluations. The results are shown in Fig. 4.14. These results show that the DKGA is able to find the optimum on most of the repetitions after 13000 function evaluations while the micro-GA and the NSGA-II are not able to find the absolute optimum in any of the repetitions.

A final test was performed with a different test function. It is known that the behavior of the benchmark functions and an engine are not necessarily equal so in order to have a closer view of the algorithms with a real case, the response surface calculated in section 5.3 for the non-evolutionary optimization with 6 parameters was used to test the performance of the DKGA, micro-GA and NSGA-II. The results are shown in Fig. 4.15. Similar to the previous tests, the DKGA is faster and more robust than the rest of the algorithms. Although the reasoning behind it is unclear, the NSGA-II and micro-GA were outperformed by the DKGA. For that reason, it was chosen for this study and was coupled with KIVA-3v.

4.4.4.2 DKGA setup parameters

The DKGA coupled with the benchmark fitness function for 22 variables and n=25 was tested to determine the best values for the algorithm parameters. The main parameters of the DKGA are the σ that controls the

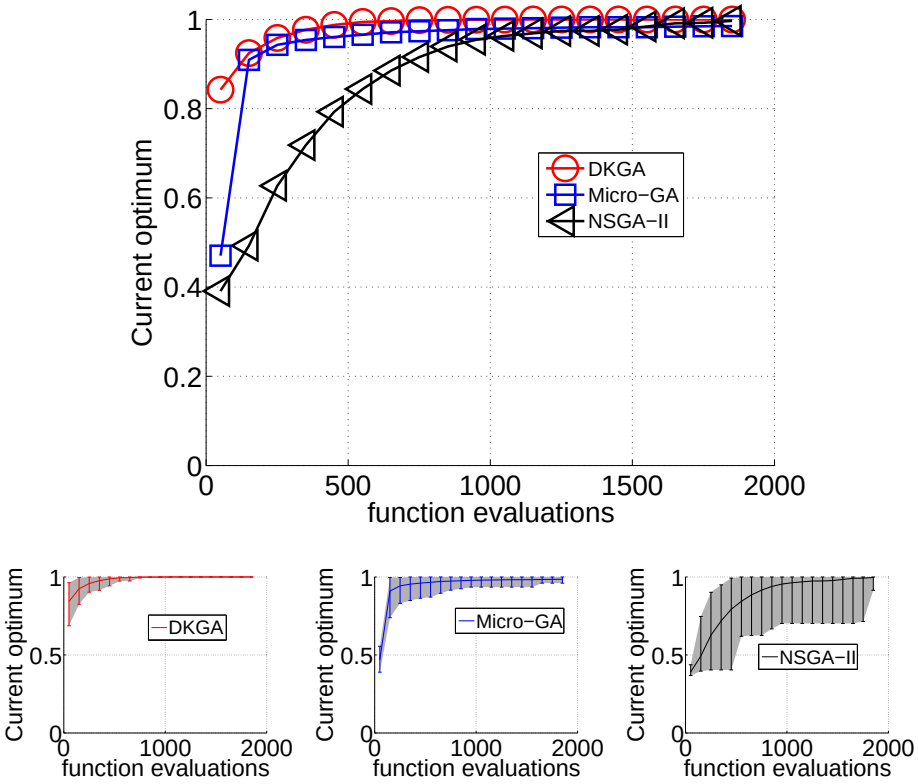

Figure 4.13. *Optimization results for the benchmark function with 2 variables and n=25 with DKGA algorithm, micro-GA and NSGA II. Top figure compares the average result for 100 repetitions with the three optimization algorithms. The bottom figures show the average result of 100 optimizations with a line and the dispersion with a gray shade.*

convergence law, the population and the maximum number of generations. Fig. 4.16 shows the average results for different σ after 100 repetitions. It can be seen that for higher σ values, the algorithm shows a faster converge rate because the mutation range is quickly restricted and the case is forced to converge. However, if σ is too high, the algorithm has more difficulties to avoid local optimums. In this case the optimum seems to be at $\sigma = 7$ were there is a compromise between a fast convergence but enough mutation range.

Additionally, different populations were tested and the results are shown in Fig. 4.17. The results show that higher population always improve the

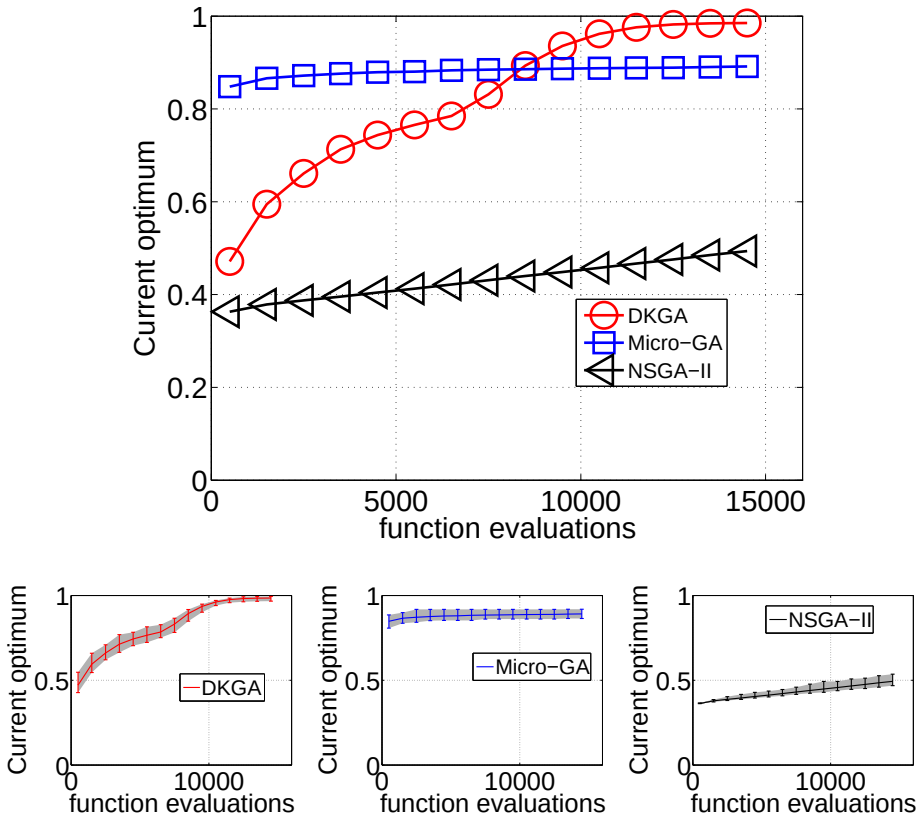

Figure 4.14. *Optimization results for the benchmark function with 22 variables and n=25 with DKGA algorithm, micro-GA and NSGA II. Top figure compares the average result for 100 repetitions with the three optimization algorithms. The bottom figures show the average result of 100 optimizations with a line and the dispersion with a gray shade.*

results. This behavior was expected since for the same amount of generations, the higher the population the higher the chances of finding a better optimum each generation. Therefore, a population of 529 cases per generation was chosen because it was the maximum capability for the available resources. It has to be taken into account that higher population means more simulations but since they are all done simultaneously, increasing population does not increase the time cost of the optimization significantly, contrary to increasing maximum number of generations.

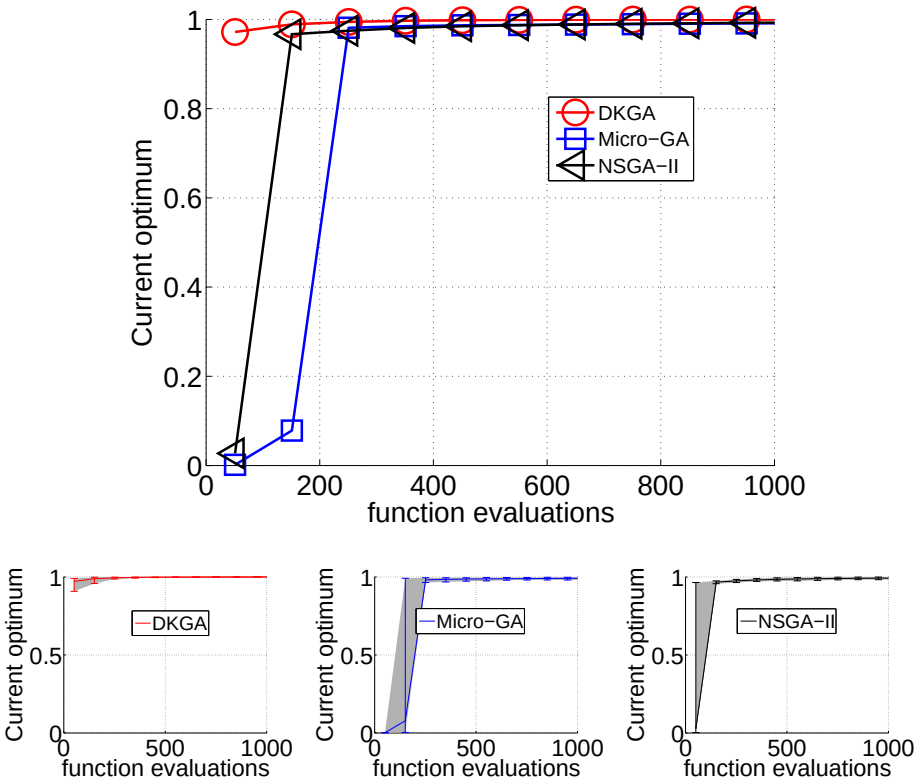

Figure 4.15. *Optimization results for the RSM generated in the non-evolutionary optimization with 6 parameters with DKGA algorithm, micro-GA and NSGA II. Top figure compares the average result for 100 repetitions with the three optimization algorithms. The bottom figures show the average result of 100 optimizations with a line and dispersion with a gray shade.*

Finally, a set up of 529 cases per generation and $\sigma = 7$ was used to test the effect of the maximum number of generations. Fig. 4.18 shows the results for 30, 40 and 50 maximum number of generations. It can be seen that the average results of the optimization is not very sensitive to the maximum number of generations; however, Fig.4.18 (Right) shows that the dispersion of the results for the 100 repetitions is strongly affected by this parameter. Even though the time cost of the whole optimization is proportional to the maximum number of generations and the time cost is one of the main aspects of a GA optimization, the robustness and reliability of the optimization was chosen as the main

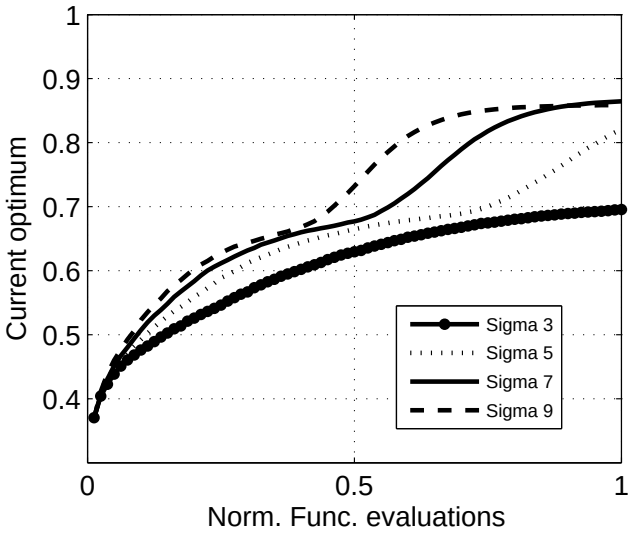

Figure 4.16. *Average optimization results for different σ values.*

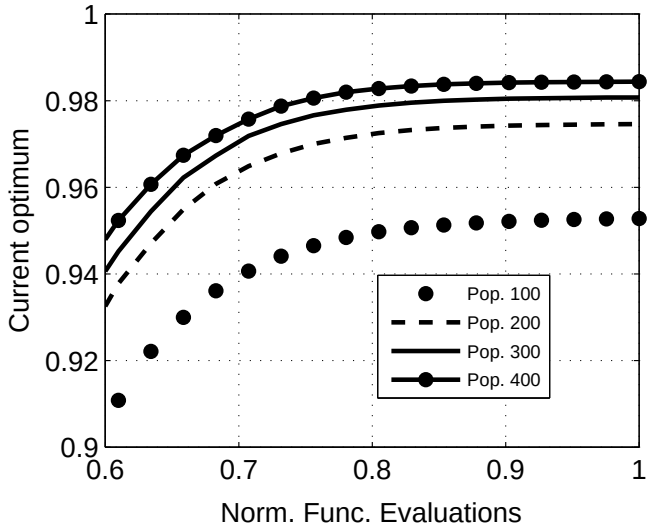

Figure 4.17. *Average optimization results for different population per generation.*

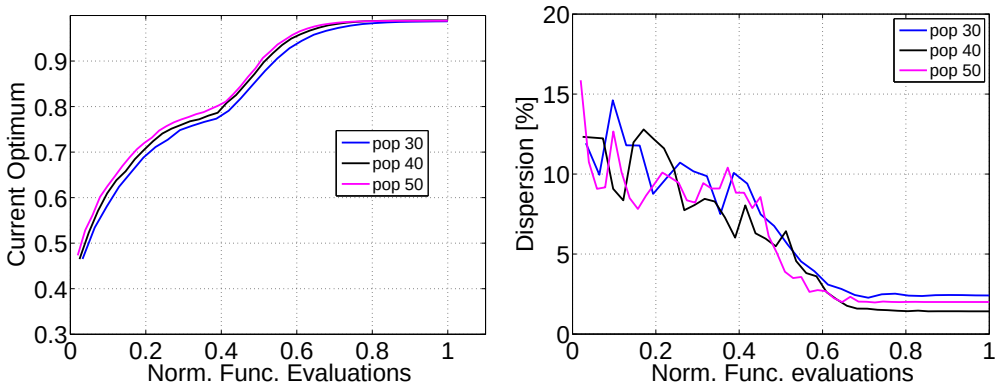

Figure 4.18. *(Left) Average optimization results for different maximum number of generations, (Right) maximum dispersion of the 100 optimization repetitions for different maximum number of generations.*

criteria for this optimization and, as seen in Fig 4.18 (Right), a value of 40 gives the best result.

4.5 Optimization methodology

Accuracy is one of the most difficult aspects when optimizing unknown processes that cannot be tested experimentally. Part of this inaccuracy comes from the CFD model but an important fraction also comes from the optimization methodology. For that reason two methodologies (based on the same principle) were developed for this study and are described in this section.

4.5.1 Non-evolutionary optimization methodology

A sketch of the methodology for non-evolutionary optimizations is represented in Fig. 4.19. The methodology described in this section has 3 different stages. Each of them has their own tools, which are described in the tools section.

The first step is the configuration of the CFD model used for the later optimization. It has to be properly calibrated and validated with experimental data because the main objective of the optimization process is to vary parameters in a given range so not having a well calibrated model could change

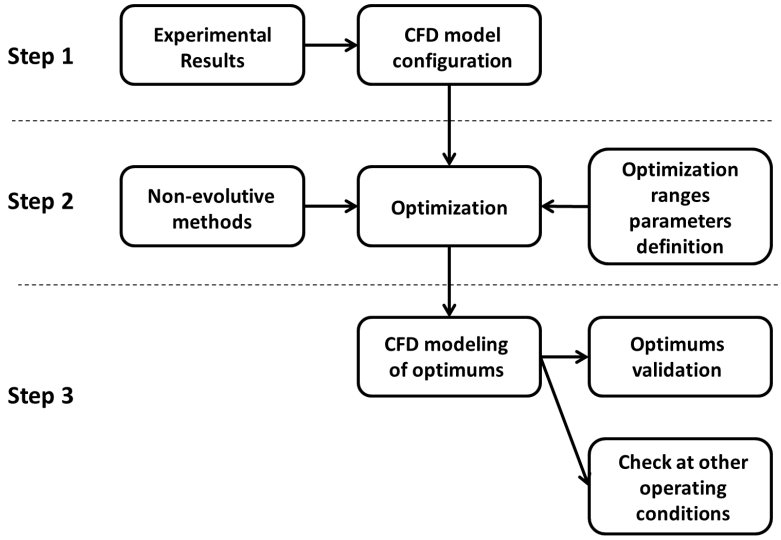

Figure 4.19. *Sketch of the methodology for non-evolutionary optimizations.*

the trends provided by the engine. The following stage is dedicated to the optimization of the combustion system. The methodology for this optimization is based on RSM methods. The final stage focuses on validating the optimums. Once the RSM is applied, a series of convenient optimums are obtained from the response surface and those optimums have to be validated with the CFD model to ensure the accuracy of the method. Additional validations at other operating conditions are necessary to check if the new set up has a better performance than the original in well-representative points of the engine map. Finally, the optimum configuration has to be validated experimentally to check is the results predicted by the CFD are correct.

4.5.2 Evolutionary optimization methodology

A sketch of the methodology for evolutionary optimizations is represented in Fig. 4.20. The methodology described in this section has 3 different stages. Each of them has their own tools, which are described in the tools section.

The first step is common with the non-evolutionary optimization, the configuration of the CFD model has to be properly calibrated and validated with experimental data. This step becomes a hard task when the optimization is focused on new combustion concepts or fuels because the experimental

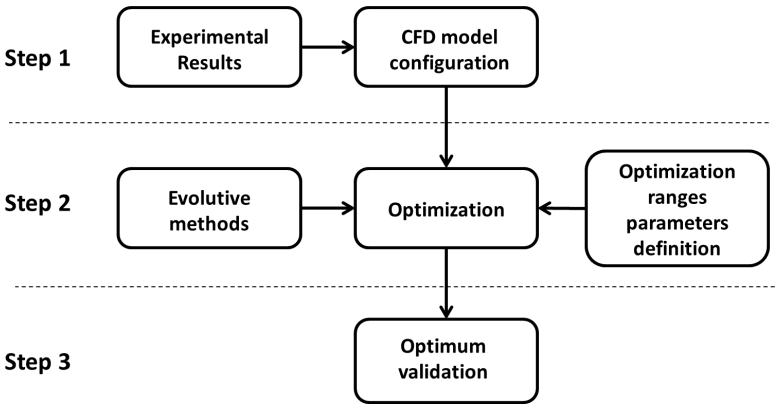

Figure 4.20. *Sketch of the methodology for evolutionary optimizations.*

data available is limited, accordingly new ways of validation have to be found. An example of this issue can be found in the validation of the CFD model working with a DME fueled diesel engine, the results are presented in section 4.3.2.2. The second stage is dedicated to the optimization of the combustion system. The methodology for this optimization is based on genetic algorithms, particularly the DKGA. This method was selected due to its superior performance compared to other algorithms. Finally, the optimum obtained from the optimization process has to be validated experimentally.

4.5.2.1 Optimization methodology improvements

Most of the tools presented in this chapter were developed and coded for this work except for the CFD codes and part of the DKGA code. The CFD codes can not be modified but the GA code, which is the key of the optimization, was modified to be more robust and faster. Even though not all the ideas ended up with successful results, some of them are presented in this section.

Mutation generation

It was said in the description of the DKGA algorithm that the mutated values were a random number from a normal distribution with its mean set to the non-mutated value and the standard deviation controlled by the DKGA. That definition work well when the non-mutated value is far from the input range limit but when the mean value of the normal distribution is close or

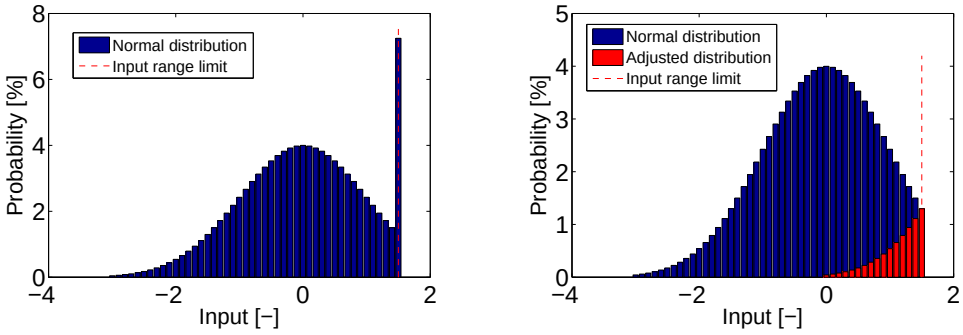

Figure 4.21. *Mutation normal distribution for (Left) original behavior, (Right) improved behavior. Input range limit represented by a red line.*

at the range limit, all the values higher than the boundary are set to the maximum value allowed, generating an increasing probability of mutating to the limit value. This behavior can be seen in Fig. 4.21 (Left). That aspect of the GA was noticed because many input parameters were located at the boundaries of the input ranges after a few iterations and they were not able to properly scan the rest of the domain. In order to solve the problem it was proposed to treat the boundary as a mirror. The behavior of the new proposed method is represented in Fig. 4.21 (Right). The performance of both approaches was tested for the same problem and the results proved the superiority of the new approach.

After the mutation operator improvement the calculations and the input values distributions were closely monitored and a potential new problem was noticed. The NA of many optimizations was guided towards a high value (usually 90 deg or close) because that way the spray did not have to interact with the geometry and then, once the air management and injection settings were optimized, the NA was reduced and the geometry was finally optimized. This behavior has a negative impact on the optimization because the geometry (15 parameters out of the 22 optimization parameters) has almost no influence for half of the optimization and many resources are wasted during those generations. The solution proposed was to force the algorithm to divide the NA optimization range in sections, as seen in Fig.4.22, and always keep at least two children in each of the NA range sections (two children per section are kept with the elitism mechanism). However, after several tests the new approach was rejected, mainly because forcing the elitism mechanism to store children with different NA values is equivalent to divide the potency of the

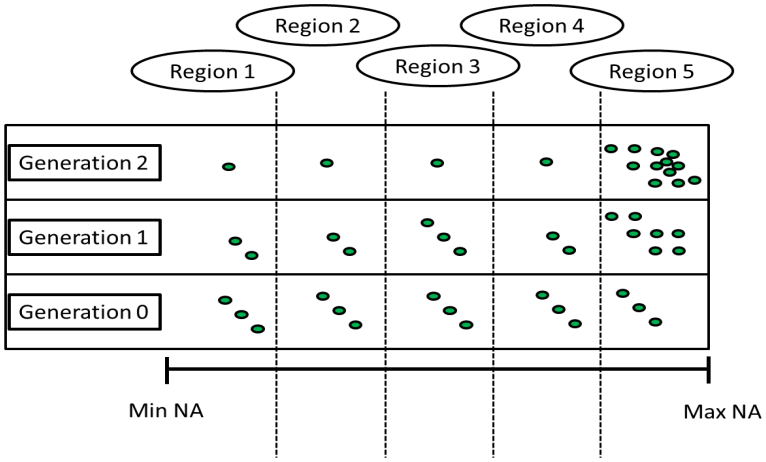

Figure 4.22. *Range of NA parameter divided in 5 sections.*

algorithm into the number of NA sections and the results proved to be worse in all cases.

Restriction function

This idea was born due to the difficult task of programming an automatic mesh generator for Kiva. Once the bowl geometry is generated by the input parameters and bezier curves, it has to be converted into a mesh readable by Kiva. However, the Kiva mesh generator has not been updated for a long time and that means that it is very rigid, the curves have to be correctly structured into blocks and the cells have to be properly described. Knowing the flexibility of the geometry generator tool presented in section 4.4.2 it is understandable that some critical shapes (note that not all the shapes are as good looking as the ones presented in this chapter) can not be properly converted into a mesh and the CFD cases would not work. For that reason, when the first attempts to run the complete system was successful it was noticed that about 20% of cases produced some kind of error due to the geometry and that error was reduced progressively while the optimization advanced due to the convergence nature of the algorithm. That 20% of the cases that do not work imply that the effective population of the optimization is reduced by a 20% and lower population reduces the effectiveness and robustness of the optimization.

The solution to the problem was to apply a double check to each generated case in each generation of the optimization with a function called *restrictions*. The double check consists on checking the Kiva mesh generator software

output to make sure that the mesh is properly generated and no inversion cells are found. This solution increased the time needed to generate a complete new generation of cases by about 1 hour but was able to reduce the amount of error cases to less than 2%. The *restrictions* function was further expanded to other aspects of the optimization process and the error cases per generation was finally reduced to less than 1%.

DKGA coupled with COSSO

One of the main problems with CFD optimization coupled with genetic algorithms is the time cost. Usually, CFD simulations of ICE engines take several hours or even days to finish so reducing the number of generations that a genetic algorithm needs to converge is one of the main research topic in this field. For that reason a new approach was proposed, the coupling of the DKGA algorithm with the COSSO tool, a non-parametric [1] regression model based on the Component Selection and Smoothing Operator (COSSO) [27]. The sketch of the new optimization methodology is presented in Fig. 4.23.

The main idea behind this approach is that the COSSO tool does not affect the genetic algorithm process when the predictions of COSSO are not good enough, but when the predictions of COSSO are good enough, then that optimum obtained form the COSSO tool is added to the elitism group. With this approach a new complementary convergence criteria was added, if the COSSO tool finds three times in a row an optimum that becomes the fittest individual of the next DKGA generation, then the optimization is considered converged. The approach was tested several times with different number of generations and populations but the COSSO tool was never able to improve the predictions of the DKGA. Therefore, this approach was removed because it increased the postprocess time cost.

4.6 Summary and conclusions

The theoretical and experimental tools used in this Thesis were presented in detail in this chapter. In the experimental tools section, the experimental facilities used to obtain the validation data for the CFD models calibration were presented. In the theoretical tools section, the CFD softwares and the in-house codes developed for this Thesis were presented. Additionally, all the genetic algorithms presented in the review chapter (see section 3.4 to find the

[1] Non-parametric regression models are models that do not have a predefined predictor form. That means that they are more flexible and able to better adjust diverse data shapes but at the same time they need more data to be trained.

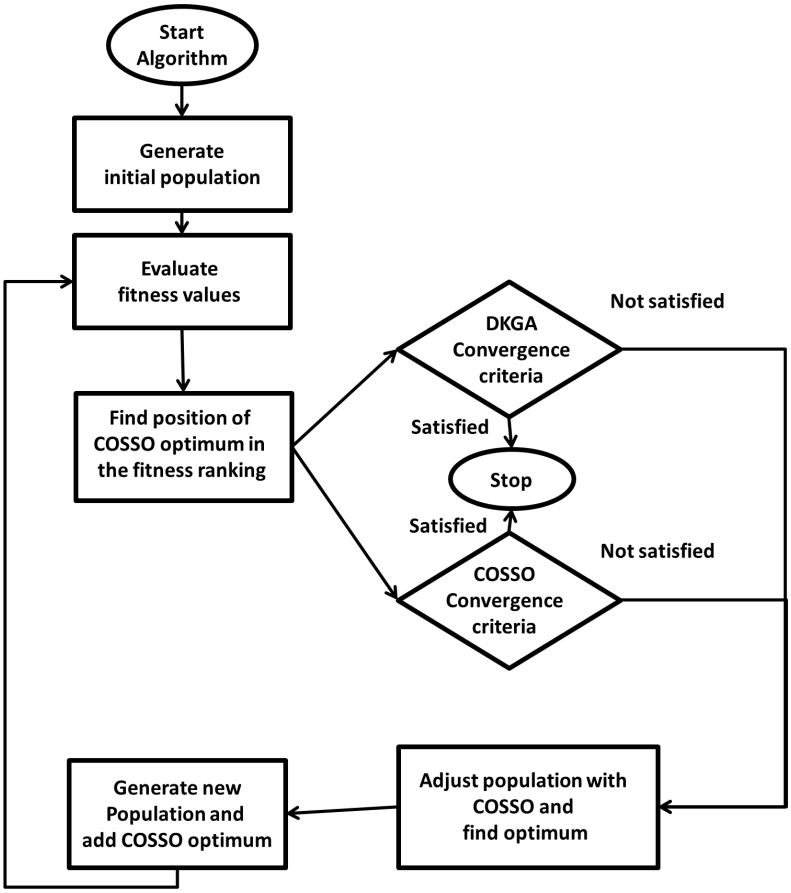

Figure 4.23. *Sketch of the structure of a DKGA algorithm coupled with COSSO.*

explanation of why non-evolutionary algorithms are used for CDC engines and evolutionary algorithms are used for DME fueled engine.) were compared and the results proved a clear superiority of the DKGA code. Finally the set up constants for the DKGA were tested and optimized, ensuring that all the tools presented in this chapter were ready to use in it optimal condition. Finally, the methodologies followed during the optimizations performed for this thesis and the most relevant improvements were described.

The tools and methodologies presented in this chapter, together with the knowledge obtained from the literature review chapters ensures that the objectives proposed for this Thesis can be achieved.

References

[1] Lapuerta M, Armas O and HernÃ¡ndez JJ. "Diagnosis of DI Diesel combustion from in-cylinder pressure signal by estimation of mean thermodynamic properties of the gas". *Applied Thermal Engineering*, Vol. 19 n^o 5, pp. 513–529, 1999.

[2] Payri F, Molina S, MartÃn J and Armas O. "Influence of measurement errors and estimated parameters on combustion diagnosis". *Applied Thermal Engineering*, Vol. 26 n^o 2, pp. 226–236, 2006.

[3] Bosch W. "The fuel rate indicator: a new measuring instrument for display of the characteristics of individual injection". *SAE Technical Paper*, 1966.

[4] Siemens. *STAR-CD METHODOLOGY. Version 4.18.* 2012.

[5] Colin O and Benkenida A. "The 3-zones extended coherent flame model (ECFM3Z) for computing premixed/diffusion combustion". *Oil & Gas Science and Technology*, Vol. 59 n^o 6, pp. 593–609, 2004.

[6] Karlsson A, Magnusson I, Balthasar M and Mauss F. "Simulation of soot formation under diesel engine conditions using a detailed kinetic soot model". *SAE Technical Paper*, 1998.

[7] Hiroyasu H and Kadota T. "Models for combustion and formation of nitric oxide and soot in direct injection diesel engines". *SAE Technical Paper*, 1976.

[8] Huh KY and Gosman AD. "A phenomenological model of diesel spray atomization". *Proceedings of the international conference on multiphase flows*, Vol. 2, pp. 515–518, 1991.

[9] Reitz RD and Diwakar R. "Structure of high-pressure fuel sprays". *SAE Technical Paper*, 1987.

[10] Habchi C, Lafossas FA, BÃ©ard P and Broseta D. "Formulation of a one-component fuel lumping model to assess the effects of fuel thermodynamic properties on internal combustion engine mixture preparation and combustion". *SAE Technical Paper*, 2004.

[11] Yakhot V and Orszag SA. "Renormalization group analysis of turbulence. I. Basic theory". *Journal of scientific computing*, Vol. 1 n^o 1, pp. 3–51, 1986.

[12] Angelberger C, Poinsot T and Delhay B. "Improving near-wall combustion and wall heat transfer modeling in SI engine computations". *SAE Technical Paper*, 1997.

[13] Issa RI. "Solution of the implicitly discretised fluid flow equations by operator-splitting". *Journal of computational physics*, Vol. 62 n^o 1, pp. 40–65, 1986.

[14] Amsden AA. "KIVA-3V, release 2, improvements to KIVA-3V". *Los Alamos National Laboratory, Los Alamos, NM, Report No. LA-UR-99-915*, 1999.

[15] Beale JC and Reitz RD. "Modeling spray atomization with the Kelvin-Helmholtz/Rayleigh-Taylor hybrid model". *Atomization and sprays*, Vol. 9 n^o 6, 1999.

[16] Ra Y and Reitz RD. "A reduced chemical kinetic model for IC engine combustion simulations with primary reference fuels". *Combustion and Flame*, Vol. 155 n^o 4, pp. 713–738, 2008.

[17] Abani N, Munnannur A and Reitz RD. "Reduction of numerical parameter dependencies in diesel spray models". *Journal of Engineering for Gas Turbines and Power*, Vol. 130 n^o 3, pp. 032809, 2008.

[18] Perini F. "Optimally reduced reaction mechanisms for Internal Combustion Engines running on biofuels". *PhD, UniversitÃ diModena e Reggio Emilia*, 2011.

[19] Han Z and Reitz RD. "Turbulence modeling of internal combustion engines using RNG K-e models". *Combustion science and technology*, Vol. 106 n^o 4-6, pp. 267–295, 1995.

[20] Kokjohn SL and Reitz RD. "Investigation of the roles of flame propagation, turbulent mixing, and volumetric heat release in conventional and low temperature diesel combustion". *Journal of Engineering for Gas Turbines and Power*, Vol. 133 n^o 10, pp. 102805, 2011.

[21] Pan L, Kokjohn SL and Huang Z. "Development and validation of a reduced chemical kinetic model for dimethyl ether combustion". *Fuel*, Vol. 160, pp. 165–177, 2015.

[22] Abraham J. "What is adequate resolution in the numerical computations of transient jets?". *SAE Technical Paper*, 1997.

[23] Abani N, Kokjohn S, Park SW, Bergin M, Munnannur A, Ning W, Sun Y and Reitz RD. "An improved spray model for reducing numerical parameter dependencies in diesel engine CFD simulations". *SAE Technical Paper*, 2008.

[24] Munnannur A. *Droplet Collision Modeling in Multi-dimensional Engine Spray Computation*. ProQuest, 2007.

[25] O'Rourke Peter J and Amsden AA. "A spray/wall interaction submodel for the KIVA-3 wall film model". *SAE Technical Paper*, 2000.

[26] Benajes J, Novella R, De Lima D, TribottÃ© P, Quechon N, Obernesser P and Dugue V. "Analysis of the combustion process, pollutant emissions and efficiency of an innovative 2-stroke HSDI engine designed for automotive applications". *Applied Thermal Engineering*, Vol. 58 n^o 1, pp. 181–193, 2013.

[27] Lin Y. and Zhang H. "Component selection and smoothing in smoothing spline analysis of variance models". *Annals of Statistics*, Vol. 5, 2006.

,

Chapter 5

Conventional combustion engine optimization with non-evolutionary optimization methods

Contents

5.1 Introduction

The research work reported in this chapter describes the results obtained from the first optimization performed for this Thesis. It is important to remember that pollutant emission standards are becoming difficult to achieve and due to the promising long life of the diesel engines it is compulsory to keep

researching in this topic. For that reason, this chapter focuses on optimizing the combustion system of a MD 4-cylinder 4-stroke CDC engine following the non-evolutionary optimization methodology developed for this Thesis.

The optimization process carried out is divided in 2 stages, an initial and simpler optimization with 4 parameters mainly focused on geometry hardware, and a second more complete and complex optimization with 6 parameters that includes air management and injection parameters. Each stage follows the methodology developed for non-evolutionary optimizations.

- The initial part presents the optimization setup, this is, the parameters that are going to be optimized and the ranges of those parameters. Additionally, the objective of the optimization and the restrictions imposed for pollutant emissions are presented. Note that the first step where the CFD models are validated and calibrated discussed in the methodology section and will not be included in this chapter.

- The second part presents and analyzes the results. The optimum configuration is described and understood. In addition, the cause/effects of the inputs and outputs are detailed to clarify the reasons behind the new optimum configuration. Finally, the optimum configuration is applied to other operating conditions to ensure that the new configuration performs well in all engine operating points.

- The last part of the methodology includes the experimental validation of the optimums obtained from the CFD calculations. This step was not applied to the 4 parameter optimization since the benefits observed after the optimization were marginal, therefore there is only experimental data of the 6 parameter optimization optimums.

Both stages focus on two objectives: improve ISFC while keeping NOx-soot trade-off (Opt 1) and improve NOx-soot trade-off while keeping ISFC (Opt 2). It is important to highlight how despite the well-known trade-off existing between ISFC and BSFC, specially when the boost pressure is adjusted, the analysis was carried out considering ISFC and not BSFC since this research focuses on understanding the requirements of the combustion system to optimize the energy conversion from heat to work respecting emission constraints. These processes are intrinsically controlled by the combustion process, while the mechanical losses (including pumping losses) are not accounted for since they depend on external factors not directly controlled by the combustion process such as the lubrication and surface finish (friction

losses), the mechanical efficiency of auxiliary systems (auxiliary losses) or the turbocharging system efficiency and its matching (pumping losses).

Most of the RSM calculations are now shown in the results section but a detailed description of the process and the mathematical models used for this section can be found in annex 5.A.

5.2 Stage 1: 4 parameters DOE optimization

This section presents the results of the first optimization performed for this Thesis. It is the simplest optimization with only 4 parameters, this means that not all the important parameters can be considered, however, it also means that it is fast, needs less resources and provides early useful information for future stages. For that reason, this stage optimizes mainly geometric parameters aiming to obtain early information about the effect of the geometry over the combustion system.

5.2.1 Optimization parameters and setup

This stage focuses on investigating the impact of the engine hardware and nozzle configurations on emissions and fuel consumption, this is, the combustion chamber geometry, NA (note that in this Thesis the acronym NA refers to half included nozzle angle) and swirl number. These inputs were chosen trying to follow an optimization path based on designing a quiescent combustion system with low swirl and non-reentrant bowl shape, which is expected to improve engine efficiency by reducing the convective HT to the combustion chamber walls. The optimization focuses on finding both Opt1 and Opt2 (see table 4.5) for the medium speed/load condition, evaluating later the optimum configurations at low speed/load and high speed/load operation conditions. Air management and injection settings were kept constant at their reference values. Then, a double shot injection (pilot plus main) at the reference timings and IP were considered. The engine CR was also kept constant at the reference values shown in Table 4.1.

The bowl geometry was parametrized by means of two geometrical relations, the ratio between the rip bowl diameter (d) and the cylinder bore (B) and a second parameter (K) defined specifically to control the reentrant shape of the bowl avoiding the artificial generation of extremely deformed bowl shapes. Due to its definition, included in Fig. 5.1 together with the geometry of the central point of the DOE, the higher the K the more reentrant bowl shape.

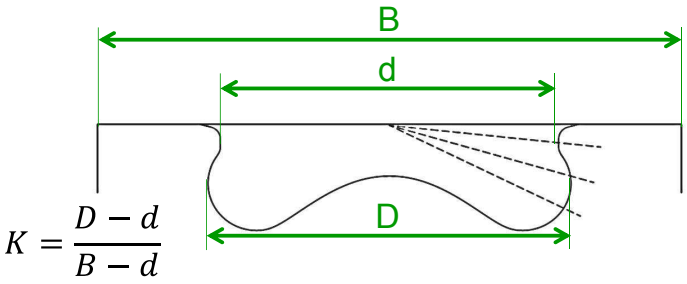

Figure 5.1. *Sketch of the bowl geometry for the central point of the DOE and definition of the K factor.*

Table 5.1. *Ranges of the input factors for the optimization Stage 1.*

	d/B	**K**	**swirl**	**NA**
	[-]	[-]	[-]	**[deg]**
Ref	0.57	0.14	2	74
min	0.53	0	0.5	70
max	0.63	0.2	2.5	78

In order to implement these geometric inputs in the optimization, the geometry generator tool presented in section 4.4.2 was simplified, the original 15 geometric parameters were combined into two final inputs, d/B and K, limiting the flexibility of the original tool to match the resources available for this optimization. The ranges for the input parameters used in Stage 1 are shown in Table 5.1.

As said in the methodology section, a CCD design defined the DOE test plan and a total of 25 simulation were needed. The distribution of the 25 cases compared to the baseline case are shown in Fig. 5.2.

5.2.2 Results and discussion

Before presenting the optimum and understanding the reasons behind its improvement, it is mandatory to understand the effect of each parameter optimized and why the optimum followed that optimization path. Fig. 5.3 and 5.4 show the effect of bowl geometry (d/B and K) and the effect of swirl and NA respectively on the end of combustion angle (CA90abs), ISFC and

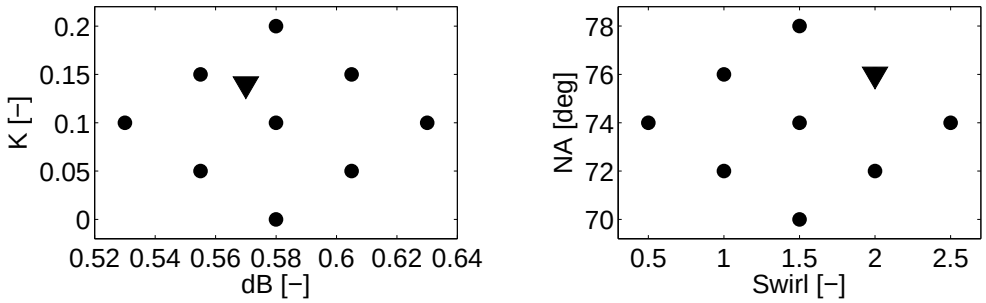

Figure 5.2. *DOE test plan for the input parameters in Stage 1. Reference engine represented as a triangle.*

NOx-Smoke emissions. In these figures, the red line[1] shows the isolated effect of the represented input parameter when the other inputs are set at constant values. The shade represents the results of the response surface, which contrary to the red line, takes into account the coupled effects between the inputs.

The general behavior of the inputs are already known so these red lines are only used to check if the isolated effects of each parameter are consistent, this is, if the RSM method and the CFD model are capturing properly the engine behavior. In this case it can be seen how the isolated effect of the swirl is well known [1]. Higher swirl values help the mixing process producing an improvement in ISFC followed by a NOx increase and a Smoke reduction. Regarding the geometric parameters, it is known that their effect over the combustion parameters is case specific so they are considered correct [2].

Focusing on the main general trends observed in Fig. 5.3, it can be seen that the geometric parameters have little effect over the engine behavior. Increasing bowl diameter (d/B) results in a slightly later CA90abs but ISFC stays unaffected. Higher d/B also decreases NOx but its effect is moderate and the engine is able to achieve the emissions target for almost every d/B value. In terms of the reentrant shape of the bowl (K), more reentrant bowls advance the CA90abs while decreasing ISFC. NOx emissions also decrease for higher K but Smoke was much less affected.

Switching to the most relevant trends observed in Fig. 5.4, increasing swirl advances CA90abs and increases combustion efficiency reducing ISFC. Higher

[1] In some figures the red line is not present because it is located over the axis range.

Table 5.2. *Optimized combustion systems after Stage 1.*

	d/B	**K**	**swirl**	**NA**
	[-]	[-]	[-]	[deg]
S1 Opt1 (best ISFC)	0.605	0.15	2	76
S1 Opt2 (best NOx-Smoke)	0.595	0.06	2	75

swirl also increases NOx and reduces Smoke making it impossible to satisfy Smoke target levels with low swirl levels. Finally, increasing NA provided better results in terms of ISFC with advanced CA90abs but increases NOx emissions. The Smoke emissions, just like with other inputs, is able to reach any wanted value for any NA value.

On the light of the results, Table 5.2 describes the two optimum combustion systems defined following two different optimization paths, minimizing ISFC keeping emissions (S1 Opt1), and improving the NOx-Smoke trade-off accepting 2% ISFC penalty (S1 Opt2). The optimized bowl profiles compared to that of the reference combustion system are shown in Fig. 5.5. Observing this data, both optimization paths resulted in similar bowl diameter, with d/B around 0.6, but more reentrant shape was required for the minimum ISFC criterion compared to the improving NOx-Smoke trade-off criterion. In all cases higher NA than the reference engine were obtained, specially for the minimum ISFC combustion system configuration, and swirl levels were forced to be high to improve ISFC and control Smoke.

The two optimized configurations were modeled by CFD for their first validation and the results are included in Fig. 5.6 compared to those of the reference engine. It is shown how S1 Opt1 (best ISFC) provided slightly decreased fuel consumption by less than 0.5%, while NOx slightly increases by 1.4% and the Smoke level is nearly unchanged, keeping Smoke below 0.1 FSN. For S1 Opt2 (best NOx-Smoke trade-off) NOx decreases by 17% with Smoke still below 0.1 FSN at the expense of a minor increment in ISFC by 0.7%, below the acceptable limit. The two optimized piston bowl geometries were also evaluated at the other two operating conditions, 1800 rpm - high load and 1200 rpm - low load. Results shown in Fig. 5.6 confirm that both optimized piston bowl geometries also work adequately in these other operating conditions.

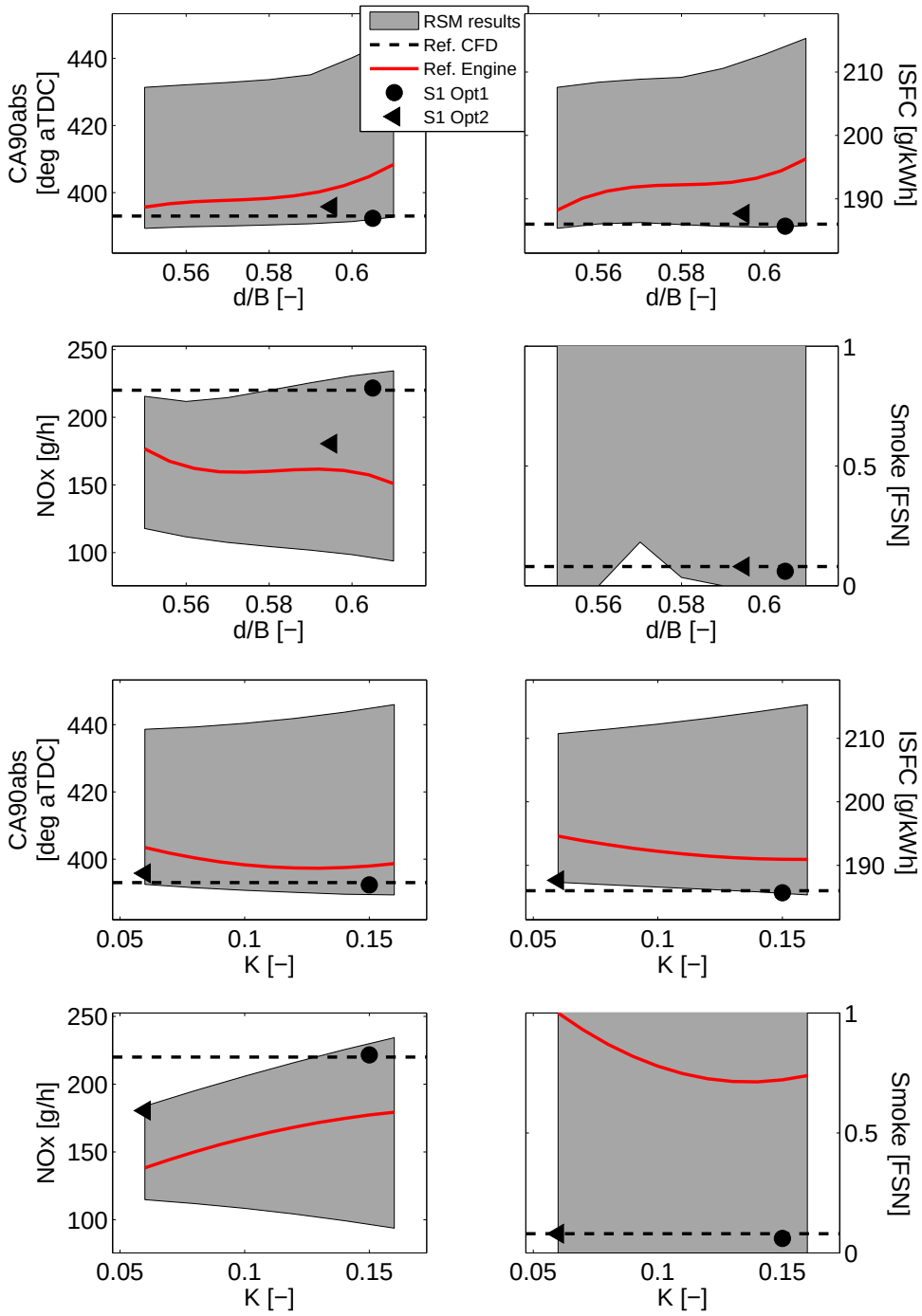

Figure 5.3. *Effect of d/B (top) and K (bottom) on key combustion, emissions and performance parameters. Reference engine levels are included as dashed lines.*

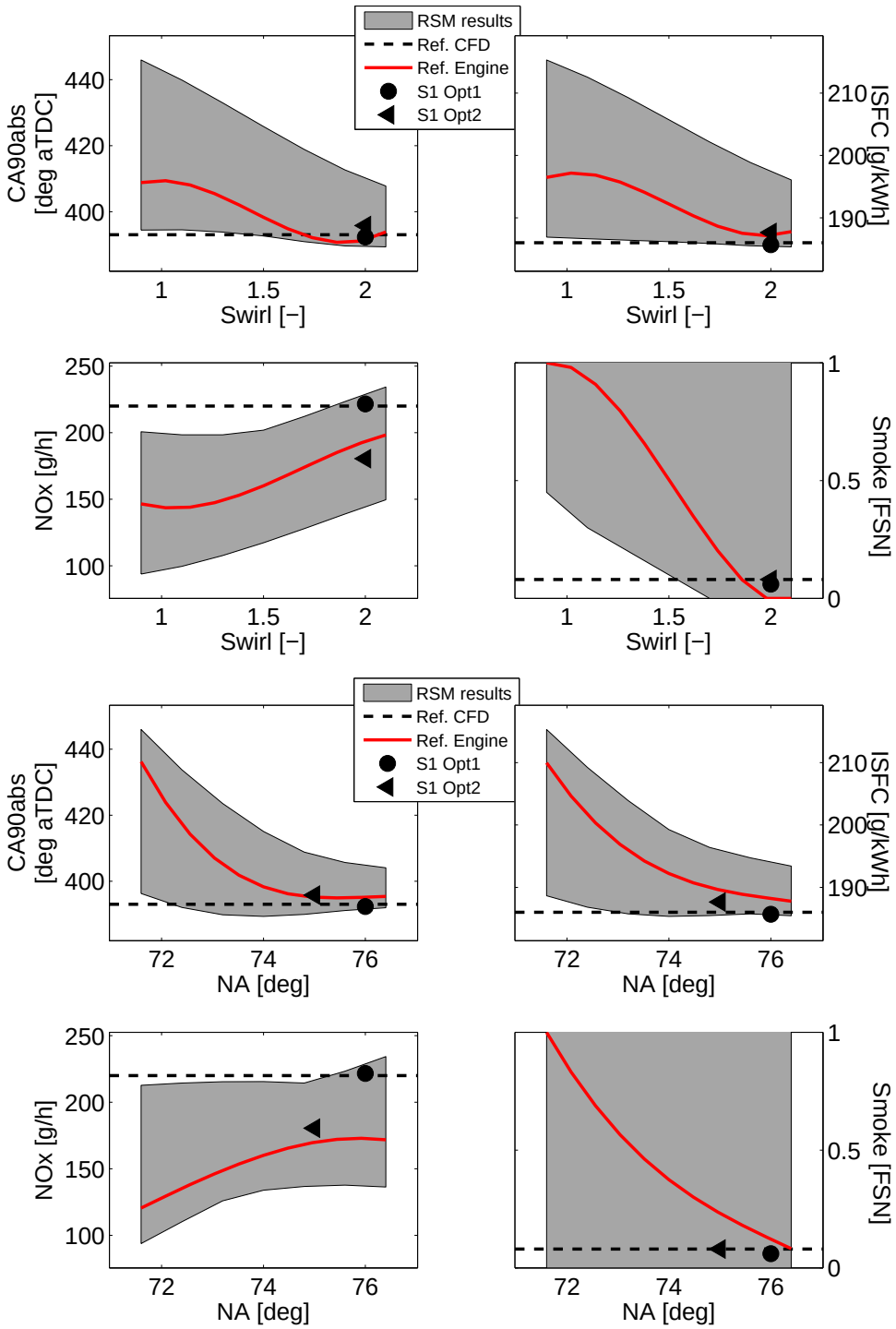

Figure 5.4. *Effect of swirl (top) and Nozzle included angle (bottom) on key combustion, emissions and performance parameters. Reference engine levels are included as dashed lines.*

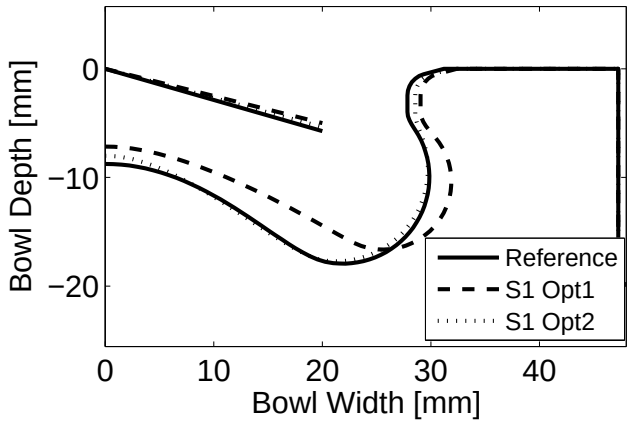

Figure 5.5. *Optimum combustion systems after Stage 1.*

As a key conclusion of this Stage 1, the implementation of the original attractive optimization path based on designing a quiescent combustion system with low swirl and non-reentrant bowl shape was not possible because low swirl would increase ISFC and Smoke emissions, at least keeping the reference air management and injection settings defined by the current engine technology. Additionally, this Stage 1 evidences the low potential of improvement in terms of ISFC while keeping constant emissions attainable by optimizing only the combustion chamber geometry of the engine. This very limited improvement encourages the definition of a second optimization stage adding the key air management (PIVC and EGR) and injection settings (SOI of the main injection and IP) for further investigating the potential for ISFC reduction.

5.3 Stage 2: 6 parameters DOE optimization

This section presents the results of the second optimization performed for this PhD project. From the results obtained in the first stage it was concluded that the inputs optimized in Stage 1 were insufficient and could not show the full potential of the geometry, therefore air management and injection settings were considered together with the geometric parameters to perform the next optimization.

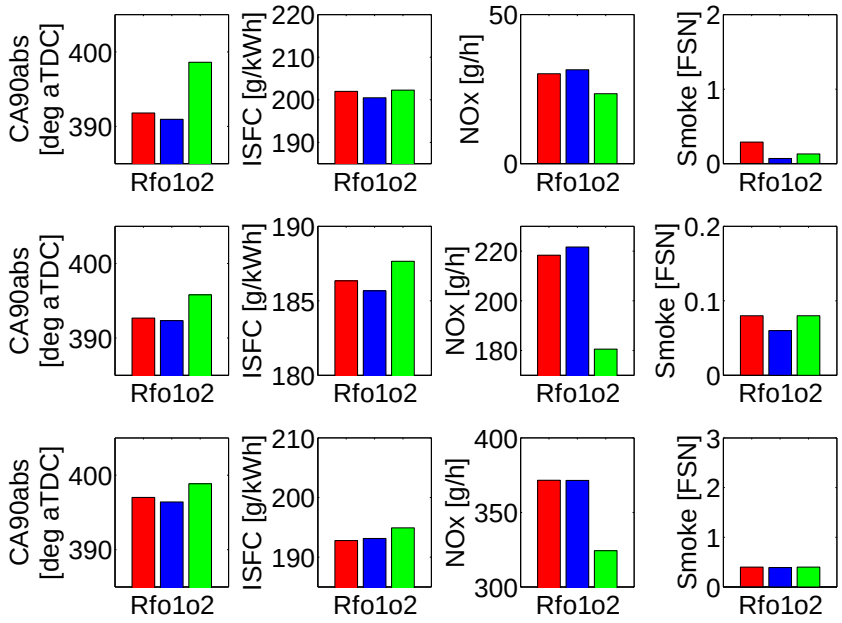

Figure 5.6. *Stage 1 optimized combustion system assessment at 1200 rpm - low load (top), 1600 rpm - half load (mid) and 1800 rpm - full load (bottom). Rf refers to the reference combustion system, o1 to the S1 Opt1 and o2 to the S1 Opt2 combustion systems.*

5.3.1 Optimization parameters and setup

From the knowledge generated in Stage 1, this Stage 2 focuses on defining a set of optimum combustion chambers, injection settings and air management settings to improve ISFC while keeping pollutants under the reference engine levels (see table 4.5). Since the maximum number of optimization parameters considered as suitable to have an acceptable time cost is six, and the reference NA and swirl level were both quite optimized, only the two geometrical parameters related to the bowl shape (d/B and K) were kept for Stage 2. The rest of the air management and injection settings were kept constant at their reference values. This optimization is also performed at the medium speed/load operating condition, evaluating the performance of the optimized combustion systems in the other two operating conditions. The ranges for the input parameters used in Stage 2 are shown in Table 5.3.

Table 5.3. *Ranges of the input factors for the optimization Stage 2.*

	Geometry		**Air manag.**		**Injection**	
	d/B	**K**	**PIVC**	**EGR**	**IP**	**SOI**
	[-]	[-]	**[bar]**	[%]	**[bar]**	**[deg aTDC]**
Ref	0.57	0.14	2.28	13	1230	-0.5
min	0.53	0	2.28	13	1200	-4.5
max	0.63	0.2	2.48	23	1600	1.5

The geometric parameter definition can be found in section 5.2.1 and the engine volumetric CR was kept constant at the reference value shown in Table 4.1.

The test plan for the Stage 2 optimization needed a total of 77 simulations. The distribution of the cases compared to the baseline case are shown in Fig. 5.7.

5.3.2 Results and discussion

The impact of the input parameters over the output responses was analyzed in order to establish clear cause/effect relationships. Fig. 5.8 shows the effect of bowl geometry (d/B and K), Fig. 5.9 the effect of air management settings (PIVC and EGR) and Fig. 5.10 the effect of injection settings (IP and SOI) on the end of combustion angle (CA90abs), ISFC and NOx-Smoke emissions. In these figures, the red line shows the isolated effect of each input parameter when the other inputs are set at constant values. The shade represents the results of the response surface.

Similar to the previous section, red lines are only used to check if the isolated effects of each parameter are consistent. Higher IP and PIVC help the mixing process and improve ISFC but increase NOx emissions [3]. Higher EGR has a strong effect over NOx but worsens ISFC and Smoke levels at the same time [4]. Finally earlier SOI is able to improve ISFC while increasing NOx [5].

Focusing on the main optimization trends observed in Fig. 5.8, increasing bowl diameter (d/B) clearly delays CA90abs and increases ISFC even compensating its effect by adjusting the other five input parameters. The impact on NOx and Smoke emissions is moderate and both can be easily

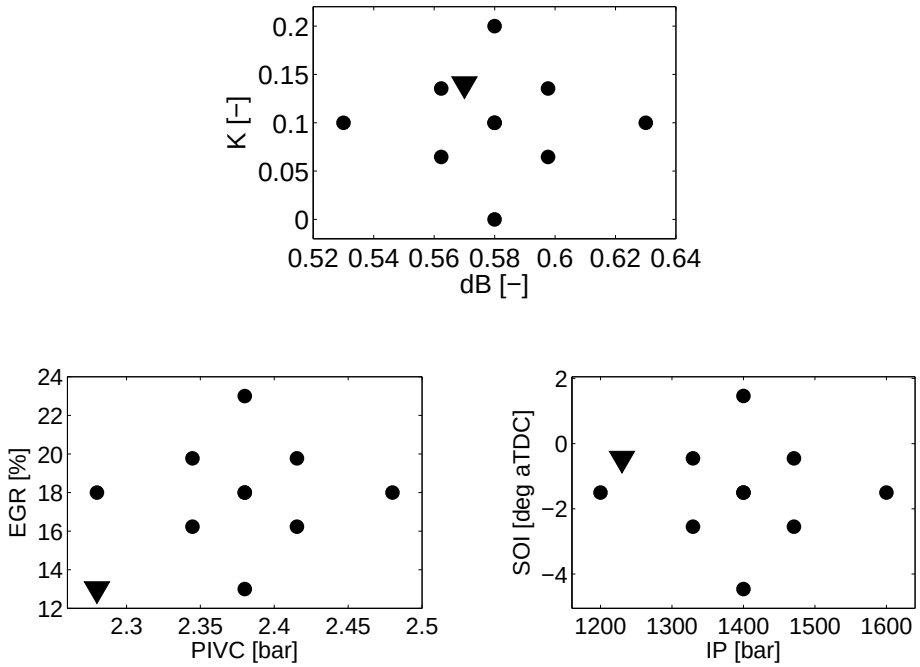

Figure 5.7. *DOE test plan for the input parameters in Stage 2. Reference engine represented as a triangle.*

controlled. Increasing K has a moderate impact on CA90abs and ISFC but, contrarily to what was observed in Stage 1, now its effect can be compensated by combining properly the other input factors and the optimum has shifted towards a value of 0.1. Additionally, NOx emissions increase with K while Smoke only increases for highly re-entrant bowl shapes.

Regarding the impact of air management settings shown in Fig. 5.9, increasing PIVC results in a slightly earlier CA90abs and then in a reduction in ISFC. The impact on NOx and Smoke emissions is moderate and levels below those generated by the reference engine can be easily attained at all PIVC levels. Increasing EGR retards CA90abs and then increases ISFC but, on the contrary, NOx emissions are sharply reduced while Smoke emissions can be controlled by adjusting the other parameters.

Closing this analysis by observing the effects of injection settings included in Fig. 5.10, CA90abs advances and ISFC decreases by increasing IP, and the

impact on NOx and Smoke can be also minimized by adjusting the other input parameters. Advancing SOI advances CA90abs and then decreases ISFC. NOx emissions increase while Smoke can be kept at levels below the reference engine for all SOI values.

Results confirm how the bowl shape is strongly coupled to the injector nozzle configuration and, in this case, the NA is slightly narrow (74 deg) and then the optimized combustion systems shifts towards bowls with lower d/B values. Additionally, the path for optimizing ISFC starts by advancing SOI to decrease it significantly and introducing the suitable rates of EGR in order to control NOx emissions keeping a moderate impact on ISFC, while adjusting IP and PIVC helps to compensate the negative effect of EGR over ISFC and control Smoke emissions. This path fits with the current trends followed in the field of diesel engine development.

The NOx-ISFC trade-offs obtained after Stage 1 and Stage 2 are included in Fig. 5.11 (left). It shows the limited potential for optimization provided by modifying only the geometry (Stage 1), while this potential increases significantly by including the air management and injection settings (Stage 2). However, an important limitation was detected after the analysis of the Stage 2 related to the relation between maximum cylinder pressure (Pmax) and ISFC observed in Fig. 5.11 (right). It is evident how ISFC is constrained by Pmax, generating an additional trade-off that must be carefully considered. In fact, the current engine ISFC level cannot be further improved without increasing Pmax, even optimizing the combustion chamber geometry and air management/injection settings altogether.

As in Stage 1, the same two optimization paths were followed for the optimization, the first based on minimizing ISFC and the second on improving the NOx-Smoke trade-off accepting a small ISFC penalty of 2%. The S2 Opt1 was selected following the first path, while the S2 Opt2 was selected considering the second path. The combustion system definitions for those optimal configurations are included in Table 5.4, and the bowl profiles compared to the reference combustion system and Stage 1 optimums are shown in Fig. 5.12.

In this Stage 2 the two optimization paths provided quite similar bowl geometries, with d/B 0.56 for best ISFC against 0.55 for best NOx-Smoke and K equal to 0.1 in both cases. Injection settings were also similar with the highest IP of 1520 bar and the earliest SOI of -3.3 deg aTDC, and they even share the highest PIVC equal to 2.44 bar. Therefore, the key difference between both optimization paths is observed in the EGR level, which shifts from 17% for the best ISFC to 21% for the best NOx-Smoke.

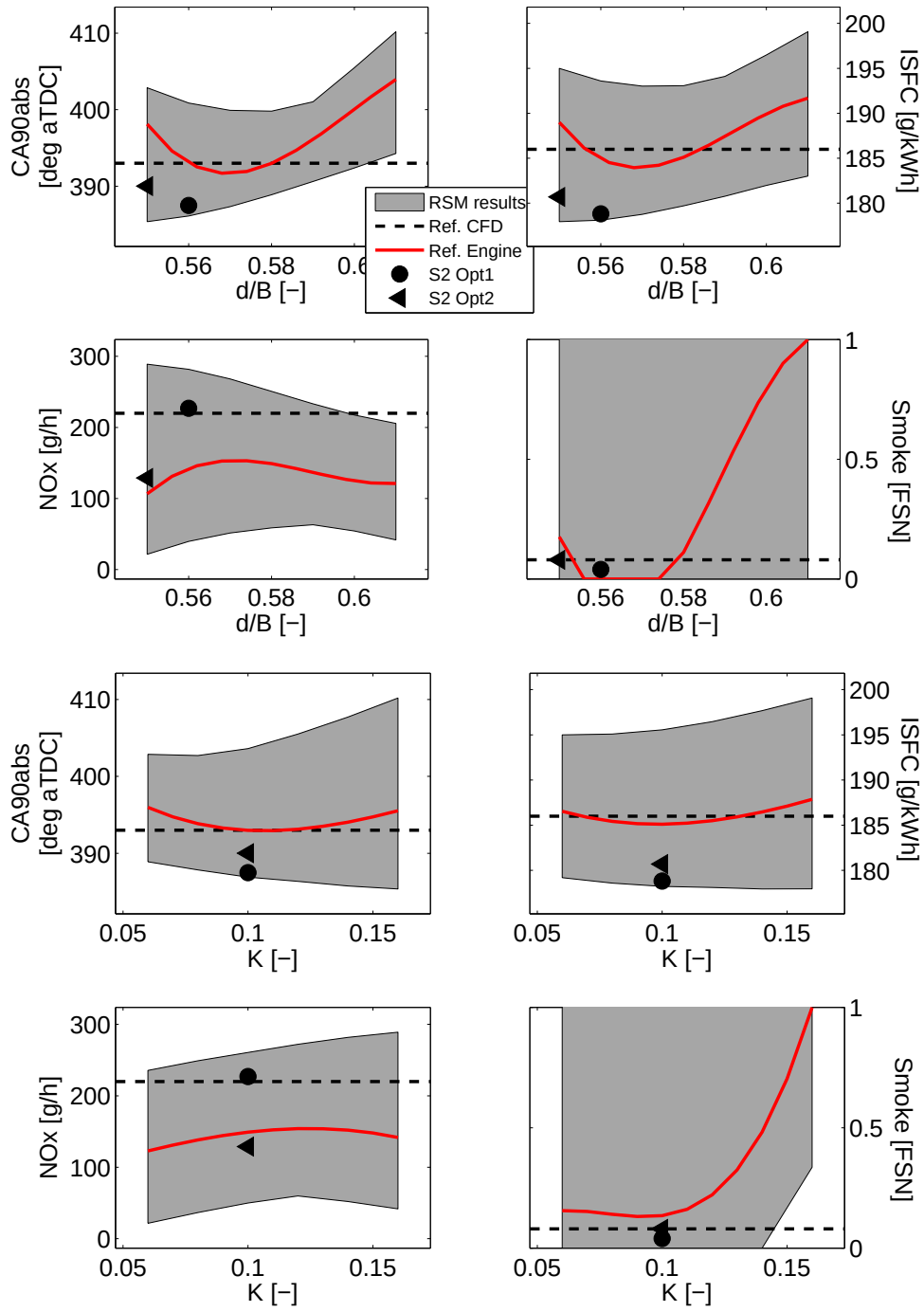

Figure 5.8. *Effect of d/B (top) and K (bottom) on key combustion, emissions and performance parameters. Reference engine levels are included as red lines.*

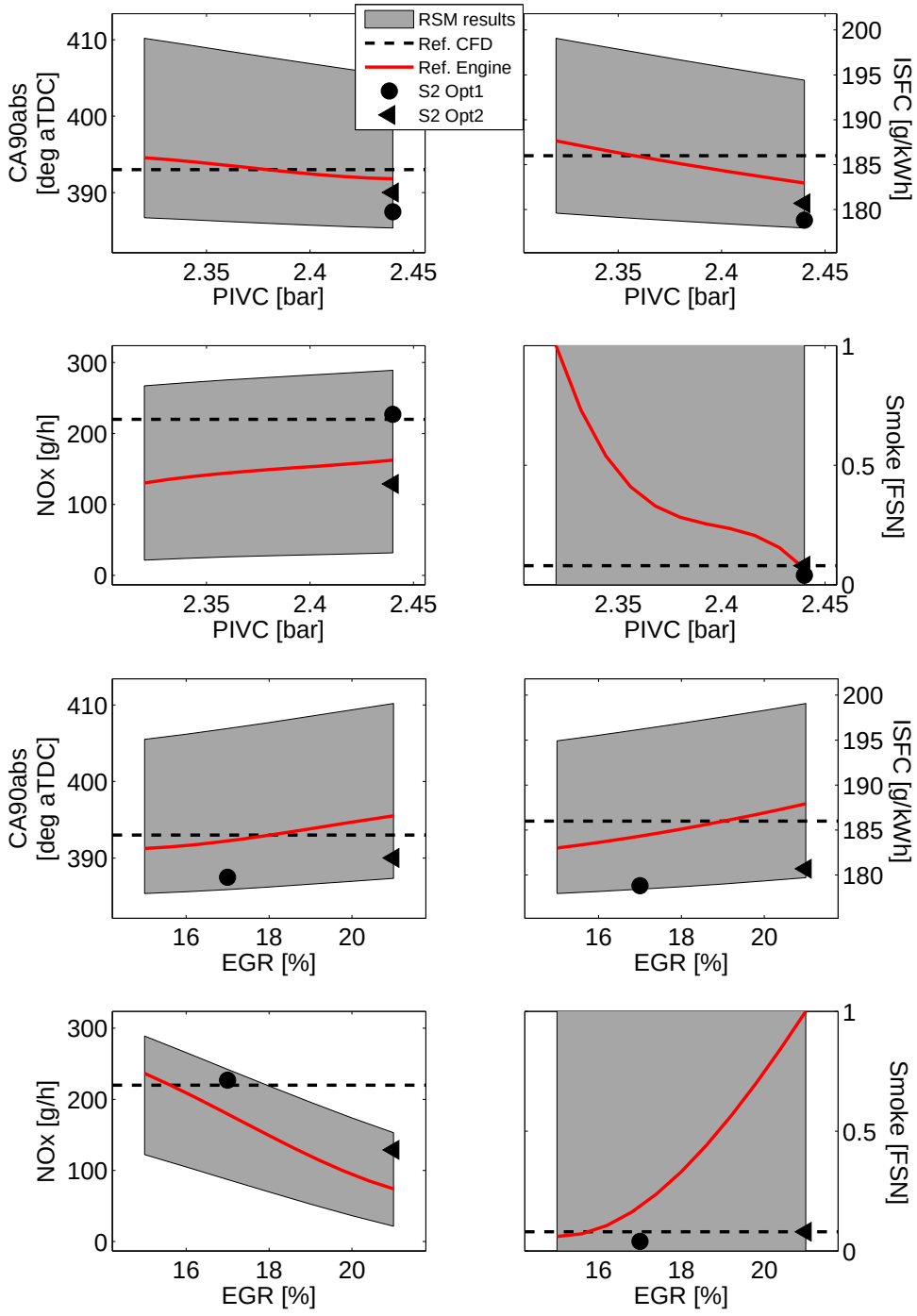

Figure 5.9. *Effect of PIVC (top) and EGR (bottom) on key combustion, emissions and performance parameters. Reference engine levels are included as red lines.*

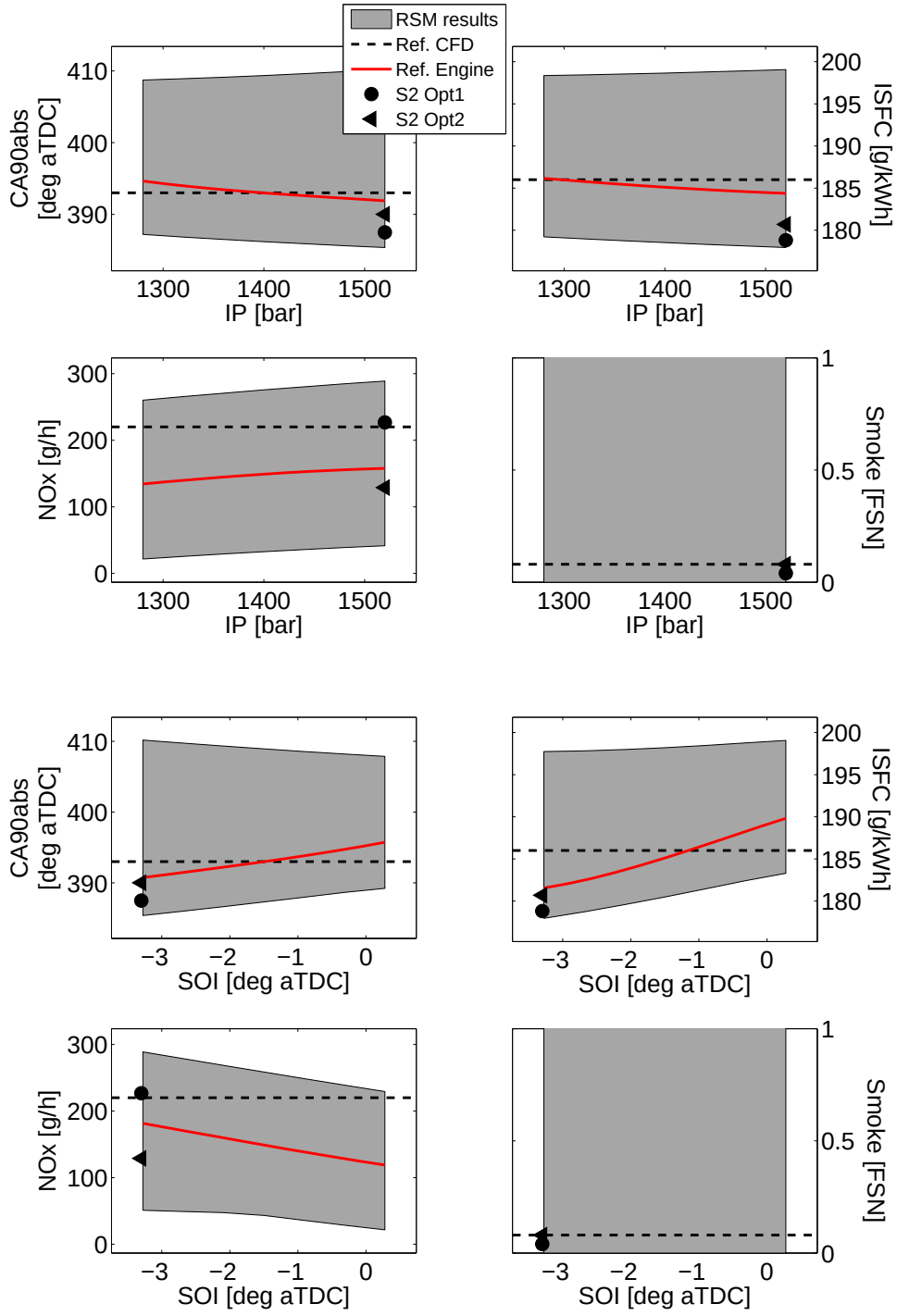

Figure 5.10. *Effect of IP (top) and SOI (bottom) on key combustion, emissions and performance parameters. Reference engine levels are included as red lines.*

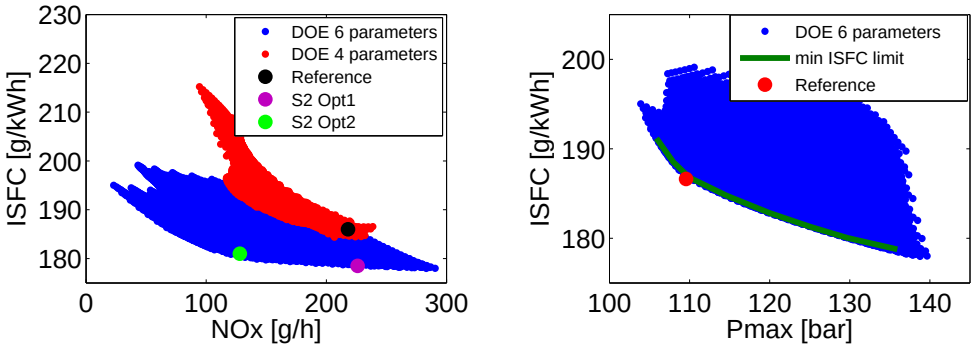

Figure 5.11. *(Left) NOx and ISFC trade-off for both optimization stages. (Right) Pmax and ISFC trade-off detected from the results of Stage 2.*

Table 5.4. *Optimized combustion systems after Stage 2.*

	d/B	K	PIVC	EGR	IP	SOI
	[-]	[-]	[bar]	[%]	[bar]	[deg aTDC]
S2 Opt1 (best ISFC)	0.56	0.1	2.44	17	1520	-3.3
S2 Opt2 (best NOx-Smoke)	0.55	0.1	2.44	21	1520	-3.3

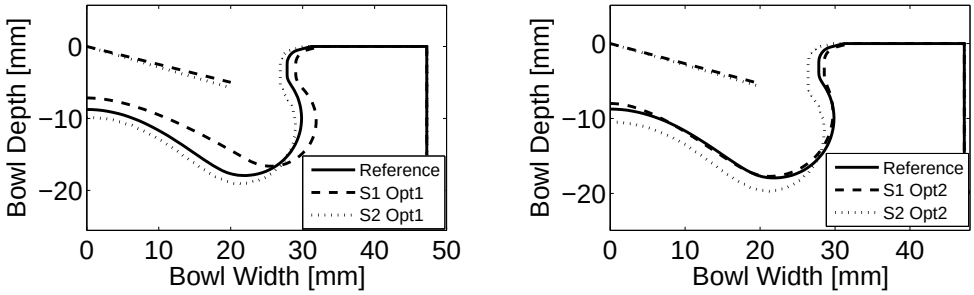

Figure 5.12. *Optimized piston bowl profiles for best ISFC (left) and for best NOx-Smoke (right).*

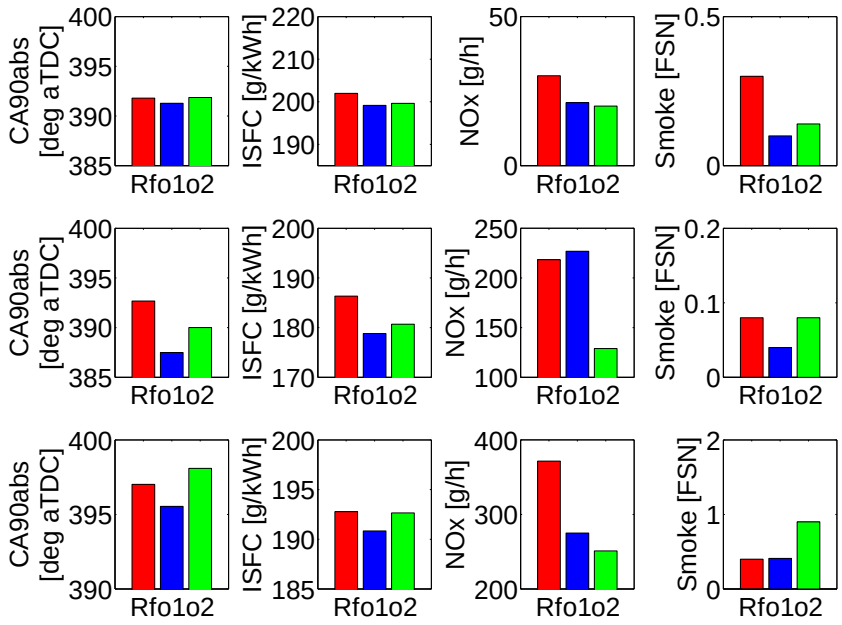

Figure 5.13. *Stage 2 optimized combustion systems assessment at 1200 rpm - low load (top), 1600 rpm - half load (mid) and 1800 rpm - full load (bottom). Rf refers to the reference combustion system, o1 to the S2 Opt1 and o2 to the S2 Opt2 combustion systems.*

Fig. 5.13 compares the CFD results of the two optimized configurations from Stage 2 with those obtained with the reference combustion system. According to these results, S2 Opt1 and S2 Opt2 decrease fuel consumption by 4.3% and by 3.2% respectively, NOx slightly increases by 1% for S2 Opt1 but sharply decreases by 43% for S2 Opt2. Smoke level is kept controlled at FSN levels below 0.1 in both cases.

As shown in Fig. 5.13 the optimized piston bowl geometries were also evaluated for the other two operating conditions, 1800 rpm - high load and 1200 rpm - low load. The S2 Opt1 combustion system also works adequately under high-load conditions. It is noticeable how the S2 Opt2 further improves the NOx emissions and keeps a modest reduction in ISFC and Smoke except at 1800 rpm - high load that suffers a noticeable Smoke increase.

The study was further expanded and the analysis was focused on the effect of the input parameters over the optimum configuration S2 Opt1. Fig. 5.14 presents the effect of air management and injection settings over the

performance of the optimum configuration. The first thing to notice is that the effect of the input parameters over ISFC and NOx has not changed (compared to Fig. 5.8 to 5.10) and no correlated effects are present in these figures, meanwhile the Smoke behavior is different. For most of the domain, the input parameters have moderate effect over Smoke and the optimum configuration is able to keep Smoke emissions under the reference engine levels for any value of PIVC and SOI. However, IP is required to have high values combined with medium EGR levels to be able to control Smoke. The only exceptions are combinations of extreme values of EGR with other inputs because the mathematical accuracy of the RSM is lower for combinations of extreme values of the inputs. In this case the PIVC, SOI and IP of the S2 Opt1 are the maximum value allowed so the response surface loses accuracy when EGR is also at the extreme, as seen in Fig. 5.14. This drawback is easily solved by validating with CFD the results obtained from the RSM or limiting the RSM to avoid combinations of extreme values of the inputs.

5.3.3 Experimental validation

The piston geometries for both optimized combustion systems were machined and installed in the engine with the aim of validating the quality of the CFD optimization results. The injection and air management settings of the CFD optimums were implemented in order to replicate the exact conditions for both S2 Opt1 and S2 Opt2 combustion systems. Both cases were tested experimentally at medium speed/load and the performance was compared with the CFD results in Fig. 5.15.

In general, the agreement is good, confirming how the CFD model setup and the optimization methodology performed well. According to the experimental results, the main objective, ISFC, was reduced by 5% and 4% with S2 Opt1 and S2 Opt2 respectively, fairly similar to the 4.3% and 3.2% predicted by the CFD, while the NOx and Smoke were kept constant or improved compared to the reference. In addition, the emission optimum, S2 Opt2, was able to reduce almost 40% NOx emissions with slightly higher ISFC following also the trends predicted by CFD. Finally, the pressure gradient increases by 10% in both cases, showing a possible noise restriction, what was also captured accurately by the CFD except for a small underprediction with the S2 Opt1.

As a result, the error between the CFD predictions and the experimental validation results is below 3% in the emissions, 2% in ISFC and 5% in pressure gradient, proving the robustness and accuracy of the new method.

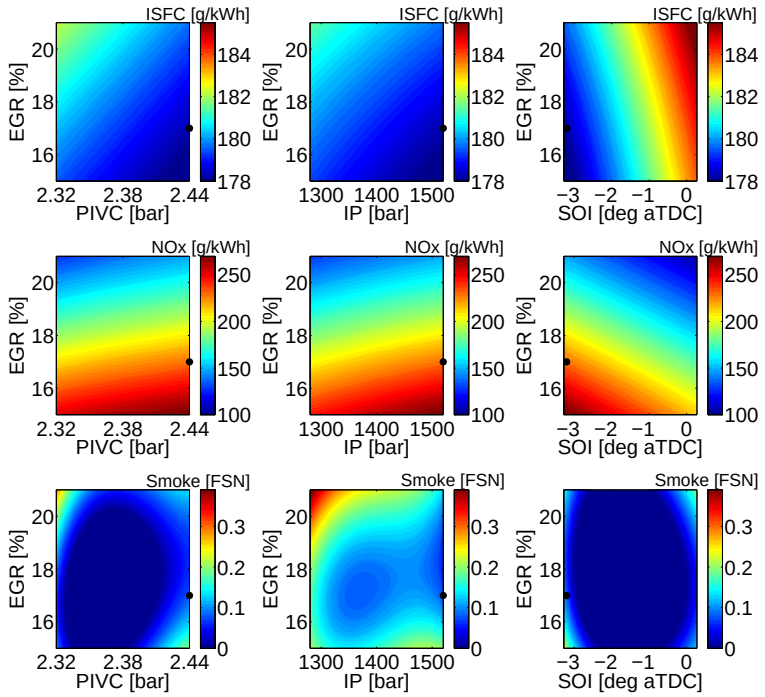

Figure 5.14. *Response surface of the combined effects of IP,PIVC, SOI with EGR over ISFC, NOx and Smoke. The S2 Opt1 optimum value for every input is represented as a black dot.*

Following the structure of the section, the optimum bowls were evaluated at the other operating conditions, 1200 rpm - low load and 1800 rpm - high load, keeping their respective reference settings and the results are shown in Table 5.5 and 5.6. However, in the particular case of 1800 rpm - high load the air management and injection settings were slightly re-adjusted to fulfill the mechanical restrictions of the engine along the experiments.

As concluded at the end of Stage 1, the impact of the geometry itself on ISFC is very limited, while the effect on pollutant emission levels is higher. At the low speed/load case both optimized bowls are able to reduce NOx emissions by around 15%, keeping ISFC almost constant with less than a 0.5% difference. At the high speed/load case the trend is very similar with a reduction by 6.3% NOx for S2 Opt1 bowl and by 5% for S2 Opt2 bowl compared to the reference, together with a reduction in ISFC of less than 1% for both optimized bowls. Soot emission levels show little discrepancies that,

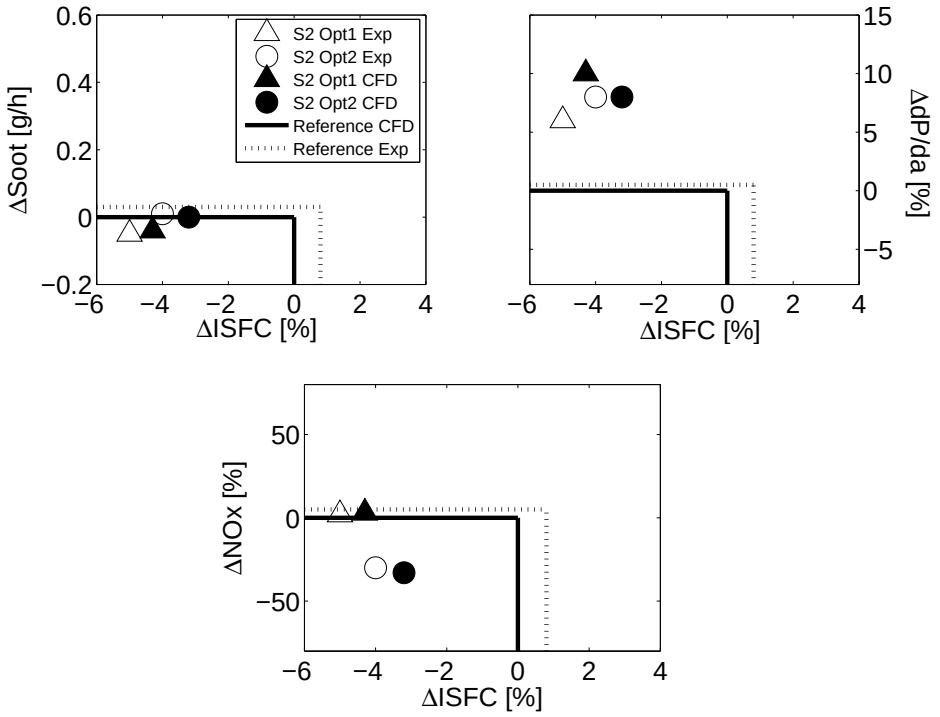

Figure 5.15. *Comparison of experimental and CFD results for the optimum combustion systems.*

Table 5.5. *Experimental results for S2 Opt1 and S2 Opt2 at 1200 rpm - low load.*

	ISFC [g/kWh]	**NOx** [g/h]	**Soot** [g/h]	**dP/da** [bar/cad]
Reference	197.72	9.52	0.04	3.92
S2 Opt1	198.23	8.07	0.03	4.79
S2 Opt2	197.52	8.18	0.05	4.5

Table 5.6. *Experimental results for S2 Opt1 and S2 Opt2 at 1800 rpm - high load.*

	ISFC	**NOx**	**Soot**	**dP/da**
	[g/kWh]	**[g/h]**	**[g/h]**	**[bar/cad]**
Reference	181.29	103.69	0.02	4.95
S2 Opt1	179.95	94.19	0.07	5.04
S2 Opt2	179.32	98.43	0.05	5.14

due to the low value of the experimental measurements, could be explained by experimental errors and/or inaccuracies in the soot model predictions. Nonetheless, the optimum bowl geometries provide competitive soot levels compared to the reference bowl, even following the trends predicted by the modeling results. Focusing now on pressure gradient, it increases by around 18% in the low load case and by 2% in the high load case, also according with the trends previously predicted.

As a final remark, these results confirm how the reference bowl geometry was already optimized in terms of ISFC and therefore, the potential for further improvement by reoptimizing the bowl geometry is very limited. As a consequence, other air management and injection setting in addition to the bowl geometry must be included in the optimization in order to decrease ISFC by improving the combustion system.

5.4 Summary and conclusions

An optimization methodology based on a combination of CFD modeling and RSM methods were applied to a MD 4-cylinder 4-stroke CDC engine in order to reduce ISFC while keeping the main pollutants constant. This methodology provided not only the optimum configurations but also the cause/effect relations between the control and target parameters. This improves the understanding of the requirements of the conventional diesel combustion system and what parameters are more attractive for being optimized.

In a first optimization stage, it has been found how the combustion system geometry could only improve ISFC by 0.5% without increasing NOx and Smoke emissions levels, showing the low potential of optimizing only the geometry. The study also indicated that a swirl-supported with re-entrant

bowl shape combustion system is still required for this engine and the swirl number was removed for later optimizations.

After that, injection and air management settings were included in order to increase the potential of the optimization and to be able to significantly reduce ISFC (around 5%), for constant emissions, as confirmed by the second optimization stage. It is also noticeable that 40% NOx reduction can be obtained keeping constant ISFC and soot emissions. Optimization path leads to advanced SOI for improved ISFC, increased EGR in order to control NOx emissions keeping a moderate impact on ISFC, while adjusting IP and PIVC helps to control soot emissions. This path fits with the current trends followed in the field of diesel engine development. Then the optimums were validated at other operating conditions and the results showed that they also work adequately at these other operating conditions.

Additionally, strong trade-off between ISFC and NOx, and between ISFC and Pmax were found. The NOx-ISFC trade-off proved that there is a very limited potential of improving this engine optimizing just the geometry. However, after adding the air management and injection settings as optimization parameters, the potential of the optimization process increased significantly. On the contrary, the ISFC-Pmax trade-off demonstrated that it is now possible to improve the ISFC without increasing at the same time the Pmax. That means that if there is a mechanical limitation in terms of Pmax, there is no potential for improving for this engine.

Finally, an experimental validation of the results was performed. The results confirmed the superior performance of the new optimum configurations proving the robustness and accuracy of the optimization method. The optimum piston bowl geometries were also tested in other operating conditions confirming that both configurations also work adequately in these other operating conditions.

From the study performed in this chapter it can be concluded that the optimization methodology provides accurate results within a reasonable time cost, therefore it is a design tool with a lot of potential. However, the optimization was limited to a maximum of 6 parameters and that limited the potential of the optimums. Additionally, further reduction in NOx emissions would penalize the ISFC (see Fig. 5.11), therefore future emission standards are not reachable keeping the efficiency levels. That suggests that the CDC engines are already optimized and are difficult to improve, therefore other optimization strategies such as after-treatment or alternative fuels are needed.

5.A Annex: Response surface functions

The mathematical model used to correlate the optimized input and the outputs of the Stage 1 are shown below.

$$\begin{gathered} Output = C1 + db * C2 + k * C3 + Swirl * C4 + \\ + NA * C5 + db^2 * C6 + k^2 * C7 + Swirl^2 * C8 + \\ + NA^2 * C9 + db * Swirl * C10 + db * k * C11 + db * NA * C12 + \\ + k * Swirl * C13 + k * NA * C14 + Swirl * NA * C15 + db * k * Swirl * C16 + \\ + db * k * NA * C17 + k * Swirl * NA * C18 + db * Swirl * NA * C19 + \\ + db * k * Swirl * NA * C20 + Swirl^3 * C21 + db^3 * C22 + NA^3 + C23 \end{gathered} \tag{5.1}$$

Where the inputs db, k, Swirl and NA as calculated as the example below.

$$db = \frac{dbvalue - \frac{dbmax+dbmin}{2}}{\frac{dbmax-dbmin}{2}} \tag{5.2}$$

being dbvalue the value of db that want to be calculated, dbmax the maximum value of db in the range used for the optimization and dbmin the minimum value of db in the range used for the optimization.

The coefficients C1 to C23 are described in Table 5.7.

A study of the significance level of the coefficients was performed. The results obtained from the ANOVA for each coefficient is shown in Table 5.8.

All the coefficient shown in Table 5.8 proved to be significant at least for one of the outputs studied in this paper so as a matter of simplifying the calculations, they were all kept. In order to show the fit of the surfaces compared to the original data, Table 5.9 shows the R^2 values.

It can be seen that, except for the pressure gradient that shows a lower fitting level than the other, all the surfaces can accurately predict the values of the original DOE points.

The mathematical model used to correlate the optimized input and the outputs of the Stage 2 are shown in Table 5.3.

Table 5.7. *RSM coefficients for the Stage 1.*

	Mathematical fit coefficients					
Output	**Pmax**	**dP/da**	**NOx**	**Smoke**	**ISFC**	**CA90abs**
C1	106.645	4.277	160.159	2.911	192.207	398.306
C2	0.809	0.030	5.365	-0.118	0.367	2.625
C3	1.321	0.005	27.339	-0.806	-2.668	-4.482
C4	1.438	-0.064	38.838	-4.533	-9.701	-18.410
C5	0.421	0.003	29.962	-3.121	-8.638	-13.717
C6	0.513	0.014	3.692	-0.069	0.035	3.724
C7	1.134	0.016	-8.132	0.659	1.392	4.845
C8	0.132	0.006	12.259	-0.169	-0.079	3.014
C9	0.193	0.031	-14.017	1.293	6.670	17.469
C10	1.547	0.041	7.776	-0.485	-2.338	-3.830
C11	-0.523	-0.007	-27.225	2.281	4.958	7.690
C12	0.464	-0.037	23.413	-0.537	-4.443	-8.081
C13	1.462	0.001	17.723	2.436	1.411	2.702
C14	1.278	-0.034	38.268	-1.751	-3.512	-3.262
C15	-1.166	0.016	-21.264	3.060	10.073	19.932
C16	0.023	-0.022	-6.944	0.733	-1.686	-4.781
C17	0.030	-0.020	13.047	-2.269	-3.828	-8.712
C18	-0.586	0.011	-14.584	1.698	1.479	0.082
C19	-0.378	0.005	21.693	-0.588	0.884	5.400
C20	-0.156	-0.040	49.228	-5.027	0.929	4.656
C21	-	-	-12.957	1.496	5.349	10.925
C22	-	-	-18.227	2.481	3.684	3.728
C23	-	-	-4.325	-0.451	-2.468	-6.683

Table 5.8. *P-value for all the coefficients used in the RSM for Stage 1.*

	P-values for all coefficients					
Output	**Pmax**	**dP/da**	**NOx**	**Smoke**	**ISFC**	**CA90abs**
C1	0.0000	0.0000	0.0000	0.0000	0.0000	0.0000
C2	0.0050	0.0020	0.2764	0.0542	0.0501	0.0432
C3	0.0000	0.0579	0.0031	0.2592	0.0442	0.0328
C4	0.0000	0.0000	0.0012	0.0007	0.0160	0.0003
C5	0.0036	0.1753	0.0028	0.0012	0.0118	0.0001
C6	0.0095	0.0046	0.0182	0.0656	0.6413	0.6588
C7	0.0068	0.0698	0.0002	0.0226	0.3081	0.5701
C8	0.0001	0.0072	0.3220	0.0186	0.0386	0.0689
C9	0.0000	0.2239	0.0159	0.2703	0.0198	0.1567
C10	0.0002	0.0045	0.4115	0.6025	0.0063	0.1781
C11	0.0207	0.4582	0.0258	0.4750	0.0298	0.0031
C12	0.0318	0.0071	0.0430	0.5656	0.0332	0.0260
C13	0.0002	0.9531	0.0967	0.0384	0.1038	0.3432
C14	0.0005	0.0101	0.0070	0.1011	0.0420	0.2622
C15	0.0007	0.1135	0.0580	0.0172	0.0147	0.0006
C16	0.8189	0.4682	0.8249	0.6217	0.1711	0.0371
C17	0.7649	0.5000	0.6897	0.8537	0.0769	0.2885
C18	0.1299	0.8362	0.6595	0.5325	0.3079	0.1662
C19	0.0845	0.6659	0.5401	0.8495	0.1938	0.2591
C20	0.4563	0.6451	0.0168	0.7431	0.0088	0.6117
C21	-	-	0.1891	0.0303	0.8195	0.5569
C22	-	-	0.032	0.3963	0.06325	0.0042
C23	-	-	0.7656	0.2488	0.0062	0.8537

Table 5.9. *R^2 values for the surfaces obtained for every output in Stage 1.*

Output	**Pmax**	**dP/da**	**NOx**	**Smoke**	**ISFC**	**CA90abs**
R^2	0.9888	0.9409	0.9918	0.9838	0.9975	0.9986

$$\begin{aligned}
Output = {} & C1 + db * C2 + k * C3 + PIVC * C4 + EGR * C5 + IP * C6 + SOI * C7 + \\
& + db^2 * C8 + k^2 * C9 + PIVC^2 * C10 + EGR^2 * C11 + \\
& + IP^2 * C12 + SOI^2 * C13 + PIVC * IP * C14 + \\
& + PIVC * EGR * C15 + PIVC * SOI * C16 + PIVC * db * C17 + \\
& + PIVC * k * C18 + EGR * IP * C19 + EGR * SOI * C20 + EGR * db * C21 + \\
& + EGR * k * C22 + IP * SOI * C23 + IP * db * C24 + IP * k * C25 + \\
& + SOI * db * C26 + SOI * k * C27 + db * k * C28 + \\
& + db^3 * C29 + k^3 * C30 + PIVC^3 * C31 + EGR^3 * C32 + \\
& + IP^3 * C33 + SOI^3 * C34 + db^2 * k * C35 + \\
& + db * IP * PIVC * C36 + db * k * PIVC * C37 + db * k * EGR * C38 + \\
& + db * k * IP * C39 + db * k * SOI * C40 + EGR * IP * SOI * C41 + EGR * PIVC * k * C42 + \\
& + db^2 * PIVC * C43 + PIVC * IP * k * C44 + PIVC * IP * SOI * C45 + PIVC * k * SOI * C46 + \\
& + db^2 * k^2 * C47 + db * k * IP * SOI * C48 + db * k * IP * PIVC * C49 + db * k * IP * EGR * C50
\end{aligned} \tag{5.3}$$

Where the inputs db, k, PIVC, EGR, IP and SOI as calculated as the example below.

$$db = \frac{dbvalue - \frac{dbmax+dbmin}{2}}{\frac{dbmax-dbmin}{2}} \tag{5.4}$$

The coefficients C1 to C50 are described in Table 5.10.

Table 5.10: RSM coefficients for the Stage 2

	Mathematical fit coefficients					
Output	**Pmax**	**dP/da**	**NOx**	**Smoke**	**ISFC**	**CA90abs**
C1	120.017	4.454	149.017	0.485	185.110	393.201
Continued on next page						

Table 5.10 – from previous page

Output	Pmax	dP/da	NOx	Smoke	ISFC	CA90abs
C2	0.016	-0.040	-29.074	4.132	5.690	6.148
C3	2.220	-0.022	24.229	0.284	0.186	-1.707
C4	4.323	0.122	12.870	-0.294	-2.336	-1.322
C5	-2.108	-0.150	-90.032	0.745	2.467	2.076
C6	3.742	0.110	12.108	0.817	-0.892	-1.576
C7	-16.124	0.007	-31.926	-0.698	4.501	2.818
C8	-0.793	0.056	-35.064	2.079	5.223	7.165
C9	-0.290	0.054	-26.282	1.487	3.123	4.153
C10	-0.093	0.051	-2.743	0.432	0.190	0.037
C11	-0.190	0.060	6.215	0.292	0.348	0.229
C12	-0.115	0.051	-2.924	0.117	0.156	0.191
C13	2.105	0.032	1.256	0.610	0.571	0.088
C14	0.061	-0.006	1.561	0.084	-0.053	-0.031
C15	0.100	-0.031	0.401	-0.179	-0.528	-0.306
C16	-0.540	0.008	-3.760	0.120	0.070	0.035
C17	0.191	0.003	1.728	-1.926	-1.543	-0.728
C18	-0.041	-0.019	3.879	0.152	-0.527	-0.487
C19	-0.302	0.039	-5.705	0.021	-0.099	-0.160
C20	0.414	0.001	10.982	-0.117	0.072	0.089
C21	0.506	-0.032	17.965	1.574	1.045	0.223
C22	-0.321	-0.016	-9.766	0.149	0.113	-0.054
C23	-0.772	-0.016	-1.329	0.126	-0.507	-0.232
C24	-1.044	-0.029	-14.468	2.219	1.923	1.240
C25	0.780	-0.003	-3.073	-0.584	1.119	1.162
C26	0.631	-0.001	20.299	-2.074	-2.873	-2.897
C27	-0.129	-0.005	6.356	0.021	-2.061	-1.948
C28	-2.940	-0.010	-65.452	4.177	7.212	8.576

Continued on next page

Table 5.10 – from previous page

Output	Pmax	dP/da	NOx	Smoke	ISFC	CA90abs
C29	2.071	0.011	36.321	-2.335	-4.346	-4.082
C30	-0.529	0.008	-5.271	1.339	-0.564	-0.674
C31	0.008	0.015	3.204	-0.506	-0.009	0.024
C32	0.142	0.010	8.861	-0.057	-0.003	0.000
C33	-0.413	0.031	-0.448	-0.435	-0.007	0.148
C34	2.327	-0.021	0.582	-0.256	-0.368	-0.221
C35	-	-	-	7.720	-	-
C36	-	-	-	0.310	-	-
C37	-	-	-	0.759	-	-
C38	-	-	-	0.223	-	-
C39	-	-	-	-2.115	-	-
C40	-	-	-	0.979	-	-
C41	-	-	-	0.354	-	-
C42	-	-	-	0.406	-	-
C43	-	-	-	-2.684	-	-
C44	-	-	-	0.488	-	-
C45	-	-	-	-0.587	-	-
C46	-	-	-	-0.653	-	-
C47	-	-	-	1.517	-	-
C48	-	-	-	25.523	-	-
C49	-	-	-	1.793	-	-
C50	-	-	-	-2.335	-	-

A study of the significance level of the coefficients was performed. The results from the ANOVA for each coefficient is shown in Table 5.11.

Table 5.11: P-value for all the coefficients used in the RSM for Stage 2

	P-values for all coefficients					
Output	**Pmax**	**dP/da**	**NOx**	**Smoke**	**ISFC**	**CA90abs**
C1	0.0000	0.0000	0.0000	0.0000	0.0000	0.0000
C2	0.0000	0.0000	0.0000	0.0000	0.0000	0.0000
C3	0.0000	0.0091	0.0000	0.0000	0.0000	0.0000
C4	0.0000	0.0000	0.0000	0.0000	0.0000	0.0000
C5	0.0000	0.0000	0.0000	0.0000	0.0000	0.0000
C6	0.0000	0.0000	0.0000	0.0000	0.0000	0.0000
C7	0.0000	0.0230	0.0000	0.0000	0.0000	0.0000
C8	0.5700	0.6420	0.0398	0.4825	0.0747	0.0127
C9	0.1705	0.2001	0.0329	0.5237	0.0000	0.0185
C10	0.6505	0.5300	0.0000	0.3154	0.0000	0.1019
C11	0.0245	0.5276	0.2360	0.0587	0.5424	0.0000
C12	0.1376	0.2663	0.1135	0.0000	0.5721	0.6085
C13	0.0176	0.3975	0.0556	0.6393	0.6081	0.4058
C14	0.1405	0.9186	0.0000	0.6269	0.2372	0.0011
C15	0.0309	0.0329	0.0575	0.3139	0.0000	0.0000
C16	0.0000	0.6125	0.0000	0.4784	0.1610	0.0001
C17	0.0013	0.6125	0.0000	0.0000	0.0000	0.0000
C18	0.3005	0.1559	0.0000	0.3973	0.0000	0.0000
C19	0.0001	0.0243	0.0000	0.8713	0.0664	0.5043
C20	0.0000	0.7598	0.0000	0.5138	0.1373	0.0021
C21	0.0000	0.0613	0.0000	0.0000	0.0000	0.0000
C22	0.0001	0.2106	0.0000	0.3973	0.0443	0.0000
C23	0.0000	0.2818	0.0001	0.4613	0.0000	0.0001
C24	0.0000	0.0449	0.0000	0.0000	0.0000	0.0000
C25	0.0000	0.7598	0.0000	0.0092	0.0000	0.0000

Continued on next page

Table 5.11 – from previous page

Output	Pmax	dP/da	NOx	Smoke	ISFC	CA90abs
C26	0.0000	0.9186	0.0000	0.0000	0.0000	0.0000
C27	0.0103	0.7598	0.0000	0.8945	0.0000	0.0000
C28	0.0000	0.2818	0.0000	0.0000	0.0000	0.0000
C29	0.0431	0.0531	0.2179	0.1067	0.0591	0.3849
C30	0.3313	0.0378	0.0370	0.5781	0.2798	0.1015
C31	0.2462	0.3716	0.1160	0.3768	0.0182	0.5971
C32	0.5816	0.5454	0.4214	0.6973	0.5600	0.0435
C33	0.0410	0.6538	0.0184	0.0547	0.3020	0.2457
C34	0.3848	0.0909	0.0458	0.3099	0.6375	0.3593
C35				0.0081		
C36				0.0522		
C37				0.0142		
C38				0.0063		
C39				0.0026		
C40				0.0463		
C41				0.0469		
C42				0.0421		
C43				0.0021		
C44				0.0333		
C45				0.025		
C46				0.0194		
C47				0.1311		
C48				0.0289		
C49				0.021		
C50				0.011		

All the coefficient shown in Table 5.11 proved to be significant at least for one of the outputs studied in this paper so as a matter of simplifying

Table 5.12. *R^2 values for the surfaces obtained for every output in Stage 2.*

Output	**Pmax**	**dP/da**	**NOx**	**Smoke**	**ISFC**	**CA90abs**
R^2	0.9981	0.9597	0.998	0.9904	0.9978	0.9934

the calculations, they were all kept. In order to show the fit of the surfaces compared to the original data, Table 5.12 shows the R^2 values.

It can be seen that, except for the pressure gradient that shows a lower fitting level than the other, all the surfaces can accurately predict the values of the original DOE points.

References

[1] Genzale C. L., Reitz R.D. and Wickman D.D. "A computational investigation into the effects of spray targeting, bowl geometry and swirl ratio for low-temperature combustion in a heavy-duty diesel engine". *SAE Technical paper*, n^o 2007-01-0119, 2007.

[2] Miles P.C. and Andersson O. "A review of design considerations for light-duty diesel combustion systems". *International Journal of Engine Research*, Vol. 17 n^o 1, pp. 6–15, 2016.

[3] Han S. and Bae C. "The influence of fuel injection pressure and intake pressure on conventional and low temperature diesel combustion". *SAE Technical Paper*, n^o 2012-01-1721, 2012.

[4] Lázaro L, Aparecida C and Lacava P. "Strategies for emission control in diesel engine to meet Euro VI". *Fuel*, n^o 104, pp. 183–193, 2013.

[5] Kweon C.B., Okada S., Stetter J.C., Christenson C.G., Shafer M.M., Schauer J.J. and Foster D.E. "Effect of injection timing on detailed chemical composition and particulate size distributions of diesel exhaust". *SAE Technical Paper*, n^o 2003-01-1794, 2003.

Chapter 6

Advanced mixing-controled combustion concept optimization using evolutionary optimization methods

Contents

6.1 Introduction

The research work reported in this chapter describes the results obtained from the second block of optimizations performed for this Thesis. The first block was focused on CI engines because they are one of the most efficient thermal engines in the world. They are known as economical and robust, but also for their smoke and NOx emissions levels [1]. However, according to the previous chapter results, CDC systems are already optimized so future emissions standards are expected to be reached after suffering an efficiency degradation. For that reason this chapter leaves behind the CDC systems and focuses on alternative systems, less known but with a lot of potential aiming to achieve future emission standards with better efficiency. DME was considered the best alternative to enable high efficiency and low emissions because it forms little to no soot emissions even under stoichiometric operation allowing to have diesel like efficiency with significantly lower emissions.

The optimization process carried out is divided in 2 stages, an initial stage aiming to achieve current emission standards and a second optimization aiming to achieve future emission standards. Each stage follows the methodology developed for evolutionary optimizations.

- The first part of these studies presents the optimization parameters, ranges, restrictions and objectives. Additionally, the optimization objective and the restrictions are presented. The validation of the CFD model can be found in section 4.3.2.2.
- In the second part the optimization results are presented and analyzed in detail, including the optimum configuration description and the cause/effects of the inputs and outputs. Finally, since an experimental optimization is not available, the evolution of the reference engine towards the optimum configuration is described to validate the individual effect of each parameter presented in the analysis section and to give a better idea of the contribution of each parameter to the optimum configuration.

It is important to highlight that in both stages the net indicated efficiency (NIE) is the main objective of the optimization, this is, the pumping work is taken into account when optimizing the DME fueled engine, because the DME lower stoichiometric air-mass/fuel-mass ratio [2] generates a noticeable improvement in pumping work compared to diesel fueled engines. Additionally, soot emissions were expected to be negligible for the DME fueled engine; accordingly, no constraint was placed on soot.

In this framework, this chapter focuses on optimizing with DKGA (see section 3.4 for explanation) a HD CI engine fueled with DME aiming to achieve current and future emissions standards. Both optimization stages focus on improving NIE while keeping NOx , PP and maximum pressure rise rate (maxPRR) under the target values. The first stage focuses on optimizing a diesel engine where diesel is directly replaced by DME while the second stage goes a step further and takes advantage of the non-sooting nature of the DME to optimize a stoichiometric combustion system coupled with a TWC. Additionally, an extra optimization with reduced number of inputs but also reduced demand of resource requirements is performed and presented in annex 6.A, whose main objective is to adapt the current optimizations to situations where only limited resources are available and evaluate its performance.

6.2 Stage 1: Lean combustion optimization

This section presents the results of the first optimization performed with the DKGA algorithm. It focuses on optimizing an engine fueled with DME aiming to control emissions and improve efficiency, compared to the diesel fueled engine used as reference. This first optimization switching to show the potential of the new engine compared to modern HD engines before aiming for future generation targets. For that reason this optimization focuses on designing an engine that achieves current US2010 emission standards without post-treatment.

6.2.1 Optimization parameters and setup

This optimization focused on maximizing NIE while keeping NOx emissions, PP, and maxPRR below the specified limits. Table 6.1 summarizes the limits used for each restriction in the optimization. The PP and maxPRR limits were set at 200 bar and 15 bar/deg, respectively. These values were selected to be comparable to a modern HD engine operating at the rated power condition and meet US2010 emission standards [3].

The optimization inputs include 15 geometric parameters and 7 injection and air management settings. The 15 geometric parameters are the minimum set required in order to allow the geometric tool, presented in section 4.4.2, to be flexible enough to be able to generate any kind of piston bowl geometry. The other 7 inputs were chosen as the most relevant in an internal combustion engine optimization and consist of SOI, EGR, PIVC, swirl, Dnoz, NA and IP.

Table 6.1. *Target values used in the optimization for the restrictions.*

NOx	**PP**	**maxPRR**
[g/kWh]	**[bar]**	**[bar/deg]**
0.268	200	15

Table 6.2. *Intervals used for the optimization parameters and ranges.*

	G1-G4	**G5**	**G6-G15**	**Dnoz**	**NA**	**SOI**	**IP**	**EGR**	**PIVC**	**swirl**
	[-]	[-]	[-]	[μm]	[deg]	[deg aTDC]	[bar]	[%]	[bar]	[-]
Min.	0.01	-0.99	0.01	200	45	-35	500	2	2.5	0.1
Max	0.99	0.99	0.99	350	90	5	2600	62	4	3

The ranges of the inputs for the optimization were taken from the limits of current technology and are shown in Table 6.2.

The optimization process consists of a population of 529 cases per generation with 40 generations having a total of 21,160 function evaluations. The number of function evaluations and generations was based on other similar optimizations carried out previously to this study (see section 4.4.4). The optimization results were analyzed using the non-parametric regression model based on the Component Selection and Smoothing Operator (COSSO) method [4]. The low root-mean-square (RMS) error of 0.12% in NIE ensures the quality of the fitting function. With this regression it is possible to complete the study by providing not only the optimum values for the inputs, but also the description of the effects of any of the inputs over the optimized NIE. The 15 piston bowl parameters are difficult to interpret; accordingly, they are transformed into 3 new geometric parameters when discussing the results. The new parameters are defined as bowl width, bowl height and reentrant parameter (Kd). Revisiting Fig. 4.7, bowl width is defined as the horizontal distance between p5 and p1, bowl height as the vertical distance between p5 and p2 and Kd as the horizontal distance between p4 and p3 being positive when the bowl has a reentrant shape.

6.2.2 Results and discussion

This section presents the optimization results, compares the optimized solution to a baseline case, and discusses the most relevant cause/effect relations between the optimized inputs and outputs.

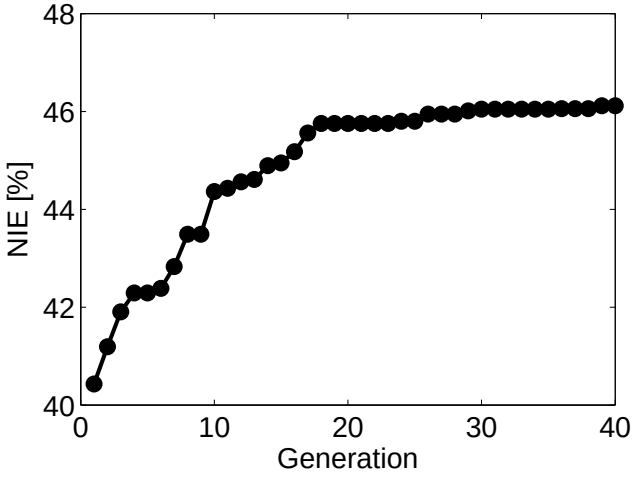

Figure 6.1. *Optimum NIE for each generation.*

6.2.2.1 Optimization results

The optimum was found after 40 generations and the NIE converged to a value of 46.11% as seen in Fig. 6.1. The set of optimum values for the 22 input parameters are shown in Table 6.3 and Fig. 6.2 compares the optimum piston geometry with the baseline shape.

The optimization process resulted in a more reentrant, narrower and less deep piston compared to the baseline case. Since the CR has to be constant, the squish has to be higher for the newly generated geometry. The optimized solution uses an injector with 300 μm hole diameter and a NA of 86.7 deg. The start of injection timing is -8.19 deg aTDC and the IP is 2500 bar. It also uses a high swirl ratio at 2.82 and 40% EGR.

The results of the optimization in terms of the inputs variables are shown in Fig. 6.3. It shows broad coverage of the design space and convergence to a solution. The peak NIE of the entire optimization was 46.41% with a NOx level of 14.53 g/kWh, maxPRR of 8.8 bar/deg, and PP of 216 bar. Both NOx and PP values of the peak NIE case exceeded the restriction values, resulting in reduced merit. The peak NIE case (unconstrained) had a wider and non-reentrant bowl geometry to that of the constrained optimum solution with a difference of 7 deg SOI advancement, 500 bar lower IP and, the main reason for the high NOx emission, 27% lower EGR.

Table 6.3. *Optimum values for the 22 inputs optimized (up/mid) geometric inputs, (bottom) injection and air management settings.*

G1	**G2**	**G3**	**G4**	**G5**	**G6**	**G7**
[-]	[-]	[-]	[-]	[-]	[-]	[-]
0.48	0.77	0.2	0.26	0.15	0.02	0.67

G8	**G9**	**G10**	**G11**	**G12**	**G13**	**G14**	**G15**
[-]	[-]	[-]	[-]	[-]	[-]	[-]	[-]
0.07	0.29	0.51	0.53	0.65	0.04	0.11	0.71

Dnoz	**NA**	**SOI**	**IP**	**EGR**	**PIVC**	**swirl**
[μ**m**]	[**deg**]	[**deg aTDC**]	[**bar**]	[%]	[**bar**]	[-]
300	86.7	-8.19	2500	40	3.25	2.82

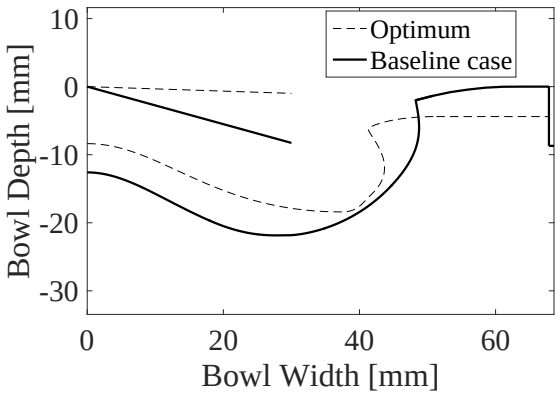

Figure 6.2. *Optimum and baseline case bowl geometry and NA configuration.*

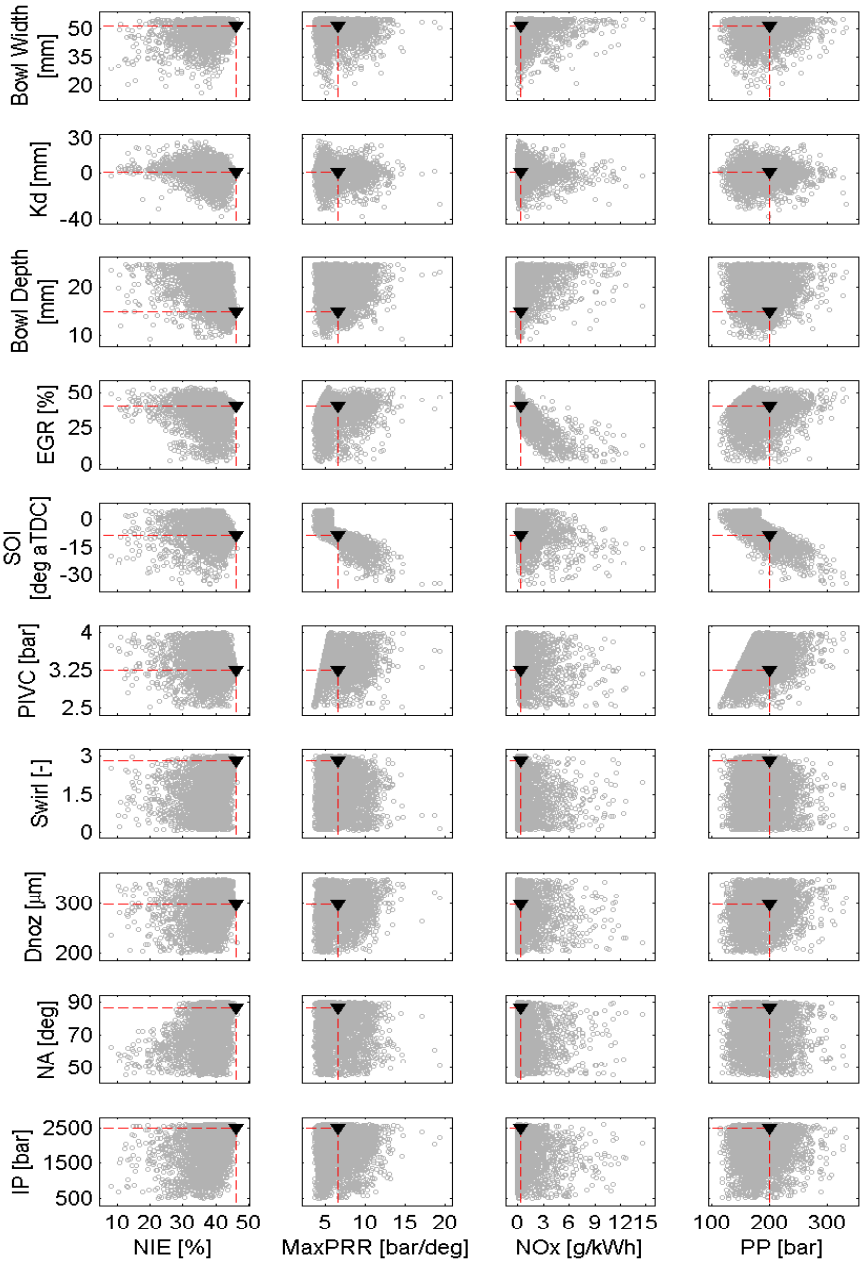

Figure 6.3. *Input versus output for all optimization cases. All data points are shown in gray circles and the optimum solution is shown by the black triangle.*

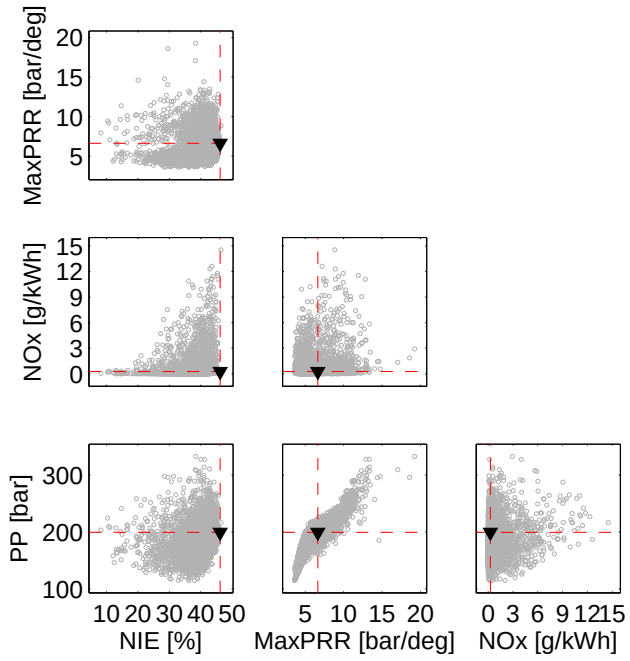

Figure 6.4. *Output versus output for all optimization cases. All data points are shown in gray circles and the optimum solution is shown by the black triangle.*

To investigate the impact of the constraints, Fig. 6.4 shows the optimization outputs plotted as functions of each other. These results show that the output space was adequately covered and that allowing operation at higher maxPRR, higher NOx levels, or higher PP levels would only enable marginal increases in NIE.

The efficiency and emissions of the optimum are shown in Table 6.4 compared to the baseline case. The baseline case selected for comparison is the validation case that corresponds to SOI -13 fueled with DME because it has the best efficiency out of the 3 cases used for validation.

The optimum configuration increased NIE by 3.3% from 42.8% to 46.1%, reducing drastically the NOx emissions from 2.81 g/kWh to the US2010 standards limit of 0.268 g/kWh. Additionally the maxPRR was kept always under the restrictions imposed for the optimization and the PP increased to 199 bar, just under its 200 bar limit imposed for the PP.

Table 6.4. *Performance and emissions for the baseline and optimum case.*

	NIE	**maxPRR**	**NOx**	**PP**
Case	**[%]**	**[bar/deg]**	**[g/kWh]**	**[bar]**
Baseline DME case	42.8	6.1	2.81	193.9
Opt. case	46.1	6.6	0.26	199.4

Table 6.5. *Energy balances for the baseline and optimum cases.*

	Gross Ind. Work	**Heat Trans.**	**Exh. Losses**	**Unburnt Fuel**	**Pump. Work**
Case	**[J]**	**[J]**	**[J]**	**[J]**	**[J]**
Baseline	4854	1926	4215	268	31
Optimum	5207	1779	4183	94	13

Table 6.5 shows the energy balances of the baseline and optimum cases. It can be seen that, even though there is an improvement in pumping work, the main difference in NIE between the optimum and the baseline case is generated by the gross indicated work. The optimum case has a 7.2% higher gross indicated work that is generated by two main sources, a reduction of 7.6% in HT and a 65% reduction in unburnt fuel. The unburnt fuel reduction means that the optimum case is able to improve the mixing process compared to the baseline case (see Fig. 6.6) and the HT reduction is caused mainly by the surface area reduction of the new geometry (from 4909 mm^2 to 3933 mm^2) and the high swirl (swirl effect over HT is later explained in detail).

Fig. 6.5 compares the HRR and Pcyl for the optimum and the baseline case fueled with DME. It can be seen how the optimum clearly promotes mixing since it is able to have a later SOI and still finish the combustion process earlier resulting in a much faster combustion process. Regarding PP and maxPRR, the optimum generates a higher PP and maxPRR due to the faster combustion process but the values are always kept under the restrictions imposed. The faster combustion process does not only affect PP and maxPRR but also increments the pressure during most of the expansion stroke that results in an increase in NIE, as seen in Table 6.4.

To explain the faster combustion, Fig. 6.6 shows the temporal evolution of the cylinder mass over several key equivalence ratios for the baseline and optimum cases. It can be seen that the optimized case has a later SOI, but it still manages to mix better and provides leaner equivalence ratios earlier than

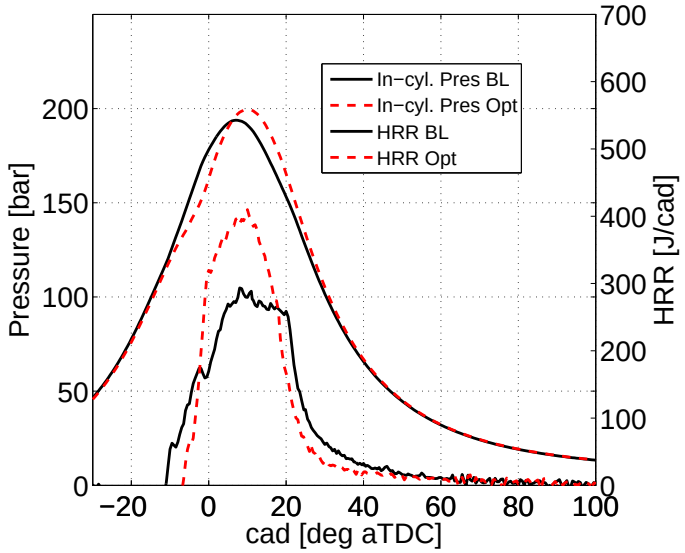

Figure 6.5. *CFD results of Pcyl and HRR using diesel and DME as fuels.*

the baseline case, leading to faster combustion as seen in Fig. 6.5. On the contrary, the baseline case is not able to completely burn all the fuel during the combustion process leaving some rich mass in the cylinder at EVO. This mixing improvement was represented in Table 6.5 where the optimum case showed an improvement in unburnt mass resulting in a gross indicated work increase.

To further illustrate the differences in mixing leading to a shorter combustion duration for the optimized case, Fig. 6.7 shows equivalence ratio contours for both cases. The baseline case is not able to reach the fresh air available in the center of the combustion chamber leading to a higher mass with equivalence ratio over 1. On the contrary, the optimized case shows a more homogeneous mixture and is able to access to more of the available fresh air.

6.2.2.2 Parametric dependence

An important aspect of an optimization is to not only provide the optimum results and compare the results with the reference case, but also to show and understand the trends of each input parameter. For that reason, all the results

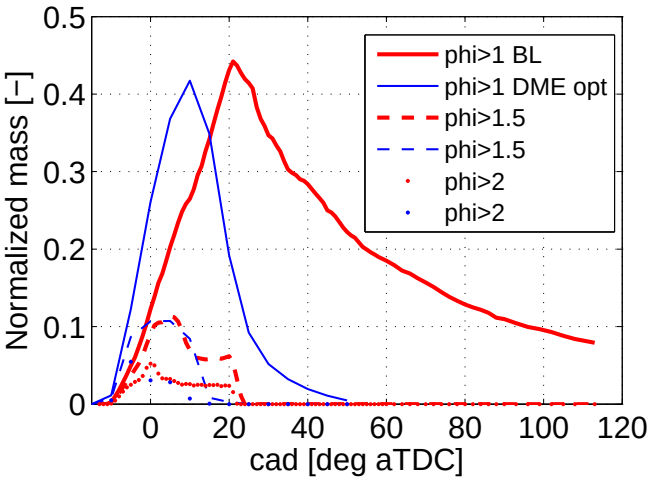

Figure 6.6. *Comparison between the baseline DME case and the optimum case of the normalized mass with equivalence ratio over 1, 1.5 and 2.*

were gathered and adjusted with COSSO and the results for the most relevant parameters are shown in Fig. 6.8. This analysis follows the same structure of the parametric study performed on the optimum configuration in section 5.3.2 for the non-evolutionary optimization, however, with a GA there is a higher concentration of cases simulated near the optimum configuration and the accuracy of this parametric study is noticeably higher. At the same time, the parametric study performed in the rest of the domain in section 5.3.2 can not be performed here due to the low density of points in the rest of the domain.

The EGR is one of the most influential inputs because it is the main tool to control NOx emissions among the parameters investigated. It has a noticeable effect on NIE that is mainly explained by the worsening of the combustion efficiency for high EGR values. Usually, the EGR has a moderate effect on NIE but for moderate to high EGR values (over 30%) the NIE becomes more sensitive. Additionally, high EGR also slows down the combustion process and that results in a reduction of PP. Focusing on NOx emissions, EGR is by far the most effective input to control NOx, higher EGR values reduce significantly the NOx emissions at the expense of worsening the combustion efficiency and lowering the maximum temperature.

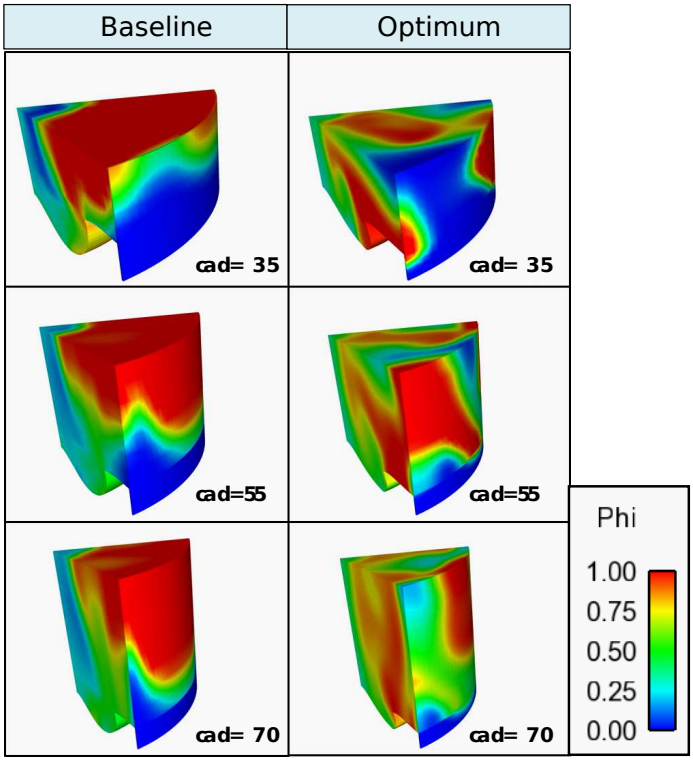

Figure 6.7. *Phi distribution on (Left column) baseline DME case and (Right column) optimum case.*

In terms of PIVC, high levels of PIVC seem to offer the best NIE. The increase in fresh air reduces the global equivalence ratio helping the mixing process and reducing the combustion duration and efficiency. This offers higher NIE, however, when the PIVC is too high, it does not seem to further improve combustion efficiency nor combustion duration and NIE values are reduced due to the increased pumping work required to achieve those pressure values. The Pcyl increases for higher PIVC and also the NOx. Similar to other inputs, better and faster combustion increases the maximum local temperatures and that increases NOx emissions.

In the case of swirl, higher swirl increases NIE. On one hand, higher swirl improves mixing, mainly in the later part of the combustion, reducing the total combustion duration and improving the combustion efficiency, resulting in a NIE increase. On the other hand, higher swirl reduces HT, contrary to the

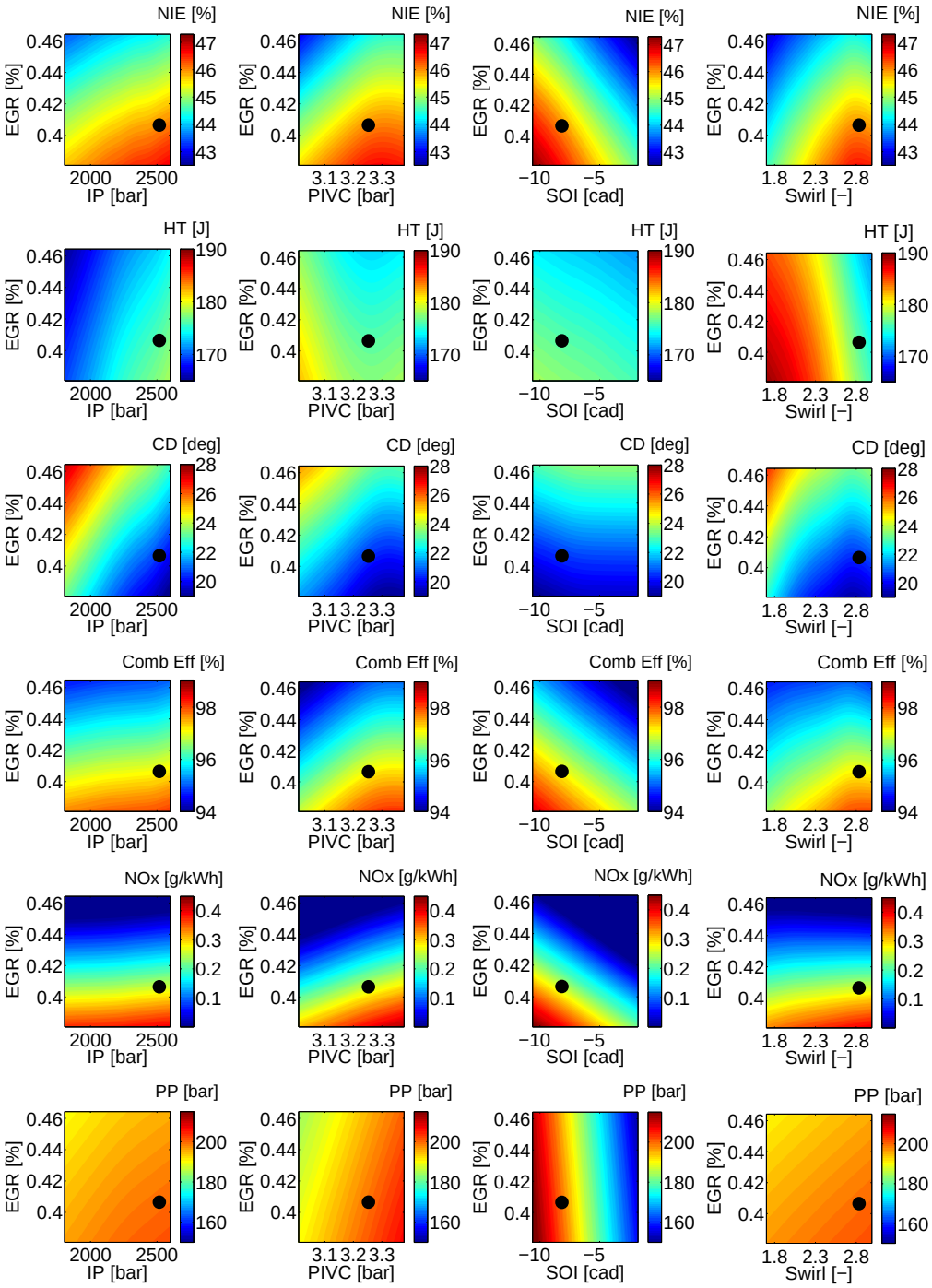

Figure 6.8. *Response surface of the combined effect of IP,PIVC with EGR over NIE, HT, combustion duration (CD), combustion efficiency, NOx and PP. The optimum value for every input is shown by the black dot.*

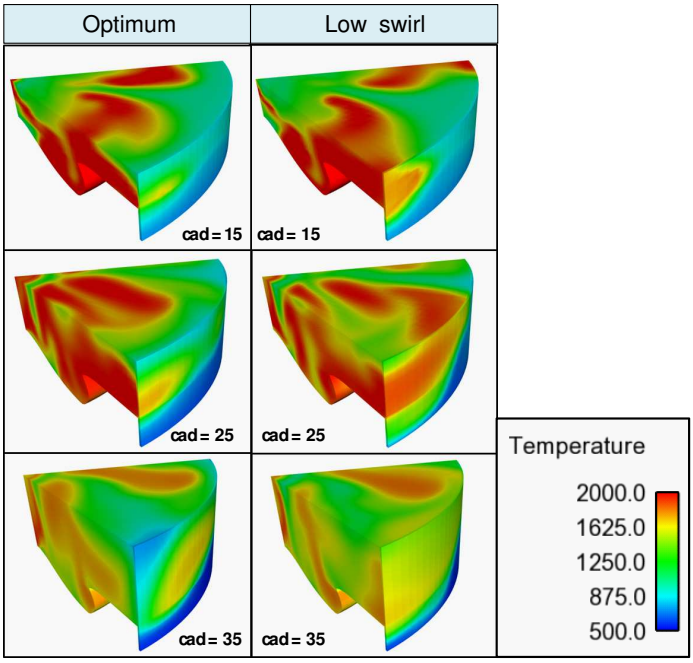

Figure 6.9. *Temperature distribution on the (Left column) optimum case and (Right column) optimum case with lower swirl.*

general trend. This happens because, as seen in Fig. 6.9, the swirl separates the flame from the liner and, even though the local temperatures are higher due to higher swirl, the temperature is lower next to the liner and the HT is reduced, what also helps to improve NIE.

The parameter SOI shows a noticeable effect on NIE, delayed SOI provides lower NIE values. This effect on NIE is also promoted by the sensitivity of the combustion efficiency to SOI where delayed SOI has a negative impact on the combustion efficiency. It also shows a big impact on PP and NOx and both of them are due to the same phenomena, earlier SOI will advance the combustion towards TDC generating higher PP and maximum local temperatures.

Finally, higher IP helps the mixing during the first and later part of the combustion improving NIE. It can be seen that contrary to the other parameters, IP has no direct effect over the combustion efficiency and focuses only on improving mixing. It also affects HT, where higher IP increases HT but like in other parameters, the combustion duration effect over NIE overcomes the HT effect.

Some of these parameters are forced to high values in order to achieve the restrictions shown in Table 6.1, like EGR, which is forced to high values to compensate NOx emissions even thought it has a negative effect over the main objective of the optimization. In the same manner, other inputs like swirl and IP focus on improving the engine NIE by improving mixing and increasing a combustion efficiency. Both trends are coupled because, as seen in Fig. 6.8, higher swirl and IP compensates the negative effect of the EGR over the combustion process and higher EGR compensates the increase in NOx emissions generated by higher swirl and IP, then the combined effect of all three parameters allows the new optimum to show better efficiency with lower NOx emissions. Additionally, higher EGR, swirl and IP produce an increase in PP that is easily controlled by adjusting SOI making possible the whole new system.

6.2.2.3 Parameter evolution

After the comparison of the optimum and the baseline cases and the isolated effects of the most relevant inputs on the engine performance are described, it is easier to understand the optimum combustion system. Starting with the geometry, the process shifted the reference shape towards a slightly more reentrant, narrower and less deep piston. This new piston geometry helps to improve HT and mixing resulting in an improvement in combustion duration and efficiency, see Fig. 6.10. Once the geometry is set, the NA is adjusted to have the best interaction possible with the optimum geometry further improving the mixing process. The EGR is the first and more sensitive parameter to be adjusted since the NOx restriction is very strong and EGR is the main strategy to improve NOx. For that reason the EGR is set to a value of 40%, reducing drastically the NOx emissions but worsening the combustion process. In order to compensate the effect of high EGR over the combustion, high IP and large Dnoz are needed to improve combustion duration and efficiency, and high swirl compensates the increase in HT by isolating the flame from the liner walls and further improves the later part of the combustion. Once the injection settings are set, PIVC is adjusted to control the equivalence ratio at a suitable level. As a result, PP is affected but it is kept under the limits by the SOI.

To illustrate the evolution of the combustion system, CFD simulations were repeated at various key points during the optimization process. Fig. 6.10 shows the results of this investigation. First, a DME case with the optimum piston bowl geometry was run keeping all of the baseline settings. This resulted in a significant increase in GIE and HT reduction. The optimum geometry

was able to improve mixing and efficiency and at the same time reduce HT, proving that for this advanced combustion system the geometry is one of the inputs with more potential to improve engine performance and is worth taking into account. Next, the case was repeated with the optimum swirl. The results show a noticeable worsening of the combustion system performance with increased incomplete combustion. Even though higher swirl number helps the mixing process, when the swirl number is too high and the sprays do not have high momentum, the sprays-to-spray interaction worsens the overall mixing process. Next, the case was repeated with the optimum NA. This resulted in an improvement in incomplete combustion and GIE due to the improved oxygen utilization generated by the matching of the new geometry with the optimum NA. Next, the case was repeated with the optimum IP. The results show that this is the best engine configuration in terms of energy balance (although NOx emissions are not under the limits). Higher IP helps to improve mixing and combustion efficiency reducing the incomplete combustion and increasing GIE from 40.7% to 46.7%. In this particular case, due to the high swirl number of the optimum configuration, higher IP helps to avoid early spray-to-spray interaction, further improving mixing. Additionally, HT increased from 13.5% to 18.1%, highlighting the importance of increasing swirl to deflect the flame and reduce HT compensating its increase caused by a higher IP. Next, the case was repeated with the optimum EGR and PIVC. This resulted in a GIE reduction. Higher EGR reduces the fresh air availability worsening the mixing and combustion efficiency of the engine which results in a GIE reduction despite the HT reduction. However, high EGR is compulsory to control the excess of NOx emissions generated after optimizing the other parameters. Finally, the case was repeated with the optimum SOI to reach the optimum configuration. This caused an increment in GIE from 45.4% to 46.2% while keeping PP just under the restriction.

6.3 Stage 2: Stoichiometric combustion optimization

The results obtained from the second stage of the DME fueled engine optimization are presented in this section. Based on the results obtained in the first stage of this chapter, the DME fuel has proven its potential to provide higher efficiency and lower emission levels than diesel fueled engines. Based on that, this section tries to go further and design an engine fueled with DME able to achieve future emission standards, in this case US2030. In order to achieve the goal, and thanks to the non-sooting nature of the fuel, it is proposed to

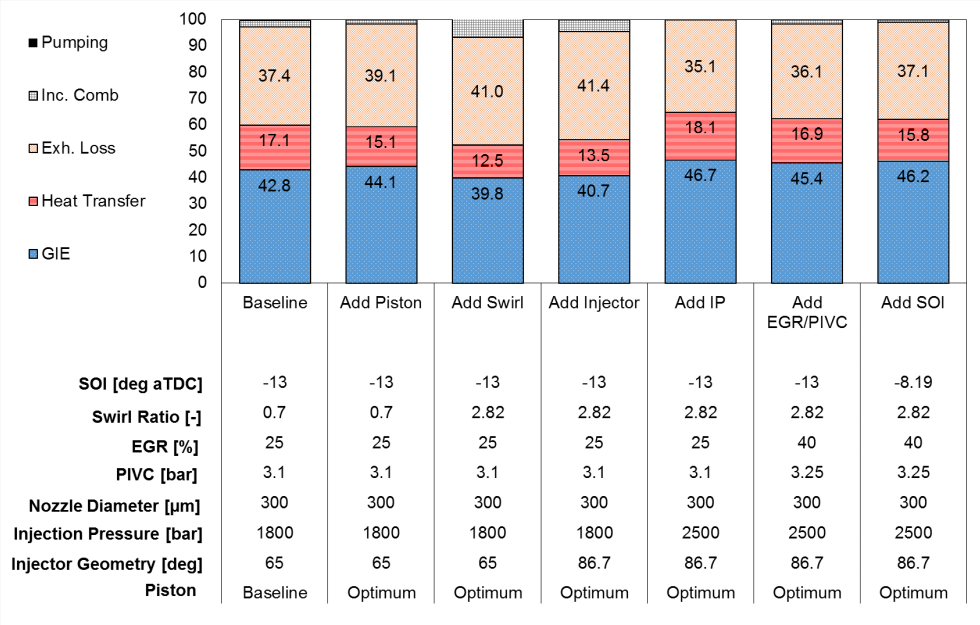

Figure 6.10. *Evolution of the optimum DME fueled lean combustion system.*

optimize an engine operating in stoichiometric combustion conditions coupled with a TWC to be able to completely control NOx emissions.

6.3.1 Optimization parameters and setup

The optimization focuses on maximizing NIE while keeping PP and maxPRR under 200 bar and 15 bar/deg., respectively. A TWC with a NOx conversion efficiency of 99% is assumed [5]. To meet a tailpipe NOx target of 0.0268 g/kWh [3], an engine out NOx constraint of 2.68 g/kWh was applied. Table 6.6 summarizes the limits used for each output restriction in the optimization.

A total of 21 input parameters are optimized. The input parameters are divided into 15 geometric parameters needed to describe the piston bowl shape and 6 important injection and air management settings. The geometric parameters are the same inputs used to describe the geometry in the previous section. The 6 injection and air management settings are SOI timing, EGR, swirl, Dnoz, NA and IP. The PIVC is adjusted with the EGR level to maintain

Table 6.6. *Target values used in the optimization for the restrictions imposed.*

NOx	**PP**	**maxPRR**
[g/kWh]	**[bar]**	**[bar/deg]**
2.68	200	15

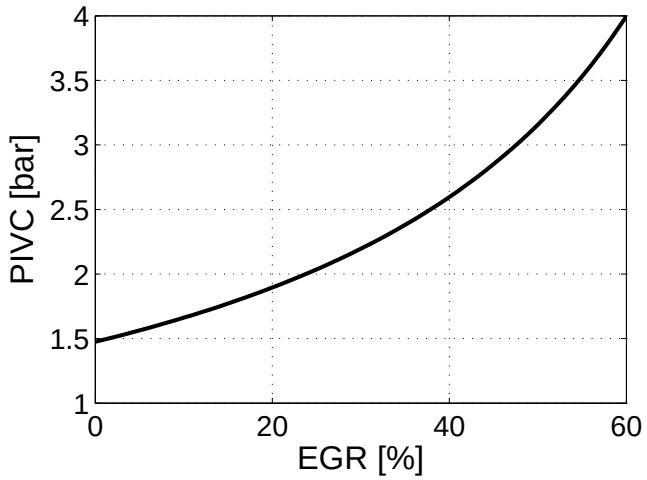

Figure 6.11. *Values of PIVC needed to achieve a stoichiometric equivalence ratio.*

Table 6.7. *Ranges used for the optimization inputs on Stage 2.*

	G1-G4	**G5**	**G6-G15**	**Dnoz**	**NA**	**SOI**	**IP**	**EGR**	**swirl**
	[-]	[-]	[-]	[μm]	[deg]	[deg aTDC]	[bar]	[%]	[-]
Min.	0.01	-0.99	0.01	200	45	-35	500	2	0.1
Max	0.99	0.99	0.99	350	90	5	2600	62	3

stoichiometric operation. The values of PIVC needed to keep a stoichiometric equivalence ratio for each EGR value are shown in Fig. 6.11.

Table 6.7 shows the ranges of design parameters considered. The parameter ranges were chosen to span the design space relevant to current and future technology.

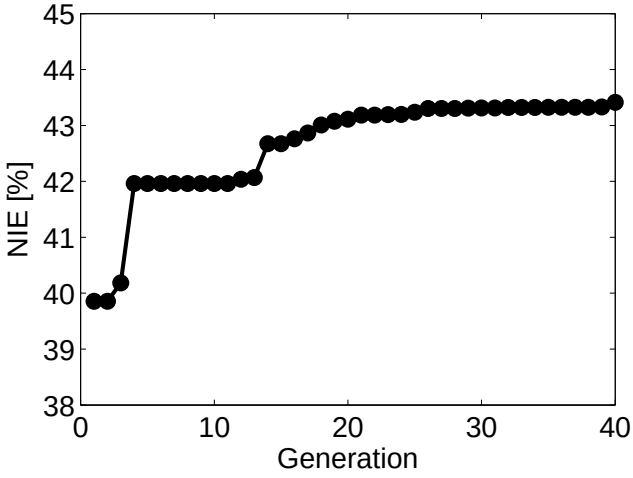

Figure 6.12. *Optimum NIE value for each generation.*

Similar to the previous optimization, a population size of 529 cases per generation and 40 generations were used, resulting in a total of 21,160 function evaluations. To analyze the effects of each of optimization parameter, the COSSO method [4] was used to fit a response surface to the outputs as a function of each input. The non-parametric fitting method showed a root-mean-square (RMS) error of 0.1% in NIE, assuring an accurate fit. Additionally, the 15 piston bowl parameters are transformed into bowl width, bowl height and reentrant parameter.

6.3.2 Results and discussion

This section is focused on the optimization results of Stage 2. The optimum is compared with the baseline case, and the most relevant cause/effect relations between the inputs and outputs are discussed.

6.3.2.1 Optimization results

The optimum was found after 40 generations and the NIE converged to a value of 43.4% as seen in Fig. 6.12. The set of optimum values for the input parameters are shown in Table 6.8.

Table 6.8. *Optimum values for the 21 inputs optimized (top/mid) geometric inputs, (bottom) injection and air management settings.*

G1	**G2**	**G3**	**G4**	**G5**	**G6**	**G7**	**G8**
[-]	[-]	[-]	[-]	[-]	[-]	[-]	[-]
0.02	0.74	0.53	0.68	0.36	0.46	0.3	0.27

G9	**G10**	**G11**	**G12**	**G13**	**G14**	**G15**
[-]	[-]	[-]	[-]	[-]	[-]	[-]
0.87	0.42	0.49	0.45	0.36	0.58	0.47

Dnoz	**NA**	**SOI**	**IP**	**EGR**	**swirl**
[μ**m**]	[**deg**]	[**deg aTDC**]	[**bar**]	[%]	[-]
330	61.7	-13.09	2594	33	2.98

Fig. 6.13 compares the optimum piston shape with the baseline geometry. The process shifted the reference piston geometry towards a non-reentrant shape. The optimum geometry is flat (i.e., the GA removed the pip) and shallower than the stock diesel bowl. The piston width is similar to the baseline engine. Additionally, the Dnoz was selected to be slightly narrower than the baseline geometry.

Fig. 6.14 shows the optimization results in terms of the input variables. It can be seen that the design space is broadly covered and the algorithm converges to the optimum solution.

In order to investigate the impact of the constraints, the optimization outputs plotted as functions of each other are shown in Fig. 6.15. It can be seen that reducing the constraints would not enable further increases in NIE because the unconstrained peak NIE case corresponds to the current optimum configuration. This is interesting because it suggests that the combustion system would be able to meet more stringent emissions regulations with minimal degradation of NIE.

The efficiency and emissions of the optimum solution and the baseline case are compared in Table 6.9. The baseline case selected for comparison is the validation case with a SOI timing of -13 deg aTDC fueled with DME (the same case used in Stage 1).

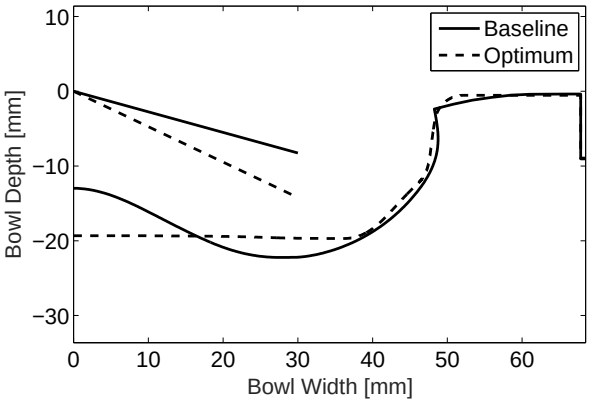

Figure 6.13. *Optimum and baseline case bowl geometry and NA configuration.*

Table 6.9. *Performance and emissions for the baseline and optimum cases.*

	NIE	**maxPRR**	**NOx**	**PP**
Case	[%]	[bar/deg]	[g/kWh]	[bar]
Baseline DME case	42.8	6.1	2.81	194
Opt. case	43.4	9.2	0.74	197

Table 6.10. *Energy balances for the baseline and optimum cases.*

	Gross Ind. Work	**Heat Trans.**	**Exh. Losses**	**Unburnt Fuel**	**Pump. Work**
Case	[J]	[J]	[J]	[J]	[J]
Baseline	4854	1926	4215	268	31
Optimum	4832	1991	4076	364	-58

The optimum configuration increased NIE from 42.8% to 43.4% and reduced the engine out NOx emissions from 2.81 g/kWh to 0.74 g/kWh. Assuming a 99% efficient TWC, the resulting tailpipe NOx would be 0.0074 g/kWh (i.e., 72% below the proposed future NOx emissions targets of 0.0268 g/kWh). Additionally, the maxPRR and PP were similar to the baseline values.

The energy balances of the baseline and optimum cases are shown in Table 6.10. It can be seen that the gross indicated work is very similar for

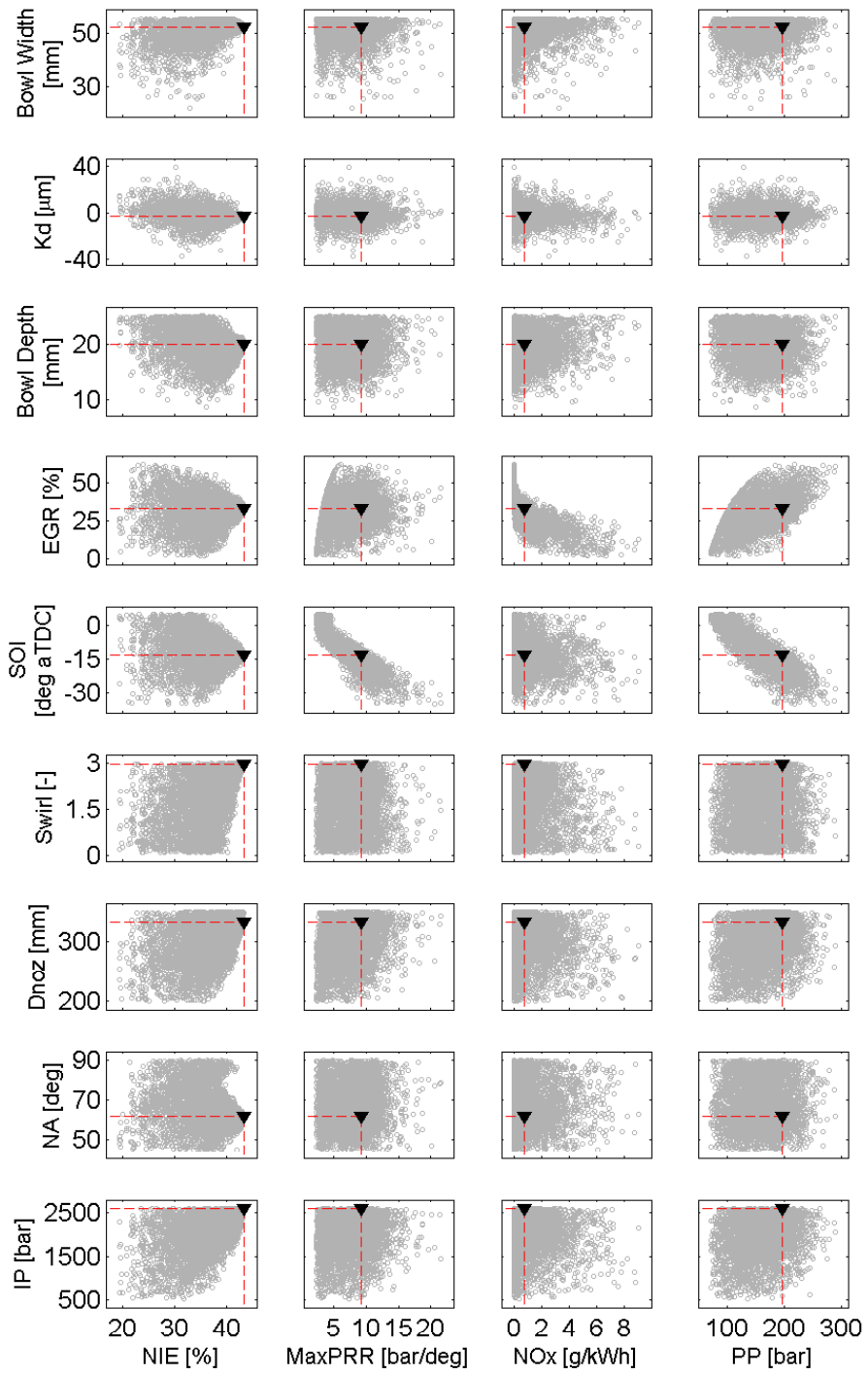

Figure 6.14. *Input versus output for all optimization cases. All data points are shown in gray circles and the optimum solution is shown by the black triangle.*

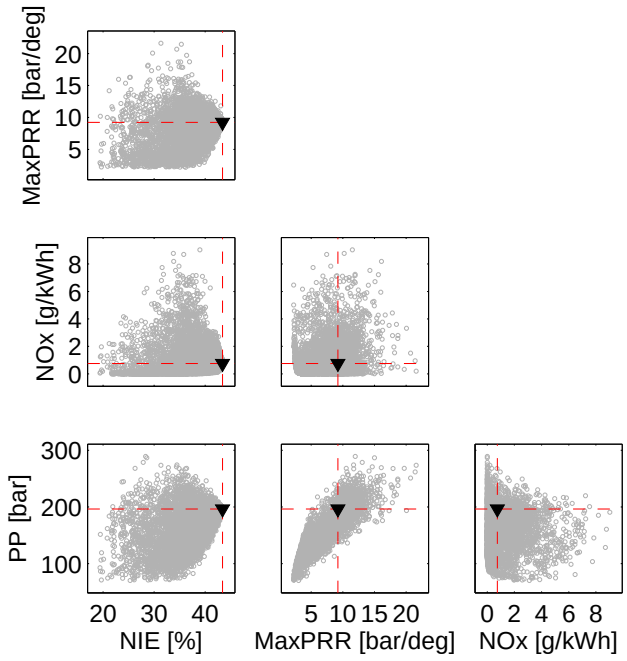

Figure 6.15. *Output versus output for all optimization cases. All data points are shown in gray circles and the optimum solution is shown by the black triangle.*

both cases. The main advantage from the optimum case can be attached to the pumping work, that is able to compensate the slightly lower gross indicated work of the optimum case, leaving an overall increase in NIE of 0.6%. This improvement in pumping work is due to the lower airflow needed to operate at stoichiometric conditions. That is, the DME case needs 0.94 bar less pressure at IVC, which reduces the pumping losses by 0.8% of the fuel energy. This effect can be seen in Fig. 6.16 where there is a noticeable difference in the pressure profile.

In terms of HRR, Fig. 6.16 shows that the optimum case is able to significantly shorten the combustion duration. This effect compensates the lower PIVC of the DME case resulting in a slightly higher PP than the baseline case. Even though the optimum case has a higher equivalence ratio and should mix slower, also seen in Table 6.10 where the unburnt fuel mass is higher for the optimum, the optimum case is able to noticeably reduce the combustion duration compared to the baseline case.

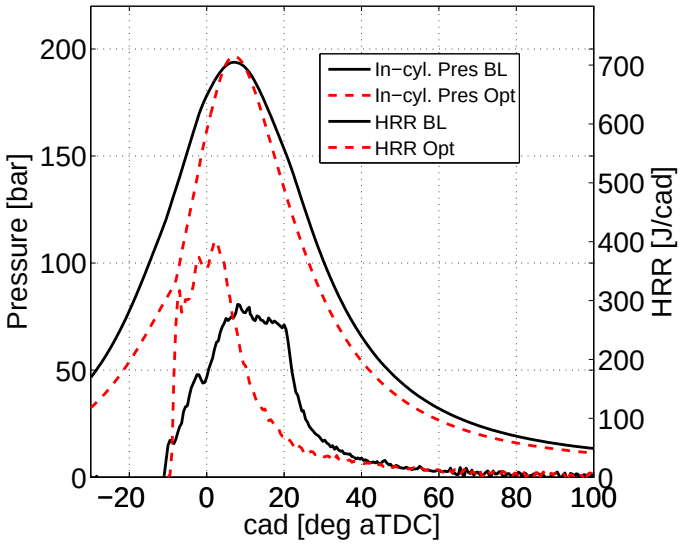

Figure 6.16. *Pcyl and HRR for the baseline and the optimum cases.*

In order to better understand the differences in combustion duration, Fig. 6.17 left shows the normalized fuel injection rate and normalized burned fuel mass. The optimum case, which keeps the same SOI as the baseline case, reaches both 90% fuel mass injected and 90% fuel burned earlier than the baseline case. However, since the injection rate is different, reaching the 90% fuel mixed mass earlier does not mean that the optimum case mixes better than the baseline case. To compare the mixing velocity for two cases with different injection profiles, Fig. 6.17 right shows the apparent combustion time (ACT) [6, 7]. ACT is defined as the time interval between the instant at which the percentage of the mass is injected and the instant at which the same percentage of fuel mass is burned, that is, shorter ACT means shorter mixing time. These results are of interest since they show that even though the combustion duration is shorter for the optimum case, the baseline case has a lower ACT for most of the combustion process, that is, it mixes better than the optimum. Then, as expected operating in stoichiometric conditions, the optimum case has difficulties mixing compared to the baseline case because there is less fresh air and in-cylinder gas density. As a direct consequence, to avoid the negative impact of the poor mixing performance of the combustion system on NIE, the optimum case is forced to compensate it by adjusting the injection settings in order to maintain a short combustion duration.

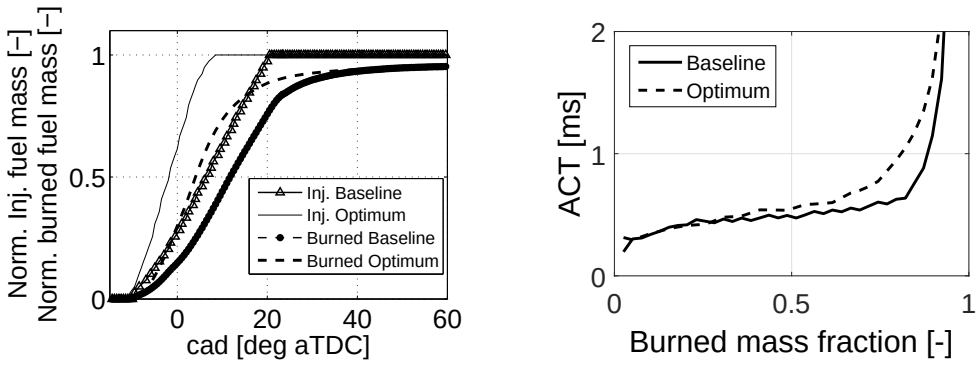

Figure 6.17. *(Left) normalized injected fuel mass and normalized burned fuel mass and (Right) apparent combustion time for the baseline and optimum cases.*

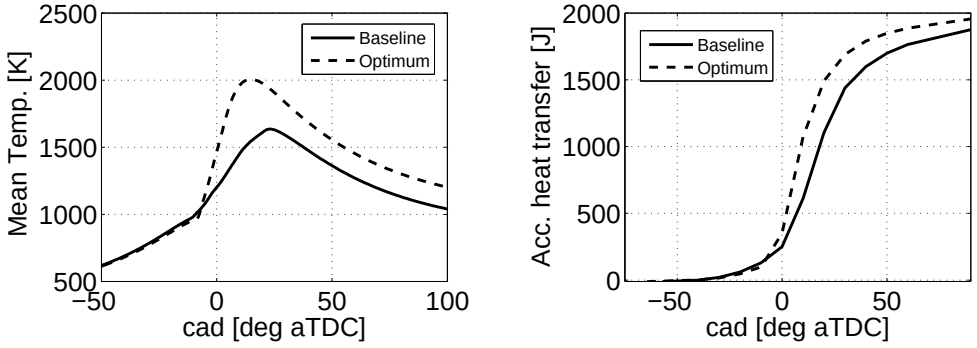

Figure 6.18. *(Left) mean in-cylinder temperature and (Right) accumulated HT for the baseline and optimum cases.*

Differences in in-cylinder temperature and HT losses can be also noticed between the optimum case and the baseline case in Fig. 6.18. As expected, the stoichiometric optimum case shows higher average temperature than the baseline case. As a consequence, the total HT through the combustion chamber walls increases by $\backsim$ 3%. It is interesting to note that, although the exhaust temperature of the optimum case is higher than the baseline case (see Table 6.10), the exhaust energy is higher for the baseline case. This is due to the lower trapped mass of the optimum case, which results in lower exhaust energy even with higher exhaust temperature.

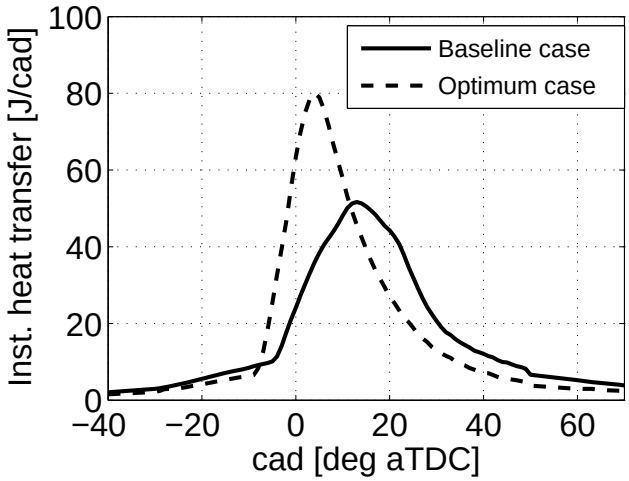

Figure 6.19. *Instantaneous HT for the baseline and optimum cases.*

To better understand the small difference in HT, Fig. 6.19 shows the HT rate. Initially, the HT rate is higher for the optimum case, but by 10 deg aTDC, the situation switches and the HT rate decreases to a value lower than that of the baseline case for the rest of the cycle. In order to understand the HT characteristics, Fig. 6.20 shows local temperature distributions for the baseline and optimum cases. It can be seen that the in-cylinder temperature of the optimum case rapidly increases due to the shorter combustion process, explaining the higher initial HT rate found in Fig. 6.19. However, the increased mixing of the optimum case results in rapid homogenization of the gas temperature. That is, by 30 deg aTDC, the in-cylinder gas temperature distribution is relatively uniform for the optimum case; however, the lower mixing rate of the baseline case results in higher local temperatures near the cylinder liner and cylinder head. This results in relatively high HT losses later in the cycle. In addition, the surface area of the optimized piston bowl is 29.7% smaller than that of the reference bowl (baseline bowl shape has a surface area of 4909 mm^2 and optimum bowl shape has a surface area of 3451 mm^2), which helps to reduce HT losses during the whole cycle.

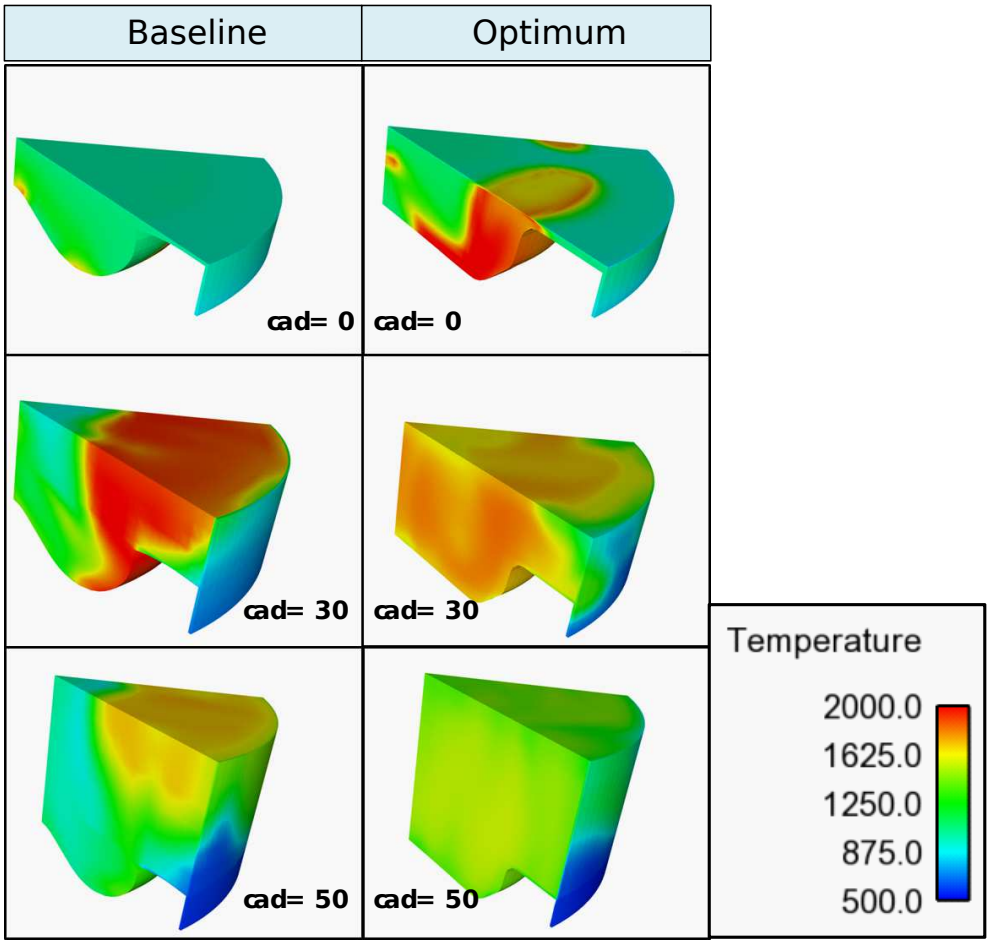

Figure 6.20. *In-cylinder temperature for (left column) the DME fueled baseline case and (right column) the optimum case.*

6.3.2.2 Parametric dependence

To identify parametric dependencies, the results were analyzed using COSSO, and the results for the most relevant inputs on the optimum configuration are presented. Fig. 6.21 shows the impact of EGR, swirl ratio, IP, and SOI timing on performance (NIE, HT, combustion duration, combustion efficiency and PP) and NOx emissions. Note that EGR, swirl ratio and IP are plotted against SOI timing due to the strong impact of SOI timing on PP and NIE.

All four parameters have a noticeable effect on NIE. Retarding SOI timing decreases combustion efficiency and increases the combustion duration, resulting in lower NIE. Similarly, retarding SOI timing shifts the combustion phasing towards the expansion stroke, decreasing PP, maximum mean temperature, peak temperature, and total HT. Although delayed SOI timing reduces HT, the effect is outweighed by the decrease in combustion efficiency and increase in combustion duration. The PP restriction imposed in this optimization limits the advance of the SOI timing to -13.09 deg aTDC.

EGR is one of the most influential inputs in the optimization. It has an effect on NIE, but it is mainly used to control the NOx emissions. The results show that, when a stoichiometric mixture is maintained, the trade-off between NOx and NIE is removed and both parameters improve with increasing EGR. Higher EGR levels reduce the oxygen mole fraction, reducing the adiabatic flame temperature and decreasing NOx emissions and peak temperature. Additionally, at a fixed equivalence ratio, higher EGR levels increase the in-cylinder trapped mass, further reducing the in-cylinder temperature and HT losses. Conversely, since the oxygen concentration is reduced, lack of free oxygen results in slower combustion (increased burn duration) and lower combustion efficiency. Evidently, the reduced HT losses outweigh the longer burn duration and lower combustion efficiency, resulting in a net increase in NIE with increased EGR.

Since the charge is stoichiometric, access to free oxygen is limited in the late stages of the combustion process. Increasing the swirl ratio allows the later injected fuel to access oxygen between the spray flames, shortening the combustion duration, and increasing combustion efficiency. However, the higher swirl ratio also increases the in-cylinder velocities, which results in higher HT losses. In contrast to the effect of EGR, where the reduced HT losses outweighed the increase in burn duration, the shorter burn duration for increased swirl ratio outweighs the increased HT. That is, NIE increases with increasing swirl ratio due to the trend of decreasing combustion duration with increasing swirl ratio.

The effect of IP is similar to that of swirl ratio. That is, increasing IP increases HT, but also shortens combustion duration and increases combustion efficiency resulting in a NIE improvement. It is interesting to note that IP and swirl ratio are complimentary. This shows the importance of the mixing process in stoichiometric DI engines.

The main restrictions in this optimization are NOx emissions and PP. It has been seen that EGR is able to control NOx and at the same time improve efficiency, breaking the NOx-NIE trade-off. However, PP is not

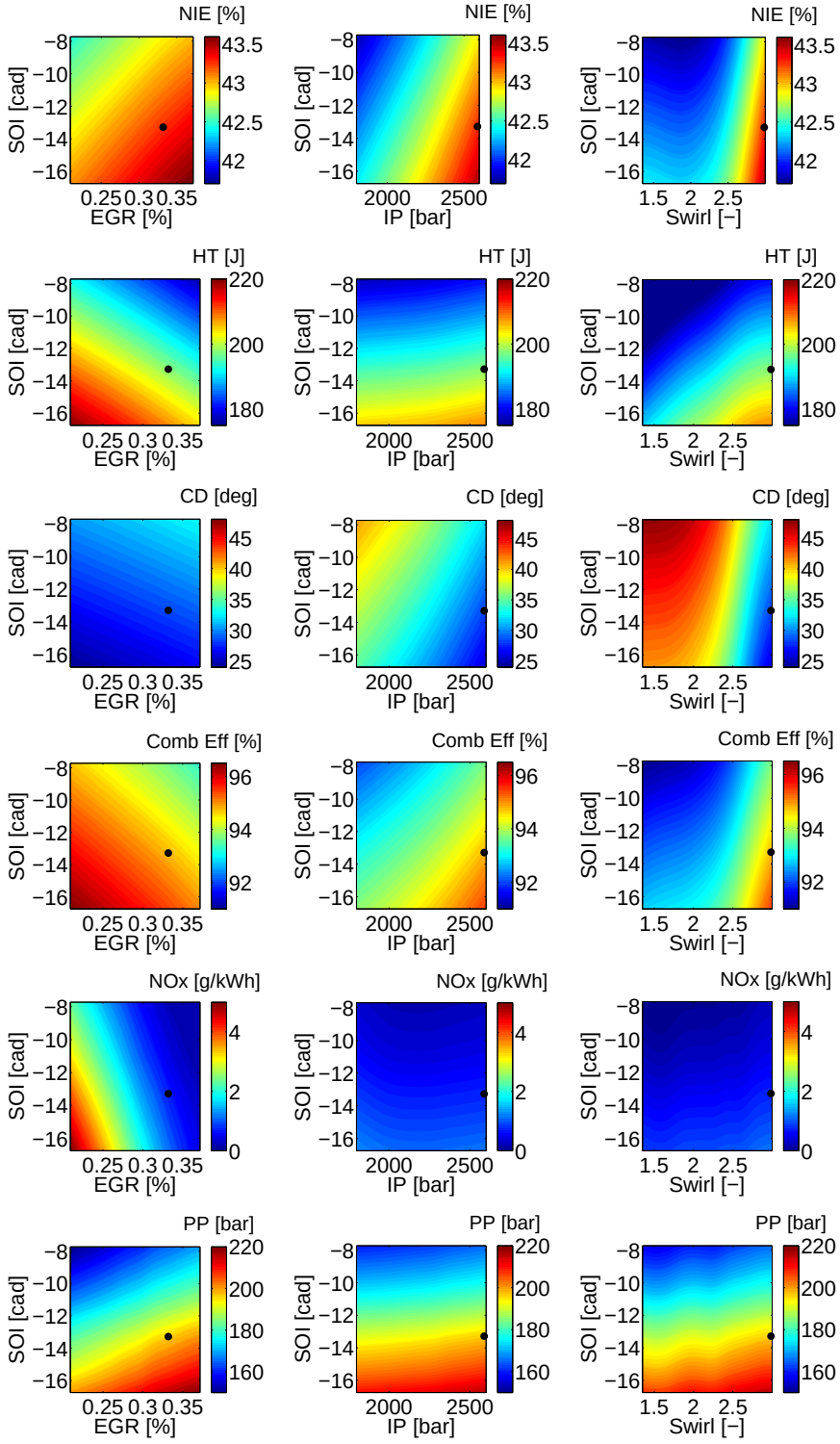

Figure 6.21. *Response surface of the combined effect of EGR, IP, swirl with SOI over NIE, HT, combustion duration (CD), combustion efficiency, NOx and PP. The optimum value for every input is shown by the black dot.*

controllable while improving NIE and it has to be reduced at the cost of increased combustion duration and reduced efficiency. It can also be seen that lower EGR ratios could solve the PP problem. That is, because the required intake pressure decreases with decreasing EGR, the PP also decreases with decreasing EGR. However, SOI timing has a stronger effect on PP than EGR. Accordingly, SOI timing was used to control PP.

6.3.2.3 Parameter evolution

In the first part of this section the optimum and the baseline case have been compared and the effects of the most relevant inputs on the engine performance are understood, therefore the optimum combustion system is now easier to understand. The process shifted the reference piston shape towards a flatter, shallower bowl than the baseline geometry to reduce the surface area to offset the increased HT associated with high IP and high swirl. The geometry is non-reentrant and has a rounded bowl rim to allow access to oxygen in the squish region. Similar to the bowl geometry, the injector geometry is adjusted to have the best interaction possible with the optimum piston geometry and improve mixing. Then the swirl ratio, IP and Dnoz are needed to shorten the combustion duration and increase efficiency. EGR is used to control the NOx emissions, but since adding EGR also increases NIE due to reduced HT, the final EGR levels are higher than the necessary levels to control NOx emissions. Finally, SOI is used to adjust PP.

To illustrate the evolution of the combustion system, CFD simulations were repeated at various key points during the design evolution. Fig. 6.22 shows the results of this investigation. First, a stoichiometric DME case was run with all of the baseline parameters. The only change from the lean DME fueled case was that the intake pressure was reduced to 2.06 bar to achieve stoichiometric operation. This resulted in a significant increase in incomplete combustion due to the difficulty for accessing free oxygen. The HT reduces slightly due to the lower combustion efficiency. The result is a reduction in GIE from the baseline value of 42.8% to 35.6%. This shows that replacing a conventional diesel fueled combustion system with a stoichiometric DME fueled combustion system with no other changes would result in poor performance. That is, the system must be re-optimized to enable peak performance. Next, the case was repeated with the optimum piston bowl geometry. This caused a reduction in HT due to the lower surface area to volume ratio and resulted in a marginal increase in GIE from 35.6% to 35.8%. Notice that most of the reduced HT losses end up as exhaust energy rather than increased work. It is also interesting to note that the combustion efficiency was approximately constant when the piston bowl

was changed from the baseline case to the optimum bowl geometry. Next, the case was repeated by changing NA from the baseline value of 65 deg to the optimum value of 61.7 deg. This caused an increase in GIE from 35.8% to 37.3% due to reduced incomplete combustion resulting from improved oxygen utilization. Note that the HT and exhaust losses are nearly unchanged. Next, the case was repeated with the optimum IP (i.e., IP was increased from the baseline value of 1800 bar to the optimum value of 2594 bar). This caused a further improvement in the mixing process, increasing the GIE from 37.3% to 40.9%. The increase in GIE is due to reduced incomplete combustion and a shorter combustion duration (i.e., reduced exhaust losses) and suggest that (together with the previous section IP results) DME fueled combustion system development efforts should focus on enabling high injection pressure operation. Notice that HT increases back to a value nearly the same as the baseline lean case. This shows the importance of the reduced HT losses resulting from the improved piston bowl geometry. That is, although the addition of the piston bowl alone does not directly improve efficiency, it reduces HT and allows higher IP to be used to improve efficiency. Next, the case was repeated with the optimum Dnoz (i.e., the Dnoz was increased from 300 μm to 330 μm). This caused a slight increase in HT and reduced the GIE from 40.9% to 40.7%. This suggests that the Dnoz has a minimal influence on the efficiency. This makes sense for a stoichiometric combustion system, as the fuel needs to both be introduced into the combustion chamber and be able to find free oxygen. The increased Dnoz addresses the fuel introduction, but does not improve access to oxygen. Next, the case was repeated with the optimum EGR (i.e., the EGR was increased from 25% to 33%). This caused a slight reduction in HT due to the increased in-cylinder mass and lower temperature, increasing GIE from 40.7% to 40.9%. Next, the case was repeated with the optimum swirl ratio (i.e., the swirl ratio was increased from 0.7 to 2.98). This caused a noticeable improvement in the mixing process, reducing the incomplete combustion, and increasing the GIE from 40.% to 43.2%. In terms of HT, it is unchanged when increasing swirl from the baseline value (0.7) to the optimum value (3), contrary to Fig. 6.21. This happens because the baseline swirl is out of the range shown in Fig. 6.21 and the behavior of HT in terms of swirl changes for very low swirl values. Finally, the next case is the optimum case after adding the optimum SOI. This caused almost no effect since the optimum SOI and the baseline SOI are almost identical, but the trends presented are consistent with the small GIE increase with advanced SOI.

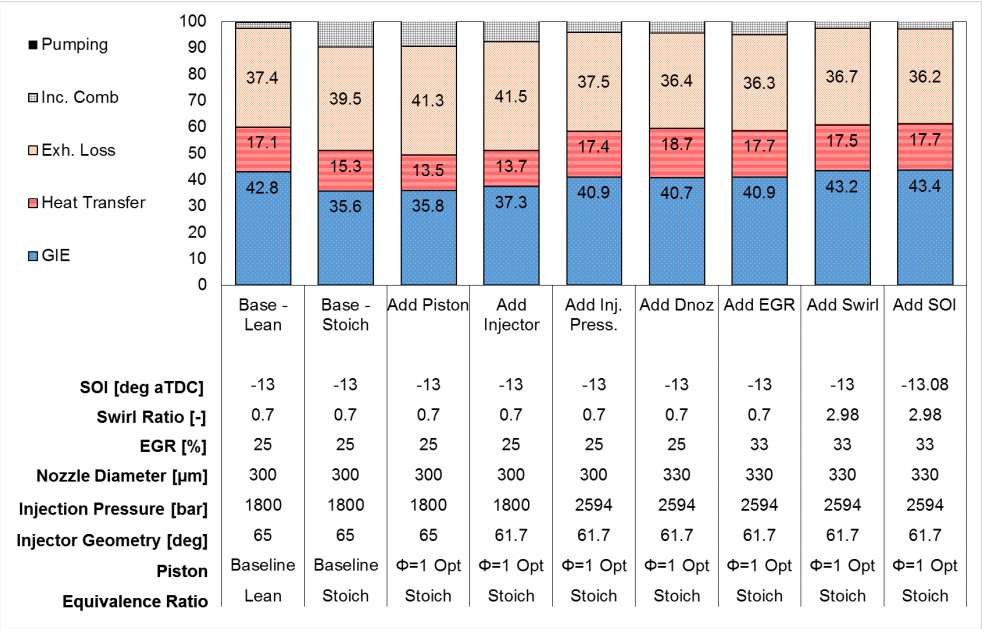

Figure 6.22. *Evolution of the optimum stoichiometric DME fueled combustion system.*

6.4 Summary and conclusions

An optimization system based on a GA algorithm coupled with CFD has been applied to a HD CI engine fueled with DME. The results not only provided the optimum configuration but also the cause/effect relations between the input and output parameters on the optimum configuration. The study was divided in two stages, a first optimization aiming to improve efficiency while keeping the NOx emissions under the current emissions standards and a second optimization aiming to achieve future emissions standards with an engine working in stoichiometric combustion.

The first optimization considered 22 input variables (15 geometric, 4 injection settings and 3 air management settings). The final optimum configuration obtained improved NIE a 3.3% and the NOx emissions, PP and maxPRR were kept under the limit values. The DME optimum combustion system resulted in a slightly more reentrant piston, narrower and less deep with an included angle of 86.7 deg. The EGR was set to a value of 40%, its effect over the combustion was compensated by high IP (2500 bar), high swirl

(2.82), early SOI (-8.19 deg aTDC), high PIVC (3.25 bar) and a large Dnoz (330 μm).

The sensitivity of the input variables was presented in order to have a better understanding of the optimum combustion system configuration. The geometry inputs mainly improved HT, combustion duration and combustion efficiency with a low effect over PP and NOx. Then EGR was the main parameter that guided the optimization. High EGR level was necessary to control NOx but it worsened noticeably the combustion duration and efficiency. Swirl, Dnoz, PIVC and IP, contrary to EGR, had to potential to improve the combustion process with a lower effect over NOx and PP (compared to EGR) and were used to compensate the effect of high EGR over the combustion. Finally, SOI showed a significant effect over PP and was used to keep PP values under the limits.

Based on the results of the first optimization, the second stage applied the optimization method to the same HD CI engine fueled with DME working under stoichiometric conditions aiming to achieve more stringent emissions standards. The optimization considered 21 input variables (15 geometric, 4 injection settings and 2 air management settings). The final optimum configuration improved NIE by 0.6% while enabling the use of a TWC for NOx reduction. Considering a 99% efficient TWC, the tailpipe NOx levels would be 0.0074 g/kWh (72% below the proposed future emission targets). That is, the proposed solution shows the potential to meet future NOx regulations while maintaining diesel-like thermal efficiency.

The new combustion system resulted in a shallow, non-reentrant piston with a flat center (i.e., the central protrusion was removed). The NA of 61.7 deg was selected to enable access to oxygen throughout the combustion chamber. The EGR was set to a value of 33% with high IP (2594 bar), high swirl ratio (2.98), early SOI timing (-13.09 deg aTDC), and a large Dnoz (330 μm). This optimum coincides with the unconstrained peak NIE case because the restriction of controlling NOx emissions is easily achievable by a stoichiometric combustion system coupled with a TWC, removing the trade-off between NIE and NOx.

Mixing and HT were proven to be the main challenges of the new combustion system. This is because the configuration operates under stoichiometric conditions, resulting in high bulk gas temperature and limited access to free oxygen. The optimum geometry was adapted to reduce surface area in order to reduce HT and the high IP and swirl improved the mixing process. The sensitivity of the input variables was analyzed using non-parametric fitting methods to identify the key optimization parameters. EGR

was the main parameter used to control NOx emissions. Contrary to the lean mixing-controlled combustion, it was found that increasing EGR also increased NIE due to reduced HT loss. Swirl, Dnoz, and IP had the potential to improve combustion duration and efficiency with a small effect on NOx and PP. Finally, SOI showed a significant effect over PP and was used to keep PP under the limits with a degradation of the combustion duration and efficiency that was compensated with higher swirl and IP levels.

This work showed that DME is a promising fuel for future generation CI engines and provides guidelines to design CI engines fueled with DME or other high cetane, non-sooting fuels. Additionally, it shows that a stoichiometric DME fueled combustion system coupled with a TWC has potential to be used for future generation CI engines. The non-sooting nature of DME together with the capability of the TWC to control NOx permits the new combustion system to completely manage NOx and soot emissions while maintaining diesel-like efficiency.

Table 6.11. *Target values used in the optimization for the restrictions imposed.*

NOx	**PP**	**maxPRR**
[g/kWh]	**[bar]**	**[bar/deg]**
2.68	200	15

Table 6.12. *Ranges used for the optimization inputs on the reduce cost optimization.*

	G1-G7	**NA**	**SOI**	**IP**	**EGR**	**swirl**
	[-]	**[deg]**	**[deg aTDC]**	**[bar]**	**[%]**	**[-]**
Min.	0.01	45	-35	500	2	0.1
Max	0.99	90	5	2600	62	3

6.A Annex: Reduced cost optimization

The main problem with optimizing with a GA algorithm coupled with CFD calculation is the cost in terms of resources and time. In this annex an extra optimization with the same targets than *"Stage 2: Stoichiometric combustion optimization"* was performed but with lower populations and number of generations. The targets of the optimization are presented in Table 6.11. However, the optimization can not be simply performed with less resources and expect to get good results, the number of inputs have to be adapted. The main source of optimization inputs is the geometry, it requires 15 parameters to be fully flexible but that number can be reduced at the cost of some flexibility, therefore the number of geometric inputs was reduced to 7, removing the capability of the geometry to be able to switch between reentrant and non-reentrant geometries. Additionally, the parameter Dnoz showed little effect on the optimum efficiency and it was removed from the reduced cost optimization. To sum up, 8 geometric parameters and Dnoz where removed as inputs in the reduced cost optimization and only 12 optimization inputs were considered. The parameters and ranges are presented in Table 6.12.

In terms of computational resources, the full cost optimization used a population size of 529 cases per generation and 40 generations were used, resulting in a total of 21,160 function evaluations, and the reduced cost optimization used 64 cases per generation and 20 generations, resulting in a total of 1280 function evaluations. Transformed into real time, the original

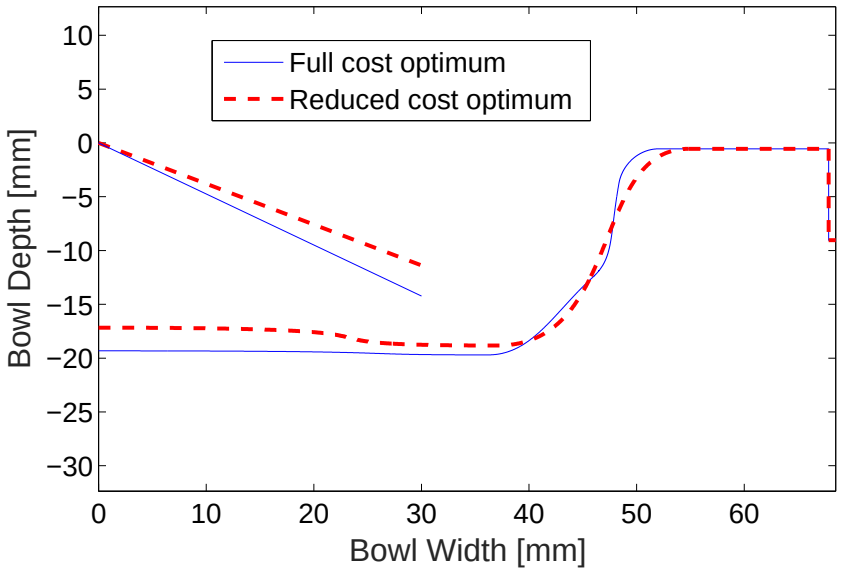

Figure 6.23. *Full cost optimization optimum geometry compared to the reduced cost optimum geometry.*

optimization took over 2 months and the reduced cost optimization was finished in less than 2 weeks.

The optimum configuration obtained in both optimizations are compared in Fig. 6.23 and Table 6.13. Focusing first on the piston bowl geometry, it can be seen that both shapes are fairly similar, except for slight differences in the center region of the bowl and the fact that the geometry obtained in the reduced cost optimization looks smoother, both geometries can be considered equal. Then in terms of injection and air management settings, both combustion systems are also very similar and only differ in 6 deg NA, 2.6 deg in SOI and 1% EGR. These similarities are also seen in the efficiency and performance in Table 6.14.

As expected due to the really similar combustion systems that both optimizations presented, the differences in efficiency and performance is minimal. Both optimum were able to improve the baseline case efficiency of 42.8% and reduce the NOx emissions under the US2030 standards while keeping maxPRR and PP under the restriction levels. In other words, the reduced cost optimization system was able to provide similar results than

Table 6.13. *Optimum values for the air management and injection settings inputs optimized.*

	NA	**SOI**	**IP**	**EGR**	**swirl**
Case	**[deg]**	**[deg aTDC]**	**[bar]**	**[%]**	**[-]**
Full cost opt.	61.7	-13.09	2594	33	2.98
Red. cost opt.	67.7	-15.66	2593	34.5	2.9

Table 6.14. *Performance and emissions for the full cost and reduced cost optimizations optimum cases.*

	NIE	**maxPRR**	**NOx**	**PP**
Case	**[%]**	**[bar/deg]**	**[g/kWh]**	**[bar]**
Full cost Opt.	43.4	9.2	0.74	197
Reduced cost Opt.	43.1	9.1	0.61	196

the full system with 16 times less function evaluations in a quarter of time. However, even though the reduced cost optimization was able to provide really good results, it can never substitute the original optimization. In order to reduce the number of inputs, the knowledge of the shape of the optimum piston geometry and the relevance of certain parameters on the engine efficiency was required and that information is unknown for new combustion concepts without a previous full cost optimization. For that reason, the reduced cost optimization is proposed as a good option to compliment the results obtained from the full cost optimization. Then, it can be used to expand the results including minor modifications of the restrictions or objectives, or it can be used to improve the optimum.

References

[1] Lázaro L, Aparecida C and Lacava P. "Strategies for emission control in diesel engine to meet Euro VI". *Fuel*, n^o 104, pp. 183–193, 2013.

[2] Arcoumanis C, Bae C, Crookes R and Kinoshita E. "The potential of di-methyl ether (DME) as an alternative fuel for compression-ignition engines: A review". *Fuel*, Vol. 87 n^o 7, pp. 1014–1030, 2008.

[3] Agency California Environmental Protection. "Heavy-Duty Technology and Fuels Assessment: Overview, Air resources board". *C.E.P. Agency*, 2015.

[4] Lin Y and Zhang HH. "Component selection and smoothing in smoothing spline analysis of variance models". *Annals of Statistics*, Vol. 34 n^o 5, pp. 2272–2297, 2006.

[5] Einewall P., Tunestal P. and Johansson B. "Lean burn natural gas operation vs. stoichiometric operation with EGR and a three way catalyst". *SAE Technical Paper*, n^o 2005-01-0250, 2005.

[6] Arrégle J, López JJ, García JM and Fenollosa C. "Development of a zero-dimensional diesel combustion model. Part 1: analysis of the quasi-steady diffusion combustion phase". *Applied Thermal Engineering*, Vol. 23 n^o 11, pp. 1301–1317, 2003.

[7] Arrégle J, López JJ, García JM and Fenollosa C. "Development of a zero-dimensional Diesel combustion model: Part 2: Analysis of the transient initial and final diffusion combustion phases". *Applied thermal engineering*, Vol. 23 n^o 11, pp. 1319–1331, 2003.

Chapter 7

General conclusions and future work

Contents

7.1 Introduction

The last chapter of this Thesis focuses on summarizing the main conclusions obtained in this research study and establish the possible relationship between them. This work is the first contact of this research group trying to optimize engines coupling 3D CFD with evolutionary and non-evolutionary algorithms and the conclusions obtained will be the base for future research paths proposed in this field.

7.2 Conclusions

Before summarizing the most important conclusions of this work, it is important to remember that the main objective of the Thesis is to optimize a MCCI combustion system to show its potential for future generation engines, this is, to improve its efficiency while keeping the emissions levels under the current and future emission standards. In order to achieve it, an automatic

optimization system and a methodology had to be developed and implemented for this study.

In Chapter 1 it is described the motivation behind this study and the methodology followed to ensure that the main objective is achieved. In order to be consistent, the same structure is followed to present the final conclusions of this Thesis.

Firstly, it was concluded in Chapter 1 that MCCI engines still have a long life in the field of HD and MD engines for on-road and off-road vehicles, therefore it is worth to follow up the development of those type of engines. For that reason, a review of the main optimization strategies and methodologies used in MCCI engine design was discussed and a valuable set of conclusions were obtained.

- Optimization strategies based on modifying the combustion characteristics of the engine (geometry, air management and injection strategies) have been used for decades with excellent results. However, the emission standards are becoming more stringent and the potential of these strategies is nowadays close to its limit in current generation engines and might not be enough to achieve the emission objectives of future generation engines. For that reason additional strategies based on aftertreatment and alternative fuels were presented as a complement to achieve future emission and fuel consumption targets. Based on that a first optimization of a CDC engine was suggested to find their maximum potential and then an alternative approach with DME is suggested to prove that MCCI engines are able to achieve more stringent emission standards and are a valid option for future generation engines.

- The main drawback attached to the increasing flexibility that the engines are offering lately is that more subsystems imply a harder optimization task, therefore advanced optimization methods are needed. Non-evolutionary methods were chosen to perform the CDC engine optimization because their combustion system is well known and then the previous experience of the research team in CDC engines permitted a reduction of optimization inputs and ranges, then a RSM method was used for this task. A RSM method was the preferred option due to its capability of capturing single and coupled trends and was the most efficient optimization method for a limited number of parameters. Then evolutionary optimization methods were chosen for the DME fueled MCCI engine because, contrary to the CDC engine optimization, the behavior of DME engines are less known and the experience of the

research group was insufficient or nonexistent. A GA method was the chosen option due to the extensive number of literature examples where they have proven success in the field of engine optimization. Concretely, the DKGA was decided as the best option for DME fueled engine optimization after testing its superior performance compared to the other GAs presented.

Then, the results of the non-evolutionary optimization were presented and the following conclusions were obtained

- The optimization methodology based on RSM methods and CFD provided accurate results and proved to be a good optimization option for CDC concepts. This statement was specially demonstrated after the experimental validation.
- The methodology not only provided the optimum configuration but also the cause/effect relationship between the inputs and outputs. This allows the research community to have a better understanding of the combustion concept and completely understand why the reference engine evolved towards the optimum configuration.
- Two optimum configurations were found in two different optimization stages, all optimums offered improved efficiency keeping the emission levels under the reference values. The first optimum was focused on improving the fuel consumption while the second optimum was focused on the NOx/ISFC trade-off. It was found that the room for improvement was very limited and that suggests that new optimization paths for MCCI engines, such as alternative fuels, are needed to achieve future emission standards without an efficiency penalization. Stage 1 optimums were limited at 0.5% ISFC improvement, showing the low potential of optimizing only the geometry and demonstrating that the idea of a quiescent combustion chamber was not achievable with the reference engine. Then, Stage 2 increased the optimization parameters from 4 to 6 (including air management and injection settings as inputs). The optimums found were able to improve ISFC around 5% for constant emissions or 4% for a 40% NOx reduction, but further NOx reduction would not be possible without penalizing the engine ISFC.

The results from the CDC engine optimization demonstrated than adding air management and injection settings as optimization parameters increase the potential of the optimization method but they also suggested that CDC

engines are already optimized and future standards are hardly reachable with this combustion concept. For that reason an alternative path was proposed, MCCI engine fueled with DME, a fuel with diesel-like combustion properties coupled with a non-sooting nature. The optimization was performed and a series of conclusions were obtained from the DME engine optimization.

- The optimization methodology based on GAs and CFD was successfully applied to a DME fueled MCCI engine. It was adjusted to not only provide accurate results but also to provide cause/effect relationship between inputs and outputs, following the structure used in the non-evolutionary optimization.
- The first optimization tried to achieve current emission standards and maximize the engine efficiency. The final optimum provided a 3.3% NIE improvement while satisfying the US2010 standards. The EGR was the main parameter that guided the optimization process. The main restriction was the NOx emissions and the EGR was the main strategy to control it, therefore, the EGR was set to a value of 40% to ensure low NOx emissions and then the rest of the parameters were adjusted to maximize NIE compensating as much as possible the negative impact of medium to high EGR levels. The piston bowl geometry was modified, keeping the reentrant shape, to enhance mixing and reduce HT. Then the injection and air management settings were optimized also to provide faster mixing and combustion, this is, to improve efficiency.
- The second optimization tried to achieve future emission standards with a DME fueled stoichiometric MCCI concept coupled with a TWC. The results proved that it is possible to achieve stremely low NOx emissions (less than 1% of the original values or 72% lower than the target US2030 standards after the TWC) keeping competitive NIE values. This suggests that DME fueled engines can be used for future generation engines achieving US2030 or even more strict regulations maintaining diesel-like efficiencies. Similar to the previous optimization, EGR was the main tool used to control NOx but this time the EGR did not show a negative effect over NIE and the optimization algorithm pushed the EGR to a higher level than that needed to control NOx emissions. The rest of the optimization inputs had similar effects over the engine, however, the non-sooting nature of the DME allowed the use of a TWC, proving superiority to any fuel concerned with soot emissions.

The results presented in this Thesis not only show the limitations and advantages of the different optimization methods but also offer improved

analysis strategies applicable to RSM and GA. Additionally, it is shown that CDC CI engines are already optimized and can not be largely improved with the state-of-the-art MCCI engine optimization strategies (based on hardware and settings) to achieve future emission standards without an efficiency penalization. On the contrary, this work showed that DME is a promising fuel for future generation engines, specially stoichiometric DME fueled MCCI concepts coupled with a TWC, that are able to achieve future emission standards while maintaining diesel-like efficiency.

7.3 Future work

When a research work is finished, it is not possible to deepen in all the concepts and aspects equally, therefore, it has to be shifted to future projects. Additionally, after analyzing the results obtained there are always new challenges and questions that have to be answered. This Thesis is not an exception and after the detailed summary performed in this chapter, there are new research paths that can be investigated to complement this Thesis. Focusing first on the optimization tools and methodologies.

- One of the main problems when generating the CFD cases was the geometry generator because the codes used for this study are already outdated in several aspects. Then this work could be performed in other CFD codes with improved performance to see the real potential of the methodologies without the restrictions imposed by the software.

- The RSM methods are already mature methods that have demonstrated great performance so it is suggested to combine them with evolutionary optimization methodologies trying to improve the accuracy and speed of the optimization. This idea is based on the approach followed in section 4.5.2.1 with the COSSO fitting tool.

- When an optimization is performed with GAs, the algorithm provides the optimum configuration but the analysis of the cause/effect relationships are done in post-process with external softwares. This aspect is specially important when the optimizations are applied to new combustion concepts that are still unknown and the understanding of the path followed by the algorithm is really valuable. For that reason, even though in this Thesis it has been tried to provide this information, it can be further improved and other analysis approaches should be tested.

- The evolutionary optimization method chosen to perform the DME engine optimization was GA because the literature review proved that optimization methodologies based on GA provide robust and accurate results when applied to MCCI engines. However, the other algorithms presented, like PSA, are gaining reliability and should be tested and compared to the GA performance. Then it is proposed to keep investigating the field of optimization methodologies and test alternative evolutionary algorithms like PSA. The main reason behind the interest on PSA algorithms is that they are less likely to converge into a local optimum and, since the real behavior of the DME engine is unknown (i.e. shapes of the response surface), it is worth to try new and more robust alternatives.

The provided optimum configurations presented really good properties and proved their potential for current and future generation engines, then the following future work is proposed.

- The stoichiometric combustion DME engine proved that it could provide lower NOx emissions that the targets proposed for this Thesis with minimal NIE penalization. In this context, it is proposed to keep optimizing the engine with more stringent targets to find the maximum potential of the engine.
- In this Thesis only the DME was proposed as an alternative, however, there are new fuels every year that are worth investigating. Then, it is proposed to modify the code to easily switch the fuel of the MCCI engine and test the potential of alternative fuels to achieve future emission standards.

References

-.
Automobile Production 1900 - 2003.
http://www.carhistory4u.com/the-last-100-years/car-production. (cited on pp. v, 2)

Abani N, Kokjohn S, Park SW, Bergin M, Munnannur A, Ning W, Sun Y and Reitz RD.
An improved spray model for reducing numerical parameter dependencies in diesel engine CFD simulations.
SAE Technical Paper, 2008. (cited on p. 71)

Abani N, Munnannur A and Reitz RD.
Reduction of numerical parameter dependencies in diesel spray models.
Journal of Engineering for Gas Turbines and Power, Vol. 130 n^o 3, pp. 032809, 2008. (cited on pp. 68, 71)

Abraham J.
What is adequate resolution in the numerical computations of transient jets?
SAE Technical Paper, 1997. (cited on p. 70)

Agarwal A.K., Singh A.P. and Maurya R.K.
Evolution, challenges and path forward for low temperature combustion engines.
Progress in Energy and Combustion Science, Vol. 61, pp. 1–56, 2017. (cited on p. 15)

Agarwal A.K., Srivastava D.K., Dhar A., Maurya R.K., Shukla P.C. and Singh A.P.
Effect of fuel injection timing and pressure on combustion, emissions and performance characteristics of a single cylinder diesel engine.
Fuel, Vol. 111, pp. 374–383, 2013. (cited on p. 29)

Agency California Environmental Protection.
Heavy-Duty Technology and Fuels Assessment: Overview, Air resources board.
C.E.P. Agency, 2015. (cited on pp. 31, 135, 149)

Alimin A.J., Benjamin S.F. and Roberts C.A.
Lean NO x trap study on a light-duty diesel engine using fast-response emission analysers.
Journal of Engine Research, Vol. 10 n^o 3, pp. 149–164, 2009. (cited on p. 30)

Amsden AA.
KIVA-3V, release 2, improvements to KIVA-3V.
Los Alamos National Laboratory, Los Alamos, NM, Report No. LA-UR-99-915, 1999. (cited on p. 68)

Amstrong J.
Electronic fuel injection: A history lesson.
http://www.autonews.com/article/20040823/SUB/408230807/electronic-fuel-injection:-a-history-lesson, 2004. (cited on p. 28)

Angelberger C, Poinsot T and Delhay B.
Improving near-wall combustion and wall heat transfer modeling in SI engine computations.
SAE Technical Paper, 1997. (cited on p. 67)

Arcoumanis C, Bae C, Crookes R and Kinoshita E.
The potential of di-methyl ether (DME) as an alternative fuel for compression-ignition engines: A review.
Fuel, Vol. 87 n^o 7, pp. 1014–1030, 2008. (cited on pp. 32, 33, 134)

Armanli A., Yuksel B., Ileri E. and Karaoglan a.D.
Response surface methodology based optimization of a diesel-n-butanol-cotton oil ternary blend ratios to improve engine performance and exhaust emission characteristics.
Energy Conversion and Management, Vol. 90, pp. 383–394, 2015. (cited on p. 47)

Armas O.
Diagnostico experimental del proceso de combustion en motores Diesel de inyeccion directa.
PhD Thesis, 1998. (cited on p. 16)

Arrégle J, López JJ, García JM and Fenollosa C.
Development of a zero-dimensional diesel combustion model. Part 1: analysis of the quasi-steady diffusion combustion phase.
Applied Thermal Engineering, Vol. 23 n^o 11, pp. 1301–1317, 2003. (cited on p. 156)

Arrégle J, López JJ, García JM and Fenollosa C.
Development of a zero-dimensional Diesel combustion model: Part 2: Analysis of the transient initial and final diffusion combustion phases.
Applied thermal engineering, Vol. 23 n^o 11, pp. 1319–1331, 2003. (cited on p. 156)

Beale JC and Reitz RD.
Modeling spray atomization with the Kelvin-Helmholtz/Rayleigh-Taylor hybrid model.
Atomization and sprays, Vol. 9 n^o 6, 1999. (cited on pp. 68, 71)

Benajes J., Molina S., Novella R. and Belarte E.
Evaluation of massive exhaust gas recirculation and Miller cycle strategies for mixing-controlled low temperature combustion in a heavy duty diesel engine.
Energy, Vol. 71, pp. 355–366, 2014. (cited on p. 15)

Benajes J, Novella R, De Lima D, TribottÃ© P, Quechon N, Obernesser P and Dugue V.
Analysis of the combustion process, pollutant emissions and efficiency of an innovative 2-stroke HSDI engine designed for automotive applications.
Applied Thermal Engineering, Vol. 58 n^o 1, pp. 181–193, 2013. (cited on p. 82)

Benajes J, Novella R, Pastor JM, Hernández-López A, Hasegawa M, Tsuji N, Emi M, Uehara I, Martorell J and Alonso M.
Optimization of the combustion system of a medium duty direct injection diesel engine by combining CFD modeling with experimental validation.
Energy Conversion and Management, Vol. 110, pp. 212–229, 2016. (cited on p. 35)

Benajes J, Pastor JV, GarcÃa A and Monsalve-Serrano J.
An experimental investigation on the influence of piston bowl geometry on RCCI performance and emissions in a heavy-duty engine.
Energy Conversion and Management, Vol. 103, pp. 1019–1030, 2015. (cited on p. 23)

Benajes J., Pastor J.V., GarcÃa A. and Monsalve-Serrano J.
An experimental investigation on the influence of piston bowl geometry on RCCI performance and emissions in a heavy-duty engine.
Energy Conversion and Management, Vol. 103, pp. 1019–1030, 2015. (cited on p. 26)

Birol F.
CO2 highlights 2016.
http://www.iea.org/publications/freepublications/publication/co2-emissions-from-fuel-combustion-highlights-2016.html. (cited on pp. v, 3)

Bosch.
Pressure in diesel engines.
http://www.bosch-presse.de/pressportal/de/en/pressure-in-diesel-engines-42396.html, 2013. (cited on pp. v, 29)

Bosch W.
The fuel rate indicator: a new measuring instrument for display of the characteristics of individual injection.
SAE Technical Paper, 1966. (cited on p. 64)

Broatch A., Olmeda P., GarcÃa A., Salvador-Iborra J. and Warey A.
Impact of swirl on in-cylinder heat transfer in a light-duty diesel engine.
Energy, Vol. 119, pp. 1010–1023, 2017. (cited on p. 26)

Bruneaux G.
Study of the correlation between mixing and auto-ignition processes in high pressure Diesel jets.
SAE Paper, n^o 2007-01-0650, 2007. (cited on p. 18)

C.F. Taylor.
The Internal Combustion Engine in Theory and Practice.
The MIT Press, Vol. 2, 1985. (cited on p. 16)

Channapattana S.V., Pawar A.A. and Kamble P.G.
Optimization of operating parameters of DI-CI engine fueled with second generation Bio-fuel and development if ANN based prediction model.
Applied Energy, Vol. 187, pp. 84–95, 2017. (cited on p. 57)

Chase S., Nevin R., Winsor R. and Baumgard K.
Stoichiometric compression ignition (SCI) engine.
SAE Technical Paper, n^o 2007-01-4224, 2007. (cited on p. 31)

Choi S, Shin SH, Lee J, Min K and Choi H.
The effects of the combustion chamber geometry and a double-row nozzle on the diesel engine emissions.
Proceedings of the Institution of Mechanical Engineers, Part D: Journal of Automobile Engineering, Vol. 229 n^o 5, pp. 590–598, 2015. (cited on p. 23)

Clow B. and White T.
An evolutionary race: a comparison of genetic algorithms and particle swarm optimization used for training neural networks.
Proc. of International Conference on Artificial Intelligence, pp. 582–588, 2004. (cited on p. 48)

Coello C.A.C. and Pulido G.T.
A micro-genetic algorithm for multiobjective optimization.
EMO, Vol. 1, pp. 126–140, 2001. (cited on p. 50)

Colin O and Benkenida A.
The 3-zones extended coherent flame model (ECFM3Z) for computing premixed/diffusion combustion.
Oil & Gas Science and Technology, Vol. 59 n^o 6, pp. 593–609, 2004. (cited on p. 67)

Costa M., Bianchi G.M., Forte C. and Cazzoli G.
A numerical methodology for the multi-objective optimization of the DI diesel engine combustion.
Energy Procedia, Vol. 45, pp. 711–720, 2014. (cited on p. 57)

Curran HJ, Fisher EM, Glaude PA, Marinov NM, Pitz WJ, Westbrook CK, Layton DW, Flynn PF, Durrett RP and Zur Loye AO.
Detailed chemical kinetic modeling of diesel combustion with oxygenated fuels.
SAE Technical Paper, 2001. (cited on p. 33)

Curran HJ, Pitz WJ, Westbrook CK, Callahan GV and Dryer FL.
Oxidation of automotive primary reference fuels at elevated pressures.
Elsevier, Vol. 27, pp. 379–387, 1998. (cited on p. 33)

Deb K, Pratap A, Agarwal S and Meyarivan T.
A fast and elitist multiobjective genetic algorithm: NSGA-II.
IEEE transactions on evolutionary computation, Vol. 6 n^o 2, pp. 182–197, 2002. (cited on p. 51)

Dec J.E.
A conceptual model of DI diesel combustion based on laser-sheet imaging.
SAE Paper, n^o 970873, 1997. (cited on p. 19)

Dec J.E. and Espey C.
Ignition adn early soot formation in a D.I. diesel engine using multiple 2-D imaging diagnostics.
SAE Paper, Vol. 24 n^o 950456, 1995. (cited on pp. 17, 18)

Dec J.E. and Espey C.
Chemiluminescence imaging of autoignition in a DI diesel engine.
SAE Paper, n^o 982685, 1998. (cited on pp. 17, 18)

Dec J.E. and R.E. Canaan.
PLIF imaging of NO formation in a DI diesel engine.
SAE Paper, n^o 980147. (cited on pp. 19, 21)

DieselNet.
Emission standards.
https://www.dieselnet.com/standards. (cited on pp. v, 3)

DiGiulio C.D., Pihl J.A., Choi J.S., Parks J.E., Lance M.J., Toops T.J. and Amiridis M.D.
NH 3 formation over a lean NO X trap (LNT) system: Effects of lean/rich cycle timing and temperature.
Applied Catalysis B: Environmental, Vol. 147, pp. 698–710, 2014. (cited on p. 31)

Divekar P.S., Chen X., Tjing J. and Zheng M.
Energy efficiency impact of EGR on organizing clean combustion in diesel engines.
Energy Conversion and Management, Vol. 112, pp. 369–381, 2016.
(cited on pp. v, 25, 28)

Diwakar R. and Singh S.
Importance of spray-bowl interaction in a DI diesel engine operating under PCCI combustion mode.
SAE Technical Paper, n^o 2009-01-0711, 2009. (cited on p. 24)

Dreisbach R., Graf G., Kreuzig G., Theissl H. and Pfahl U.
HD base engine development to meet future emission and power density challenges of a DDI engine.
SAE Technical Paper, n^o 2007-01-4225, 2007. (cited on p. 25)

Egnell R.
Comparison of heat release and NOx formation in a DI diesel engine running on DME and diesel fuel.
SAE Technical Paper, n^o 2001-01-0651, 2001. (cited on p. 33)

Eiben A.E. and Smith J.E.
Introduction to Evolutionary Computing.
Springer, 2003. (cited on p. 47)

Einewall P., Tunestal P. and Johansson B.
Lean burn natural gas operation vs. stoichiometric operation with EGR and a three way catalyst.
SAE Technical Paper, n^o 2005-01-0250, 2005. (cited on pp. 31, 149)

ERTRAC.
Future light and heavy duty ICE powertrain technologies.
http://www.ertrac.org, 2016. (cited on pp. v, 4)

Fleisch T., McCarthy C., Basu A., Udovich C., Charbonneau P., Slodowske W., A.E. Mikkelsen and McCandless J.
A new clean diesel technology: demonstration of ULEV emissions on a Navistar diesel engine fueled with dimethyl ether.
SAE Technical Paper, n^o 950061, 1995. (cited on p. 33)

Flynn P.F., Durrett R.P., Hunter G.L., zur Loye A.O., Akinyemi O.C. and Dec J.E.
Diesel combustion: An integrated view combining laser diagnostics, chemical kinetics and empirical validation.
SAE Paper, n^o 1999-01-0509, 1999. (cited on pp. v, 19, 20)

Funayama Y., Nakajima H. and Shimokawa K.
A Study on the Effects of a Higher Compression Ratio in the Combustion Chamber on Diesel Engine Performance.
SAE Technical Paper, n^o 2016-01-0722, 2016. (cited on p. 23)

Ge H, Shi Y, Reitz RD, Wickman D and Willems W.
Engine development using multi-dimensional CFD and computer optimization.
SAE Technical Paper, 2010. (cited on p. 50)

Genzale C. L., Reitz R.D. and Wickman D.D.
A computational investigation into the effects of spray targeting, bowl geometry and swirl ratio for low-temperature combustion in a heavy-duty diesel engine.
SAE Technical paper, n^o 2007-01-0119, 2007. (cited on pp. 26, 104)

Goto S., Oguma M. and Suzuki S.
Research and development of a medium duty DME truck.
SAE Technical Paper, n^o 2005-01-2194, 2005. (cited on p. 33)

Guan B., Zhan R., Lin H. and Huang Z.
Review of state of the art technologies of selective catalytic reduction of NO x from diesel engine exhaust.
Applied Thermal Engineering, 2014. (cited on p. 31)

Guan B., Zhan R., Lin H. and Huang Z.
Review of the state-of-the-art of exhaust particulate filter technology in internal combustion engines.
Journal of environmental management, Vol. 154, pp. 225–258, 2015. (cited on p. 30)

Habchi C, Lafossas FA, BÃ©ard P and Broseta D.
Formulation of a one-component fuel lumping model to assess the effects of fuel thermodynamic properties on internal combustion engine mixture preparation and combustion.
SAE Technical Paper, 2004. (cited on p. 67)

Hajireza S., Regner G., Christie A., Egert M. and Mittermaier H.
Application of CFD modeling in combustion bowl assessment of diesel engines using DoE methodology.
SAE Technical Paper, n^o 2006-01-3330, 2006. (cited on p. 58)

Han S. and Bae C.
The influence of fuel injection pressure and intake pressure on conventional and low temperature diesel combustion.
SAE Technical Paper, n^o 2012-01-1721, 2012. (cited on pp. 27, 29, 110)

Han S., Kim J. and Bae C.
Effect of air-fuel mixing quality on characteristics of conventional and low temperature diesel combustion.
Applied Energy, Vol. 119, pp. 454–466, 2014. (cited on p. 14)

Han Z and Reitz RD.
Turbulence modeling of internal combustion engines using RNG K-e models.
Combustion science and technology, Vol. 106 n^o 4-6, pp. 267–295, 1995. (cited on p. 68)

Hassan R., Cohanim B., De Weck O. and Venter G.
A comparison of particle swarm optimization and the genetic algorithm.
Proceedings of the 1st AIAA multidisciplinary design optimization specialist conference, Vol. 18 n^o 21, pp. 2005. (cited on p. 49)

Heywood J.B.
Internal combustion engine fundamentals.
McGraw Hill Inc., 1988. (cited on pp. 19, 24, 34)

Higgins B, Siebers D and Aradi A.
Diesel spray ignition and premixed-burn behavior.
SAE paper, 2000. (cited on p. 17)

Hiroyasu H and Kadota T.
Models for combustion and formation of nitric oxide and soot in direct injection diesel engines.
SAE Technical Paper, 1976. (cited on p. 67)

Hountalas D.T., Kouremenos D.A., Binder K.B., Schwarz V. and Mavropoulos G.C.
Effect of injection pressure on the performance and exhaust emissions of a heavy duty DI diesel engine.
SAE Technical Paper, n^o 2003-01-0340, 2003. (cited on p. 29)

Huh KY and Gosman AD.
A phenomenological model of diesel spray atomization.
Proceedings of the international conference on multiphase flows, Vol. 2, pp. 515–518, 1991. (cited on p. 67)

Idicheria C.A. and Pickett L.M.
Formaldehyde visualization near lift-off location in a Diesel jet.
SAE Paper, n^o 2006-01-3434, 2006. (cited on p. 20)

information administration U.S. Energy.
Annual energy outlook.
https://www.eia.gov/outlooks/aeo/pdf/0383(2012).pdf, 2012. (cited on pp. v, 5)

Issa RI.
Solution of the implicitly discretised fluid flow equations by operator-splitting.
Journal of computational physics, Vol. 62 n^o 1, pp. 40–65, 1986. (cited on p. 68)

Jang J., Lee Y., Cho C., Woo Y. and Bae C.
Improvement of DME HCCI engine combustion by direct injection and EGR.
Fuel, Vol. 113, pp. 617–624, 2013. (cited on p. 33)

Jung H., Kittelson D.B. and Zachariah M.R.
The influence of engine lubricating oil on diesel nanoparticle emissions and kinetics of oxidation.
SAE Technical Paper, n^o 2003-01-3179, 2003. (cited on p. 33)

Kachitvichyanukul V.
Comparison of three evolutionary algorithms: GA, PSO, and DE.
Industrial Engineering and Management Systems, Vol. 11 n^o 3, pp. 215–223, 2012. (cited on pp. vi, 48, 49, 54, 55)

Kapus P. and Ofner H.
Development of fuel injection equipment and combustion systems for DI diesels operated on dimethyl ether.
SAE Technical Paper, n^o 950062, 1995. (cited on p. 32)

Karlsson A, Magnusson I, Balthasar M and Mauss F.
Simulation of soot formation under diesel engine conditions using a detailed kinetic soot model.
SAE Technical Paper, 1998. (cited on p. 67)

Kennedy J. and Eberhart R.
Particle Swarm Optimization.
Proceedings of the IEEE International Conference on Neural Networks, pp. 1942–1945, 1995. (cited on p. 54)

Kim B.S., Yoon W.H., Ryu S.H. and Ha J.S.
Effect of the injector nozzle hole diameter and number on the spray characteristics and the combustion performance in medium-speed diesel marine engines.
SAE Technical Paper, n^o 2005-01-3853, 2005. (cited on p. 29)

Kim M., Liechty M.P. and Reitz R.D.
Application of micro-genetic algorithms for the optimization of injection strategies in a heavy-duty diesel engine.
SAE Technical Paper, n^o 2005-01-0219, 2005. (cited on p. 50)

Kim M, Liechty MP and Reitz RD.
Application of micro-genetic algorithms for the optimization of injection strategies in a heavy-duty diesel engine.
SAE Technical Paper, 2005. (cited on p. 51)

Klos DT.
Investigations of low temperature combustion (LTC) engine design and combustion instability.
University of Wisconsin, 2015. (cited on pp. vi, 52, 53)

Kokjohn SL and Reitz RD.
Investigation of the roles of flame propagation, turbulent mixing, and volumetric heat release in conventional and low temperature diesel combustion.
Journal of Engineering for Gas Turbines and Power, Vol. 133 n^o 10, pp. 102805, 2011. (cited on p. 70)

Kosaka H., Drewes V.H., Catalfamo L., Aradi A.A., Iida N. and Kamimoto T.
Two-dimensional imaging of formadehyde formed during the ignition process of a diesel fuel spray.
SAE Paper, n^o 2000-01-0236, 2000. (cited on p. 18)

Krishnakumar K.
Micro-genetic algorithms for stationary and non-stationary function optimization.
Symposium on Visual Communications, Image Processing, and Intelligent Robotics Systems, pp. 289–296, 1990. (cited on p. 50)

Kweon C.B., Okada S., Stetter J.C., Christenson C.G., Shafer M.M., Schauer J.J. and Foster D.E.
Effect of injection timing on detailed chemical composition and particulate size distributions of diesel exhaust.
SAE Technical Paper, n^o 2003-01-1794, 2003. (cited on pp. 30, 110)

Lapuerta M, Armas O and HernÃ¡ndez JJ.
Diagnosis of DI Diesel combustion from in-cylinder pressure signal by estimation of mean thermodynamic properties of the gas.
Applied Thermal Engineering, Vol. 19 n^o 5, pp. 513–529, 1999. (cited on p. 64)

Lázaro L, Aparecida C and Lacava P.
Strategies for emission control in diesel engine to meet Euro VI.
Fuel, n^o 104, pp. 183–193, 2013. (cited on pp. 110, 134)

Lázaro L., Aparecida C. and Lacava P.T.
Strategies for emission control in diesel engine to meet Euro VI.
Fuel, Vol. 104, pp. 183–193, 2013. (cited on p. 27)

Lee S. and Reitz R.D.
Stoichiometric combustion in a HSDI diesel engine to allow use of a three-way exhaust catalyst.
SAE Technical Paper, n^o 2006-01-1148, 2006. (cited on p. 31)

Lee S. and Reitz R.D.
Effects of engine operating parameters on near stoichiometric diesel combustion characteristics.
SAE Technical Paper, n^o 2007-01-0121, 2007. (cited on p. 31)

Lin Y. and Zhang H.
Component selection and smoothing in smoothing spline analysis of variance models.
Annals of Statistics, Vol. 5, 2006. (cited on p. 95)

Lin Y and Zhang HH.
Component selection and smoothing in smoothing spline analysis of variance models.
Annals of Statistics, Vol. 34 n^o 5, pp. 2272–2297, 2006. (cited on pp. 136, 151)

Liu C., Shi J.W., Gao C. and Niu C.
Manganese oxide-based catalysts for low-temperature selective catalytic reduction of NO x with NH 3: A review.
Applied Catalysis A: General, Vol. 522, pp. 54–69, 2016. (cited on p. 31)

McCulloch W.S. and Pitts W.
A logical calculus of the ideas immanent in nervous activity.
The bulletin of mathematical biophysics, pp. 115–133, 1943. (cited on p. 55)

Miles P.C. and Andersson O.
A review of design considerations for light-duty diesel combustion systems.
International Journal of Engine Research, Vol. 17 n^o 1, pp. 6–15, 2016.
(cited on pp. 23, 24, 26, 29, 104)

Molina S.A.
Influencia de los parametrod de inyeccion y la recirculacion de gases de escape sobre el proceso de combustion en un motor diesel.
PhD Thesis, 2003. (cited on pp. v, 21)

Montgomery D.C.
Design and Analysis of Experiments.
John Wiley and Sons, 2013. (cited on pp. v, vi, 43, 44, 45, 46)

Munnannur A.
Droplet Collision Modeling in Multi-dimensional Engine Spray Computation.
ProQuest, 2007. (cited on p. 71)

Musculus M.P.B.
On the correlation between NOx emissions and the diesel premixed burn.
SAE Paper, n^o 2004-01-1401, 2004. (cited on p. 19)

Novella R.
Influencia de los ciclos Atkinson y Miller sobre el proceso de combstión y las emisones contaminantes de un motor diesel.
Editorial Reverté, 2012. (cited on pp. v, 6, 16)

O'Rourke Peter J and Amsden AA.
A spray/wall interaction submodel for the KIVA-3 wall film model.
SAE Technical Paper, 2000. (cited on p. 71)

Pacaud P., Perrin H. and Laget O.
Cold start on diesel engine: is low compression ratio compatible with cold start requirements?
SAE International Journal of Engines, Vol. 1 n^o 2008-01-1310, pp. 831–849, 2008. (cited on p. 23)

Pan L, Kokjohn SL and Huang Z.
Development and validation of a reduced chemical kinetic model for dimethyl ether combustion.
Fuel, Vol. 160, pp. 165–177, 2015. (cited on p. 70)

Park SH and Lee CS.
Combustion performance and emission reduction characteristics of automotive DME engine system.
Progress in Energy and Combustion Science, Vol. 39 n^o 1, pp. 147–168, 2013. (cited on p. 34)

Park S.H. and Lee C.S.
Applicability of dimethyl ether (DME) in a compression ignition engine as an alternative fuel.
Energy Conversion and Management, Vol. 86, pp. 848–863, 2014. (cited on p. 32)

Payri F and Desantes J.M.
Motores de combustión interna alternativos.
Editorial Reverté, 2011. (cited on pp. 23, 24, 26, 28)

Payri F, Molina S, MartÃn J and Armas O.
Influence of measurement errors and estimated parameters on combustion diagnosis.
Applied Thermal Engineering, Vol. 26 n^o 2, pp. 226–236, 2006. (cited on p. 64)

Perini F.
Optimally reduced reaction mechanisms for Internal Combustion Engines running on biofuels.
PhD, UniversitÃ diModena e Reggio Emilia, 2011. (cited on p. 68)

Plee S.L. and Ahmad T.
Relative roles of premixed and diffusion burning in DIisel combustion.
SAE Paper, n^o 831733, 1983. (cited on p. 18)

Prabhu S.S., Nayak N.S., Kapilan N. and Hindasageri V.
An experimental and numerical study on effects of exhaust gas temperature and flow rate on deposit formation in Urea-Selective Catalytic Reduction (SCR) system of modern automobiles.
Applied Thermal Engineering, Vol. 111, pp. 1211–1231, 2017. (cited on p. 31)

Praveena V. and Martin M.L.J.
A Review on Various After Treatment Techniques to Reduce NOx emissions in a CI Engine.
Journal of the Energy Institute, 2017. (cited on pp. 30, 31)

Ra Y and Reitz RD.
A reduced chemical kinetic model for IC engine combustion simulations with primary reference fuels.
Combustion and Flame, Vol. 155 n^o 4, pp. 713–738, 2008. (cited on pp. 68, 70)

Reddy A., Pratap N, Kolluri R.V., Priyedarshi A. and Singh S.N.
Effect Of Compression Ratio On The Performance Of Diesel Engine At Different Loads.
International Journal of Engineering Research and Applications, Vol. 5, 2015.
(cited on p. 23)

Reitz RD and Diwakar R.
Structure of high-pressure fuel sprays.
SAE Technical Paper, 1987. (cited on p. 67)

Saluja R.K., Kumar V. and Sham R.
Stability of biodiesel - A review.
Renewable and Sustainable Energy Reviews, Vol. 62, pp. 866–881, 2016. (cited on p. 32)

Saravanan S., Rajesh K.B., Varadharajan A., Rana D., Balaji A and Lakshmi N.G.
Optimization of DI diesel engine parameters fieled with iso-butanol/diesel blends - Response surface methodology approach.
Fuel, Vol. 203, pp. 658–670, 2017. (cited on p. 47)

Senecal P.K.
Development of a methodology for internal combustion engine design using multi-dimensional modeling with validation through experiments.
University of Wisconsin, 2001. (cited on p. 50)

Sher E.
Handbook of air pollution from internal combustion engines.
USA Academic press, 1998. (cited on p. 27)

Shi Y., Ge H.W. and Reitz R.D.
Computational Optimization of Internal Combustion Engines.
Springer Science and Business Media, 2011. (cited on pp. 42, 43)

Shi Y and Reitz RD.
Assessment of optimization methodologies to study the effects of bowl geometry, spray targeting and swirl ratio for a heavy-duty diesel engine operated at high-load.
SAE International Journal of Engines, Vol. 1 n^o 2008-01-0949, pp. 537–557, 2008.
(cited on p. 26)

Shi Y. and Reitz R.D.
Assessment of optimization methodologies to study the effects of bowl geometry, spray targeting and swirl ratio for a heavy-duty diesel engine operated at high-load.
SAE International Journal of Engines, Vol. 1 n^o 2008-01-0949, pp. 537–557, 2008.
(cited on p. 47)

Shiffman D.
The nature of code.
http://natureofcode.com/book/index, 2012. (cited on pp. 55, 57)

Sidhu S., Graham J. and Striebich R.
Semi-volatile and particulate emissions from the combustion of alternative diesel fuels.
Chemosphere, Vol. 42 n^o 5, pp. 681–690, 2001. (cited on p. 33)

Siemens.
STAR-CD METHODOLOGY. Version 4.18.
2012. (cited on pp. 67, 68)

Sperling C and Gordon D.
Two billion cars, transforming a culture.
http://onlinepubs.trb.org/onlinepubs/trnews/trnews259billioncars.pdf.
(cited on pp. v, 2)

Stamatellou A.M. and Stamatelos A.
Overview of Diesel Particulate Filter Systems sizing approaches.
Applied Thermal Engineering, 2017. (cited on p. 30)

Sung K., Kim J. and Reitz R.D.
Experimental study of pollutant emission reduction for near-stoichiometric diesel combustion in a three-way catalyst.
International Journal of Engine Research, Vol. 10, pp. 349–357, 2009. (cited on p. 31)

Teng H, McCandless JC and Schneyer JB.
Thermochemical characteristics of dimethyl ether-An alternative fuel for compression-ignition engines.
SAE Technical Paper, 2001. (cited on p. 33)

Thangaraja C. and Kannan C.
Effect of the exhaust gas recirculation on advanced diesel combustion and alternate fuels - A review.
Applied Energy, Vol. 180, pp. 169–184, 2016. (cited on p. 27)

Thomas G., Feng B., Veeraragavan A., Cleary M.J. and Drinnan N.
Emissions from DME combustion in diesel engines and their implications on meeting future emission norms: A review.
Fuel processing technology, Vol. 119, pp. 286–304, 2014. (cited on pp. 32, 33)

Turkson R.F., Yan F., Ali M.K.A. and Hu J.
Artificial neural network applications in the calibration of spark-ignition engines: An overview.
Engineering Science and Technology, an International Journal, Vol. 19 n^o 3, pp. 1346–1359, 2016. (cited on pp. vi, 56)

Yakhot V and Orszag SA.
Renormalization group analysis of turbulence. I. Basic theory.
Journal of scientific computing, Vol. 1 n^o 1, pp. 3–51, 1986. (cited on p. 67)

Yao M., Zheng Z. and Liu H.
Progress and recent trends in homogeneous charge compression ignition (HCCI) engines.
Progress in Energy and Combustion Science, Vol. 35 n^o 5, pp. 398–437, 2009.
(cited on p. 14)

Yoon E.S. and Han C.
A review of sustainable energy recent development and future prospects of dimethyl ether (DME).
Computer aided chemical engineering, Vol. 27, pp. 169–175, 2009. (cited on p. 32)

Youn I.M., Park S.H., Roh H.G. and Lee C.S.
Investigation on the fuel spray and emission reduction characteristics for dimethyl ether (DME) fueled multi-cylinder diesel engine with common-rail injection system.
Fuel processing technology, Vol. 92 n^o 7, pp. 1280–1287, 2011. (cited on p. 33)

Yuan Y, Li G, Yu Y, Zhao P and Li H.
Multi-parameter and multi-object optimization on combustion system of high power diesel engine based on response surface method.
Chinese Internal Combustion Engine Engineering, Vol. 5, pp. 005, 2012. (cited on p. 58)

Yusoff Y., Ngadiman M.S. and Zain A.M.
Overview of NSGA-II for optimizing machining process parameters.
Procedia Engineering, Vol. 15, pp. 3978–3983, 2011. (cited on p. 51)

Zhao X., Ren M. and Liu Z.
Critical solubility of dimethyl ether (DME)+ diesel fuel and dimethyl carbonate (DMC)+ diesel fuel.
Fuel, Vol. 84 n^o 18, pp. 2380–2383, 2005. (cited on p. 32)